MODULATION OPTIONS FOR OFDM-BASED WAVEFORMS

A DISSERTATION SUBMITTED TO

THE GRADUATE SCHOOL OF

ENGINEERING AND NATURAL SCIENCES

OF ISTANBUL MEDIPOL UNIVERSITY

IN PARTIAL FULFILLMENT OF THE REQUIREMENTS FOR

THE DEGREE OF

DOCTOR OF PHILOSOPHY

IN

ELECTRICAL, ELECTRONICS ENGINEERING AND CYBER SYSTEMS

By

Ahmad Mohammad Abd-alghani Jaradat

January, 2023

MODULATION OPTIONS FOR OFDM-BASED WAVEFORMS

By Ahmad Mohammad Abd-alghani Jaradat

17 January 2023

We certify that we have read this dissertation and that in our opinion it is fully adequate, in scope and in quality, as a dissertation for the degree of Doctor of Philosophy.

Prof. Hüseyin Arslan (Advisor)

Assist. Prof. Ali Görçin

Prof. Bahadır K. Güntürk

Prof. Hasari Çelebi

Assoc. Prof. Mehmet Kemal Özdemir

Approved by the Graduate School of Engineering and Natural Sciences:

Prof. Yasemin Yüksel Durmaz

Director of the Graduate School of Engineering and Natural Sciences

I hereby declare that all information in this document has been obtained and presented in accordance with academic rules and ethical conduct. I also declare that, as required by these rules and conduct, I have fully cited and referenced all material and results that are not original to this work.

Signature :

Name, Surname: AHMAD MOHAMMAD ABD-ALGHANI JARADAT

ACKNOWLEDGEMENT

First and foremost, I would like to express my most valuable appreciation to my Ph.D. advisor Prof. Hüseyin Arslan for his great support and contribution. Without his patience and sacrificing hours for me, this thesis will never be written. His wide knowledge, plentiful experience, continuous guidance, and encouragement motivated me to commit myself to research and also pursue an academic career in my future endeavors.

I would like to extend my sincere thanks to the committee members of my Ph.D. thesis: Asst. Prof. Ali Görçin, Prof. Bahadır K. Güntürk, Prof. Hasari Çelebi, Assoc. Prof. Mehmet Kemal Ozdemir for their constructive comments and valuable suggestions on my research works and thesis.

I wish to thank the Graduate School Director Prof. Yasemin Yüksel Durmaz and the staffs of the secretary office at Engineering and Natural Sciences Department for technical support throughout my stay in Medipol University. I am also grateful to my fellow lab colleagues and friends in Medipol University. I have learned a lot from each of them throughout the years, and I really appreciate their companions, help, and ideas. Their kind support and friendship have made my study and life in Turkey a wonderful time.

I would also like to acknowledge that this thesis work is supported in part by the Scientific and Technological Research Council of Turkey (TUBITAK). Without these financial supports, I would not be able to complete my Ph.D. study.

Finally, I would like to express my gratitude to my parents and family for their tremendous support and encouragement throughout my studies.

Ahmad Mohammad Abd-alghani Jaradat
January, 2023

CONTENTS

Page

LIST OF FIGURES

LIST OF TABLES

LIST OF SYMBOLS

$(\cdot)^H$	:Hermitian (conjugate transpose)
$(\cdot)^T$	:Transpose
$\|\| \cdot \|\|_F$	:Frobenius norm
$\| (\cdot) \|$	:Absolute value
$E(\cdot)$	:Expectation operation
I_N	:$N \times N$ identity matrix
F_N^{-1}	:N-point inverse fast Fourier transform (IFFT) matrix
$det(A)$	:determinant of A
σ	:Noise standard deviation
n	:AWGN
N_0	:Noise power density
B	:Bandwidth
h	:Channel coefficient vector

ABBREVIATIONS

2-D	: two dimensional
3-D	: three dimensional
3GPP	: Third Generation Partnership Project
5G	: fifth generation
NR	: New Radio
RATs	: radio access technologies
BS	: base station
SCSs	: subcarrier spacings
eMBB	: enhanced mobile broadband
mMTC	: massive machine type communications
URLLC	: ultra-reliable low-latency communication
MAC	: Medium access control
UEs	: user equipments
CP	: cyclic prefix
SWISS	: Spectrum Weighted Identification of Signal Sources
DFT	: discrete Fourier transform
FFT	: fast Fourier transform
OFDM	: orthogonal frequency division multiplexing
SM-OFDM	: Spatial modulation-OFDM
OFDM-IM	: OFDM with index modulation
OFDM-GIM	: OFDM with generalized index modulation
OFDM-SNM	: OFDM with subcarrier number modulation
OFDM-HNIM	: OFDM with hybrid number and index modulation
OFDM-SGM	: OFDM with subcarrier gap modulation
OFDM-DM	: OFDM-differential modulation
OFDM-PSM	: OFDM with pulse superposition modulation
OFDM-STSK	: OFDM-aided space-time shift keying
MBM	: media-based modulation
SAP	: subcarrier activation pattern
QAM	: quadrature amplitude modulation
PSK	: phase shift keying
mmWave	: millimeter-wave
PAPR	: peak-to-average power ratio
SE	: spectral efficiency
PE	: power efficiency
EE	: energy efficiency
ICI	: inter-carrier-interference
RRS	: radio resource scheduling
RA	: resource allocation
CSI	: channel state information
CQI	: channel quality indicator
FMCW	: frequency modulated continuous wave
TTI	: transmission time interval

OFDM TABANLI DALGA BIÇIMLERI IÇIN MODÜLASYON SEÇENEKLERI

ÖZET

Ahmad Mohammad Abd-alghani Jaradat

Elektrik-Elektronik Mühendisliği ve Siber Sistemler, Doktora

Tez Danışmanı: Prof. Hüseyin Arslan

17 Ocak 2023

5G ve sonraki ağların, değişen gereksinimlere ve yeteneklere sahip çeşitli uygulamaları destekleyebileceği tahmin edilmektedir. Bu nedenle, özellikle veri hızları, gecikme süresi ve enerji ekonomisi gibi sıkı parametrelerle uğraşırken belirli bir kullanım durumu için doğru modülasyonu seçmek çok önemlidir. Milimetre dalga kablosuz iletişim sistemleri için gelecekteki çok sayıda yöntem, seçilen modülasyon seçeneğinden etkilenir.

Verimli veri aktarımı için "alt taşıyıcı sayı modülasyonu (OFDM-SNM) ile orthogonal frekans bölmeli çoğullama" olarak adlandırılan yeni bir modülasyon sistemi sunulmuştur. Her OFDM alt bloğundaki aktif alt taşıyıcıların sayısı, bu yöntemi kullanarak very iletimini kolaylaştırmak için değiştirilir. Bu teknolojinin fikri, OFDM ve darbe genişlik modülasyonunun kombinasyonundan geldi. Darbe genişliği, belirli bir bilgi bitine karşılık gelen aktif alt taşıyıcıların sayısını gösterir. Bu, bilgilerin alt taşıyıcıların sayıları yerine indeksleri kullanılarak gönderildiği OFDM-IM'den farklıdır. Sistemin aynı bit hata oranında OFDM-IM'den daha yüksek spektral verim elde ettiği gösterilmiştir. Aktif alt taşıyıcılar, alt blok içinde herhangi bir yere yerleştirilebilir. Bu, sistem performansını daha da artırabilen kanala göre en uygun alt taşıyıcının seçilmesine olanak tanır.

Her OFDM alt bloğunda, verimli veri iletimi amacıyla yeni bir iletim şeması sunulur. Bu yöntem, aktif alt taşıyıcıların indeksini ve sayısını değiştirerek daha fazla veri gönderir. OFDM-SNM ve OFDM-IM ile karşılaştırıldığında, önerilen modülasyon yöntemi, özellikle yüksek güvenilirlik ve düşük karmaşıklık sunabilen ikili faz kaydırmalı anahtarlama (BPSK) gibi düşük modülasyon sıralarında spektral verimlilik ve enerji verimliliği açısından daha verimlidir. Sonuç olarak Nesnelerin İnterneti (IoT) uygulamalarının gereksinimlerini karşılamak için çok uygundur. Önerilen yöntem için, bit hata oranının (BER) bir performans analizi verilmiş ve simüle edilen BER'in analiz edilenle aynı olduğunu göstermek için Monte Carlo simülasyonları kullanılmıştır. Güç ve spektral verim değerleri aynı olduğunda, önerilen sistemin OFDM-IM ve geleneksel OFDM'den çok daha iyi BER performansı sağlayabildiği gösterilmiştir.

Alt taşıyıcı boşluk modülasyonu (OFDM-SGM) ile ortogonal frekans bölmeli çoğullama adı verilen bir modülasyon tekniği önerilmektedir. Önerilen teknik, her bir alt bloktaki aktif alt taşıyıcılar arasındaki boşluğu kullanarak fazladan bilgi bitlerini gömer. Önerilen sistem, bilgi bitlerini aktif alt taşıyıcıların indeksine dayalı olarak ileten OFDM-IM'den farklıdır. Bu OFDM-SGM tekniği, özellikle düşük karmaşıklıktaki IoT uygulamaları için ideal olan BPSK'ye benzer düşük takımyıldız şemaları kullanıldığında, spektral ve enerji verimliliği açısından OFDM-IM tekniğinden daha iyi performans gösterir. Teorik olarak

hesaplanan ve simüle edilen hata performansları arasındaki tutarlılığın yanı sıra, önerilen sistemin teorik hata performansının bir analizi sağlanmaktadır.

Yeni OFDM-SNM şeması, geleneksel OFDM'den daha az enerji ve spektral verimlilik kullanır. Bu, ek bilgi bitlerinin aktif alt taşıyıcılara yüklenmesinin bir sonucu olarak ortaya çıkar. Öte yandan, OFDM-SNM şemasının zirveortalama güç oranı (PAPR) yüksektir ve geleneksel OFDM'ninkine yaklaşık olarak eşdeğerdir. OFDMSNM'de, yüksek PAPR dışında, bloklar arasında genellikle bant dışı emisyon (OOBE) vardır. Yukarıda listelenen sorunları çözmek için klasik OFDMSNM'nin geliştirilmiş bir versiyonunu bulduk. Bu versiyonda aktif alt taşıyıcılar PAPR ve OOBE değerlerini düşürecek şekilde yerleştirilmiştir. PAPR'nin PSD ve CCDF'si, önerilen planın PAPR ve OOBE performansını ölçer. Simülasyonlar, PAPR ve OOBE açısından, önerilen şemanın klasik OFDM'den daha iyi olduğunu, BER performansının ise neredeyse aynı olduğunu göstermektedir.

Geniş bir hizmet yelpazesinin ihtiyaçlarını karşılamak söz konusu olduğunda, 5G New Radio (NR), çoklu numeroloji seçimine izin vererek yeni bir esneklik getiriyor. Kör numeroloji tanımlaması sayesinde bu yeni yapıyla geliştirilmiş sistem etkinliği mümkündür. Sonuç olarak, çeşitli numerolojiler için uygun bir kör tanımlama yöntemi sağlıyoruz. Zaman alanı otokorelasyonu, aday numerolojinin bileşik sinyaldeki döngüsel önek (CP) sinyalini ilişkilendirerek numeroloji tipini belirlemek için kullanılır. Her bir numerolojinin yaşadığı alt bantların güç spektral yoğunluğundaki (PSD) varyans farkı, frekans alanı konumunu belirler. Simülasyonun bulguları, frekans seçici kanallarla birlikte toplam beyaz Gauss gürültüsü (AWGN) kullanılarak elde edilir. Geleneksel karma numeroloji sisteminde kullanılan kör olmayan tanımlama stratejisiyle karşılaştırıldığında, elde edilen sonuçlar, önerilen yöntemin sağlam bir tanımlama doğruluğuna ve tatmin edici bir BER performansına sahip olduğunu göstermektedir.

Kablosuz iletişim sistemlerindeki kanal dürtü yanıtı, kanal bağlantılarının sayısı biliniyorsa (CIR) daha iyi tahmin edilebilir. Derin sinir ağlarının (DNN'ler) kullanılmasıyla, bu araştırma, mevcut bir DNN'yi değiştirdiğimiz ve yakınsama performansını analiz ettiğimiz kablosuz kanal bağlantılarının sayısının verimli bir şekilde tespit edilmesi hedefine ulaşmayı başardı. kablosuz sistem. Görüntülenen sonuçlar, uyarlanan DNN'nin, Sinyal Kaynaklarının Spektrum Ağırlıklı Tanımlanması (SWISS) adlı mevcut bir algoritmaya kıyasla, kanal bağlantılarının sayısını belirlemede üstün performans gösterdiğini göstermektedir.

Radar ve iletişimin birlikte yaşaması, orta erişim kontrolü (MAC) katmanında, özellikle programlama ve radyo kaynakları yönetimi (RRM) alanlarında çok sayıda araştırma fırsatı sunan, gelişmekte olan bir teknolojidir. Kablosuz ortamlarda çalışan artan sayıda uygulamaya uyum sağlamak için daha etkili olan programlama yöntemlerine ihtiyacımız var. Radar destekli araç haberleşme sistemi kapsamında, yankının bir hedeften yansıdığı, yankı tabanlı senaryo adı verilen bir durumu inceliyoruz. Geleneksel programlama mekanizmalarında yapıldığı gibi sadece sinyalparazitvegürültü oranına (SINR) güvenmek yerine, menzil ve hız gibi ek özellikleri bir araya getiren yeni bir radar destekli iletişim programlama algoritması sunuyoruz. zamanlama süreci. Mevcut kaynakları programlamak için gereken bilgi, önerilen algoritma tarafından radar yankısından çıkarılır. Yeni parametreler, radar destekli iletişim programlama yöntemini çok çeşitli senaryolarda daha esnek ve verimli hale getiriyor. Önerilen yöntem, B5G haberleşme sistemleri için lokalizasyon ve algılama yapılmasına olanak sağladığı için avantajlıdır.

Mevcut dinamik kaynak bloğu yapısına (D-RBS) dayalı verimli bir radyo kaynak programlama (RRS) yaklaşımı öneriyoruz. Önerilen RRS, trafik talebindeki değişikliklere daha duyarlıdır. Daha spesifik olarak, küçük boyutlu kaynak blokları (RB)'ler, trafik ihtiyaçları ve bağlantı arızalarındaki değişiklikleri işlemek için kullanıcı ekipmanlarına (UE) tahsis edilir. Önerilen yaklaşım, delinmiş mini yuva tabanlı programlama yöntemleri kullanılmadan düşük gecikmeli iletişim sağlar. Böylece, gelişmiş mobil geniş bant (eMBB) UE'lerinin veya hücrelerinin performansı, ultra güvenilir düşük gecikme süreli iletişim (URLLC) UE'lerine öncelik verilirken bozulmaz. Mevcut RB'leri tahsis etmek için, hepsini bir kez deneme (RR), orantılı adil (PF) ve en iyi kanal kalite göstergesi (BCQI) gibi geleneksel programlama algoritmaları kullanılır. Ayrıca önerilen şema, sinyalgürültü oranı (SNR) değerleri gibi belirli eşiklere dayalı olarak RR ve BCQI programlamasının dinamik olarak değiştirilmesine izin verir. Önerilen yöntemin etkinliğini standart statik kaynak blok yapısı (S-RBS) ile karşılaştırmak amacıyla, sistem düzeyinde simülasyonlar (SLS'ler) gerçekleştirilir. Simülasyon sonuçları, geliştirilen yaklaşımın çeşitli beşinci nesil (5G) hizmetler için güçlü veri hızı, sistem verimi, spektral verimlilik (SE) ve UE başına ulaşılabilir oran sağladığını göstermektedir.

Anahtar sözcükler: OFDM, Kaynak Tahsisi, Modülasyon, OFDM-SNM, OFDM-SGM, OFDM-HNIM, Dalga Formu, Kaynak Bloğu 5G, OFDM-IM, Zamanlama.

MODULATION OPTIONS FOR OFDM-BASED WAVEFORMS

ABSTRACT

Ahmad Mohammad Abd-alghani Jaradat

Ph.D. in Electrical, Electronics Engineering and Cyber Systems

Advisor: Prof. Hüseyin Arslan

17 January 2023

It is anticipated that 5G and subsequent networks would be able to support a variety of applications with varying requirements and capabilities. Therefore, it is crucial to choose the correct modulation for a given use case, especially when dealing with tight parameters like data rates, latency, and energy economy. Numerous future methods for millimeter-wave wireless communication systems are affected by the modulation option selected.

A new modulation system termed "orthogonal frequency division multiplexing with subcarrier number modulation (OFDM-SNM)" is presented for efficient data transfer. The number of active subcarriers in each OFDM subblock is varied to facilitate data transmission using this method. The idea for this technology came from the combination of OFDM and pulse width modulation. The pulse width shows the number of active subcarriers that correspond to a certain bit of information. This is different from OFDM-IM, where information is sent using the indices of the subcarriers instead of their numbers. It is shown that the system achieves greater spectral efficiency (SE) than OFDM-IM at the same bit error rate. The active subcarriers can be placed anywhere inside the subblock. This lets the optimal subcarrier be chosen based on the channel, which can improve system performance even more.

Within each OFDM subblock, a novel transmission scheme is presented for the purpose of efficient data transmission. This method sends more data by modifying the index and number of active subcarriers. Compared to OFDM-SNM and OFDM-IM, the proposed modulation method is more efficient in terms of SE and energy efficiency (EE), especially at low modulation orders like binary phase shift keying (BPSK), which can offer high reliability and low complexity. As a result, it is very suitable for meeting the requirements of Internet of Things (IoT) applications. For the suggested method, a performance analysis of the bit error rate (BER) is given, and Monte Carlo simulations are used to show that the simulated BER is the same as the one that was analyzed. When the power and SE values are the same, it has been shown that the suggested system can provide much better BER performance than OFDM-IM and traditional OFDM.

A modulation technique called orthogonal frequency division multiplexing with subcarrier gap modulation (OFDM-SGM) is suggested. By utilizing the gap between the active subcarriers in each subblock, the proposed technique embeds extra information bits. The proposed system varies from OFDM-IM, which transmits information bits based on the index of active subcarriers. This OFDM-SGM technique outperforms the OFDM-IM technique in terms of spectral and EE, particularly when employing low constellation

schemes similar to BPSK, which are ideal for low-complexity IoT applications. An analysis of the proposed system's theoretical error performance is provided, as is the consistency between the theoretically calculated and simulated error performances.

The new OFDM-SNM scheme uses less energy and SE than traditional OFDM. This occurs as a result of the loading of additional information bits onto the active subcarriers. On the other hand, the peak-to-average power ratio (PAPR) of the OFDM-SNM scheme is high and about equivalent to that of traditional OFDM. In OFDM-SNM, apart from the high PAPR, there is often out-of-band emission (OOBE) between the blocks. To solve the problems listed above, we came up with an improved version of the classic OFDM-SNM. In this version, the active subcarriers are placed in a way that reduces the PAPR and OOBE values. The PSD and CCDF of PAPR measure the proposed scheme's PAPR and OOBE performance. The simulations show that in terms of PAPR and OOBE, the proposed scheme is better than the classical OFDM, while BER performance is nearly identical.

When it comes to meeting the needs of a wide range of services, 5G New Radio (NR) brings new flexibility by allowing for a selection of multiple numerologies. Improved system effectiveness is possible with this new structure thanks to blind numerology identification. As a result, we provide a method of blind identification suitable for a variety of numerologies. Time-domain autocorrelation is used to identify numerology type by correlating the candidate numerology's cyclic prefix (CP) signal in the composite signal. The variance difference in the power spectral density (PSD) of the subbands inhabited by each numerology determines its frequency domain position. The findings of the simulation are acquired using additive white Gaussian noise (AWGN), in conjunction with frequency-selective channels. When compared to the non-blind identification strategy used in the conventional mixed-numerology system, the acquired results indicate that the suggested method possesses a robust identification accuracy and a satisfactory BER performance.

The channel impulse response (CIR) in wireless communication systems can be better estimated if the number of channel taps is known. Through the use of deep neural networks (DNNs), this research was able to achieve the goal of efficient detection of the number of wireless channel taps, where we modified an existing DNN and analyzed its convergence performance using only the transmitted and received signals of a wireless system. The displayed results demonstrate that the adopted DNN accomplishes superior performance in identifying the number of channel taps, as compared to an existing algorithm called Spectrum Weighted Identification of Signal Sources (SWISS).

The cohabitation of radar and communications is an emerging technology that presents a plethora of research opportunities in the medium access control (MAC) layer, particularly in the areas of scheduling and radio resource management (RRM). In order to accommodate the growing number of applications that operate in wireless environments, we require scheduling methods that are more effective. Within the context of the radar-aided vehicular communication system, we study a situation called an echo-based scenario in which an echo is reflected from a target. Instead of relying just on the signal-to-interference-and-noise ratio (SINR), as is done in traditional scheduling mechanisms, we present a new radar-aided communication scheduling algorithm that incorporates additional characteristics, such as range and velocity, into the scheduling process. The information needed to schedule the available resources is extracted from the radar echo by the algorithm that has been proposed. New parameters make the radar-aided communication scheduling method more flexible and efficient in a wide range of

scenarios. The suggested method is advantageous for B5G communication systems since it makes it possible to do localization and sensing.

We propose an efficient radio resource scheduling (RRS) approach based on the existing dynamic resource block structure (D-RBS). The proposed RRS is more responsive to variations in traffic demand. More specifically, small-sized resource blocks (RB)s are allocated to user equipments (UE)s to handle the changes in the traffic needs and link failures. The proposed approach enables low latency communication without the use of punctured minislot based scheduling methods. Thus, the performance of enhanced mobile broadband (eMBB) UEs or cells is not degraded while prioritizing ultra-reliable low latency communication (URLLC) UEs. Traditional scheduling algorithms such as round robin (RR), proportional fair (PF), and best channel quality indicator (BCQI) are used to allocate the available RBs. Also, the proposed scheme allows the dynamic switching of RR and BCQI scheduling based on specific thresholds, such as signal-to-noise ratio (SNR) values. For the purpose of comparing the efficiency of the suggested method to that of the standard static resource block structure (S-RBS), system-level simulations (SLSs) are carried out. The simulation results demonstrate that the developed approach provides robust data rate, system throughput, SE, and achievable rate per UE for various fifth generation (5G) services

Keywords: OFDM, Resource Allocation, Modulation, OFDM-SNM, OFDM-SGM, OFDM-HNIM, Waveform, Resource Block, 5G, OFDM-IM, Scheduling

CHAPTER 1

1. INTRODUCTION

1.1. Background

There have been many contributions in proposing new novel approaches and schemes linked to the following two study directions at the physical layer level in recent research efforts connected to 5G and beyond RATs.

- Advanced waveform designs: The purpose here is to create new, improved waveforms (other than the conventional OFDM waveform) to enhance the system performance metrics in terms of adjacent channel interference, inter-numerology interference, synchronicity, complexity, SE, reliability, and robustness to inter-carrier interference, Doppler, phase noise, etc.
- New modulation techniques: The goal here is to come up with novel modulation schemes (other than the conventional modulation schemes) to enhance the system's performance in terms of SE, PE, and reliability. Examples of techniques in this domain are shown in detail in this thesis.

However, there has been some confusion in the literature in terms of naming, where many people think waveform is modulation, as can be seen in [9], which is not very true as they are related but different from each other. To understand the difference and see if there is any relationship between them, we will resort back to the most basic, fundamental definition as follows.

Modulation is the process of intentionally varying the characteristics of the radio environment (at the transmitter) in accordance with the information signal. This definition also involves modulation as a general technique of shaping a signal to convey information. More

specifically, the definition of modulation involves changing the properties of a physical signal in the analog domain according to the incoming information. For instance, when the used carrier signal in a digital communication system is a sinusoidal function, then its properties, including amplitude, phase, and frequency, can be changed according to the incoming information bits, resulting in what is called amplitude shift keying (ASK), phase shift keying (PSK), and frequency shift keying (FSK), respectively. This is well-known in the literature as the most basic form of modulation. Also, another possible definition of modulation is the mapping of the incoming information bits to constellation symbols in the digital domain, such as binary PSK (BPSK), and then the transmission carrier changing state according to each symbol. Researchers have recently used the properties of a subblock within an OFDM symbol structure as a new type of carrier at the baseband to send extra information bits. The subblock properties in terms of the indices and number of subcarriers within a subblock [10] are used to convey extra information. These changes in the properties of the physical signal contribute to the final physical signal, which represents the waveform that can be transmitted and received over a medium.

The waveform defines the locations of the transmitted signal, i.e., lattice points and spacing. Also, the waveform includes the way information is sent, such as the shapes in hyperspace that hold energy. Any processing that can change these shapes is part of the waveform. The waveform includes noise, redundancy, precoding, etc. applied to the physical signal. The modulated signal's waveform establishes its physical shape.

From the above discussion and explanation, the differences between waveform and modulation concepts are clearly stated and concluded. This description is expected to help researchers choose appropriate terms and names for the proposed schemes, methods, techniques, etc. according to their exact functionality to avoid any confusion in the basic understanding of new concepts.

Classical single-carrier digital modulations like M-ary PSK and quadrature amplitude modulation (QAM) can map entering data bits to constellation symbols. OFDM multicarrier schemes can boost communication system data rates.

Multicarrier transmission schemes are extensively used in wireless communications due to features, like easy equalization, multi-user scheduling, and support for adaptive modulation and coding techniques, etc. [11]. The OFDM transmission scheme is arguably

considered the most promising multicarrier techniques, leading to its widespread use in various communication standards [12]. However, the conventional OFDM scheme has certain limitations, such as a high peak-to-average power ratio (PAPR) [13], which necessitates improved modulation schemes, particularly for metrics such as reliability, spectral efficiency (SE), EE, etc. [10]. The diverse user requirements, such as increased capacity and massive connectivity, render increased SE and EE imperative. These factors also dictate the appropriate modulation schemes, particularly for EE in mmWave bands [14].

Different OFDM-based modulation options have been proposed in the literature and their classification, comparison, and future directions have been provided in [10]. In conventional OFDM transmission, each constellation symbol is carried by an OFDM subcarrier. Differently, the conventional constellation symbols could be conveyed by making changes either between two consecutive subcarriers in the same OFDM symbol or the difference between two successive symbols in the same subcarrier [15]. This kind of transmission is called OFDM-differential modulation (OFDM-DM), which is characterized by its insensitivity to slowly changing amplitude and phase distortion; thus, the OFDM-DM transmission scheme enables the total elimination of equalization processes.

In addition to the conventional and differential modulation schemes for OFDM systems, some other modulation schemes utilize a third dimension besides the two dimensional (2-D) signal constellation plan with the main aim of transmitting additional information. The utilization of three dimensional (3-D) relies on the application, its requirements, and its capabilities. Each modulation technique is formed by its specific parameters, which constitute the flexibility aspect of modulation design. Spatial modulation-OFDM (SM-OFDM), OFDM-IM, OFDM-SNM, and OFDM with pulse superposition modulation (OFDM-PSM) are some examples of these 3-D emerging modulations, which are built based on some modifications in the OFDM-based waveform. The SM-OFDM [16] and OFDM-IM [17] transmission schemes are structured by the utilization of the index of active antennas and subcarriers, respectively, for an OFDM-based waveform. Therefore, the OFDM-IM and SM-OFDM schemes can be categorized under the index-based modulation family [18], in which the index of the active transmit medium is exploited to send additional data bits.

Another degree of freedom for efficient data transmission is the utilization of the number

of active transmitting resources as another dimension for conveying extra information bits. According to [19], the OFDM-SNM scheme is one of the promising candidate number-based modulation schemes in which the number of active subcarriers is used to convey extra information bits in addition to the symbols from a standard modulation alphabet. It is worth noting that, unlike the OFDM-IM method, which uses fixed indices for active subcarriers, OFDM-SNM enables floating active subcarriers within an OFDM subblock, allowing them to be positioned in any index.

Moreover, the shape dimension could be exploited to enhance the data rate of the OFDM-based transmission scheme. The OFDM-PSM scheme is considered one example of the shape-based modulation family, where N_p pulses are modulated based on the incoming bit sequence, and then they are superimposed to transmit N_p data symbols in each grid of rectangular time-frequency lattice structure. Therefore, the data rate could be enhanced to N_p times. In [20], multiple orthogonal Hermite-Gaussian (HG) carriers have been used with rectangular orthogonal frequency division multiple access to boost the bandwidth efficiency.

1.2. Motivation And Thesis Contributions

Recent research studies exhibit the urgent need for designing new advanced waveforms and modulation techniques that are capable of further increasing SE, EE, and reliability with little complexity in comparison to classical OFDM in order to accommodate the varied requirements of future 5G services [21], [22].

Fifth generation (5G) and beyond radio access technologies (RATs) need flexibility to satisfy different applications, channel conditions, and user needs. The design of modulation looks like a new degree of freedom that could help with the design of RATs for 5G. Numerous modulation techniques have been developed, each with advantages in different channel conditions and applications. Several merits cannot be achieved by the conventional modulation schemes, which necessitate the design of flexible modulation options. For example, the conventional modulation for the OFDM waveform is not flexible enough for future RAT. There is no optimal modulation that meets all user demands, i.e., each modulation scheme has some demerits in some scenarios. Therefore, it is worthy to investigate the flexibility perspective of a given modulation scheme by studying its parameters, which

facilitates a proper selection of modulation techniques for future RATs [23].

The design of modulation emerges as an additional degree-of-freedom that can be used to overcome various sorts of signal distortions and interference. By making a proper adjustment to the modulation parameters, the communication performance would be maintained. Moreover, different modulation schemes exhibit different inherent advantages. For example, the non-conventional modulation schemes for the OFDM waveform, such as OFDM-IM and OFDM-SNM, have inherent robustness against inter-carrier-interference (ICI) due to having some inactive subcarriers in their transmission block. These features are not observed in the conventional OFDM scheme, where almost all subcarriers are active. Also, some modulation techniques offer inherent advantages in certain scenarios. For example, the OFDM-SNM scheme exhibits high throughput performance at low modulation orders due to its inherent feature of conveying information via the number of active subcarriers. More flexible modulation techniques are required to address various technical challenges in next-generation communication networks in order to provide a greater degree of freedom.

Modulation selection and parameter adaptation for channel and user situations show the modulation design's adaptability, resulting in improved communication performance for all users. Another flexibility that may be offered in B5G is a hybrid scheme that intelligently blends several modulation methods to deliver varied benefits with low complexity overhead.

1.2.1. The OFDM with subcarrier number modulation

A novel modulation scheme called "spatial modulation" that exploits the spatial domain by selecting the indices of antennas along with the classical signal constellations (amplitude/phase modulation) to convey information was proposed in [24]. OFDM with subcarrier index modulation (OFDM-SIM) was proposed in [25] as an intriguing application of SM to OFDM. The information bits are transmitted using the OFDM-SIM by varying the indices of the OFDM active subcarriers in each OFDM block. A systematic subblock-based transceiver structure, named OFDM with Index Modulation (OFDM-IM), that enables selecting more than one active subcarrier among the available subcarriers in each subblock, was proposed in [17]. In [26], a generalized version of OFDM-IM named OFDM-GIM was introduced, where different activation ratios per each subblock are used

to enhance SE. Recently, a comprehensive survey of the recent advances and different variations of the index modulation (IM) concept was given in [22]. For this IM strategy, a set number of subcarriers within each subblock of the OFDM-IM signal are chosen to act as active subcarriers and send bits of data.

In this study, rather than OFDM-IM, we suggest a novel modulation approach that we call OFDM with subcarrier number modulation (OFDM-SNM). The concept of OFDM-SNM is inspired by OFDM with pulse width modulation by means of representing pulse width by the number of active subcarriers. This number is determined depending on the different combinations of incoming bits. The number of active subcarriers adds a dimension to the two-dimensional complex signal constellation scheme for data transmission. These dimensions are used to send information to the receiver based on the number of active subcarriers (rather than their indices) and symbols. Better SE is achieved with the proposed OFDM-SNM compared to both OFDM and OFDM-IM when BPSK is used. Also, the suggested OFDM-SNM system is proven to be superior to OFDM and OFDM-IM in terms of power efficiency and reliability. As is the case with OFDM-IM, OFDM-SNM has the potential to cut down on ICI as well as PAPR because it does not activate all of the subcarriers. Different from OFDM-IM, the activated subcarriers can be placed in any index or position within each subblock as the information is sent by the subcarriers' number, and thus they can be made channel-dependent, resulting in even better reliability performance. The proposed scheme's exact SE and error performance formulas are derived and shown to closely match the simulated results. This study was published in IEEE Wireless Communications Letters [19].

1.2.2. The OFDM with hybrid number and index modulation

A new way to send data that sends more information by changing the index and number of active subcarriers in each OFDM subblock is proposed. The proposed scheme is different from the conventional OFDM-SNM and OFDM-IM, in which data bits are transmitted using either a number or index of active subcarriers. The suggested OFDM with hybrid number and index modulation (OFDM-HNIM) modulation technique has better SE and EE than OFDM-SNM and OFDM-IM, especially for low modulation orders like BPSK, which can provide high reliability and low complexity, making it suitable for IoT applications. Monte Carlo simulations are used to verify the proposed scheme's bit error rate (BER)

performance analysis. More crucially, the proposed system outperforms OFDM-IM and traditional OFDM in BER at equivalent power and SE levels. This study was published in IEEE Access [27].

1.2.3. The OFDM with subcarrier gap modulation

Similar to the generic blocks of OFDM-IM and OFDM-SNM, we present a new gap-based OFDM technique called OFDM-subcarrier gap modulation (OFDM-SGM). Rather of using the indices or the number of activated subcarriers to transmit information, this unique technique makes use of the gap between them and the traditional symbols. The proposed OFDM-SGM transmission scheme improves the system's design flexibility by creating additional means of conveying information in the gap dimension. This inherent flexibility can be utilized for different purposes, such as improving the overall SE of the communication system while maintaining low detection complexity. The proposed OFDM-SGM system could enhance SE-EE tradeoff by leveraging inactive subcarriers, unlike traditional OFDM, where all subcarriers are filled by nonzero components. This study was published in the proceedings of PIMRC 2020 conference [28].

1.2.4. The floating OFDM-SNM for PAPR and OOBE reduction

The technologies that offer high data rates, mobility, and high resource utilization efficiency, are increasingly needed due to fast-growing advanced wireless applications and their eagerness for more data. For the aforementioned objectives, the renowned multicarrier transmission scheme OFDM is considered a leading solution. However, OFDM's high PAPR and out-of-band emission (OOBE) limit its practical use. These issues have gained importance, especially with the emergence of the requirements of beyond 5G (B5G) networks [29].

The high PAPR is regarded as one of the most harmful characteristics of OFDM-based modulation systems, as its high levels limit modulation. This high PAPR causes the power amplifiers to introduce nonlinear distortion and spectral spreading in the OFDM system. The PAPR performance has a direct effect on the high PA (HPA) efficiency. Therefore, it is crucial to reduce PAPR to enhance its power efficiency by running it in the saturation zone. Signal distortion approaches, multiple signaling and probabilistic methods, and coding methods are the main PAPR reduction strategies in the literature [30].

The general representation of the OFDM-SNM signal is similar to that of traditional OFDM, in which several sinusoids are superimposed in the time domain, which results in a high power at a specific moment. The sparsity distribution of the active subcarriers in the OFDM-SNM has been investigated to see if it influences its comparable PAPR performance to that of conventional OFDM [31].

The higher data rates and mobility needs could be fulfilled by utilizing more subcarriers in future OFDM-based systems [31]. However, the inherent high PAPR associated with OFDM based systems should be addressed carefully, and this can serve as the impetus for future research. So, it's best to find ways to reduce PAPR that improve the performance of communication systems while keeping complexity and cost to a minimum.

Existing methods for reducing PAPR improve PAPR performance, but they decrease bit rate, increase transmission power, or make computing more difficult [32]. Under all circumstances, there is no single technique that could be considered an all-encompassing best available method; instead, we need to select proper techniques that suit the given requirements of interest as well as the available resources.

OFDM-SNM can use PAPR reduction methods like conventional OFDM. These solutions would not work well due to the inactive subcarriers of OFDM-SNM. Therefore, an efficient PAPR reduction technique tailored to OFDM-SNM is needed. We propose a PAPR reduction technique for the OFDM-SNM scheme that involves determining the best subcarrier activation patterns (SAPs) arrangement with the lowest PAPR value. Moreover, we employ the active constellation extension (ACE) and smart gradient projection (SGP) methods to provide a further reduction in PAPR performance [33].

OFDM-based systems' main drawbacks are PAPR and OOBE. To increase OFDM system performance, the OOBE and PAPR problems should be addressed. This problem happens due to the sidelobe roll-off between adjacent subcarriers that introduces inter-carrier interference, which leads to degradation in system performance. Almost all current techniques for OOBE reduction introduce the degradation in the BER performance or otherwise the loss in SE [34], [35]. In light of the aforesaid, there is a need to design an efficient OOBE reduction technique tailored to OFDM-based transmission schemes. OFDM-IM and our proposed scheme are the possible solutions to serve this purpose. In the literature, there is

no single research study to investigate the OOBE for OFDM-SNM or OFDM-IM. Moreover, almost all existing spectral suppression methods ignore the PAPR problem as a major issue in OFDM-based systems [34], [35], which may result in misleading OOBE reduction gains.

In this research, we present a flexible OFDM-SNM strategy called "floating OFDM-SNM" to suppress PAPR and spectral sidelobes of the OFDM signal while minimizing peak power and spectral leakage without affecting transmission rate. Another advantage of our proposed scheme is that we do not introduce any addition, removal, or even modification at the conventional OFDM-SNM receiver. This study was published in the proceedings of VTC 2021-Spring conference [36].

1.2.5. Blind numerology identification for mixed numerologies

The Third Generation Partnership Project (3GPP) chose OFDM for 5G New Radio (NR) downlink and uplink transmissions. An OFDM signal is a rectangular symbol composed of orthogonal subcarriers that carry the modulated symbols. The frequency spacing between the orthogonal subcarriers equals the reciprocal of the symbol time. In 5G, the set of subcarrier spacings (SCSs) and symbol durations is flexible and known as an OFDM numerology. This mixed-numerology structure has been studied in [37]–[39] and included in the NR standards of 3GPP [40].

The mixed numerology structure provides appealing flexibility in 5G and beyond networks. As the adjustable parameters of numerology increase, it becomes more critical to find the optimum one [41]. Due to this variety in the parametrization of numerologies, distinguishing them by the user equipments (UEs) becomes crucial in the 5G NR. The UEs can identify numerology using different approaches; for instance, they can know what to look for, they can exploit higher-layer signaling (of known numerology) for informing the UE, or they can also employ a blind detection method.

Blind detection algorithms are used to increase SE by estimating the signal parameters without additional signals. There are some identification methods proposed to identify OFDM signals [42], [43]. These methods target conventional OFDM with single numerology. Therefore, they cannot be directly reflected in the mixed-numerology system.

In [44], the author introduces the concept of using numerology for blind identification.

How to recognize distinct numerologies in the space of time and frequency is the subject of this work. In order to accomplish this objective, the power spectral density (PSD) mask in the frequency domain and the cyclic prefix (CP) correlation in the time domain are utilized. With the assumption of the use of blank resources, the numerologies are identified by measuring the size and disposition of their blank resources in the PSD mask. Therefore, only numerology identification is aimed at [44], without identifying its locations in the frequency domain. It is worth noting that this work proposes identification methods without focusing on specific communication systems. For example, the flexible mixed-numerology structure with mixed numerologies has not been investigated. Furthermore, the performance evaluation of this work has not been conducted.

To our knowledge, no literature study explains blind numerology identification for mixed numerology transmissions. Our blind numerology identification method identifies numerology types and subband locations. We propose a new method for blind numerology identification, where numerology types and their subband locations can be identified. For this purpose, we apply the CP correlation based and signal variance based techniques in the time and frequency domains, respectively, to build two receiver algorithms. Our proposed method achieves high identification accuracy without any prior information. The proposed method's BER performance is compared to the standard mixed numerology OFDM system's non-blind identification methodology. This study was published in the proceedings of WCNC 2021 conference [45].

1.2.6. Identification of the number of wireless channel taps using deep neural networks

Identification of the number of channel taps is a challenging task in real-time with fast channel variations. Precise channel estimation with better restoration of transmitted signals is possible by identifying the number of taps in unknown environments with no prior information. Therefore, an effective technique to recognize these taps is needed. Various wireless channel identification techniques, like [46], [47], assume prior information at the receiver about the multipath delay profile for the channel. However, this profile is usually unknown in practical use cases.

Motivated by the potential improvements that can be accomplished over the state-of-the-art, we propose a deep neural network (DNN) to identify a sparse channel parameter called

the number of taps from transmitted and received data of a wireless system. Our proposed identification method improves the SE of the communication system because the adopted DNN doesn't need to send any extra signals besides the data that comes in and goes out of the channel.

The DNNs can create maximally sparse representations of the signals of interest. To reflect our approach to DNN modeling, we used the basic network in [1] for finding the maximum sparsity. The DNN in [1] unfolds the high-complexity Iterative Hard Thresholding (IHT) algorithm given in [48]. The research study [1] shows the superior theoretical and empirical performance of this DNN compared to the IHT method. Also, the DNN promotes the maximal sparsity of its input with incomparable complexity.

To highlight the advantages of the adopted DNN in the proposed identification solution, we chose to compare its performance with an existing algorithm called Spectrum Weighted Identification of Signal Sources (SWISS) [49]. The SWISS algorithm finds the optimal combination of the discrete Fourier transform (DFT) components in the weighted DFT of the received signal, hence solving the path-number identification problem. The resultant signal represents the reconstructed channel signal, which has the minimum Euclidean distance to the received signal. The number of channel paths is then identified by calculating the number of significant components in the weight vector. Similar to the proposed DNN-based method, the SWISS algorithm does not need prior information about the number of channel taps. This study was published in the proceedings of NEWCAS 2021 conference [50].

1.2.7. Radar-aided communication scheduling algorithm for 5G and beyond networks

When it comes to bandwidth, latency, packet loss rate, and dependability, the needs of individual 5G services can vary widely [51]–[54]. To meet the different needs of future RATs, B5G RATs need schedulers that are both efficient and flexible.

As we are heading towards B5G, introducing flexible schedulers that exploit different parameters besides signal-to-interference-plus-noise-ratio (SINR) is crucial. Futuristic applications such as vehicle-to-everything communication and indoor localization depend on

the collaborative functionalities of communication and sensing [55]. Proposing a scheduler is first step toward emerging technologies such as the coexistence of communication and sensing. Utilizing radar's sensory data at communication terminals gives an essential level of knowledge regarding the environment that is around them. Low-cost radar sensors developed for radar applications [56] or integrated communication-radar systems [57], [58] can be used to gain this awareness The use of radar signals for improving communication has been studied in [59]–[64].

This work's objective is to be the first practical example of radar-aided scheduling in a vehicular communication situation, and as such, it explores the possibility of utilizing radar sensory data to steer the scheduling problem. Our key idea is to use the information from the radar operating in a mmWave band to extract the scheduling information where communication happens. In order to feed the appropriate features into the communication modules, the created system makes use of domain knowledge for radar signal processing.

Different from the existing PHY-based resource management approaches [65], we propose a new scheduling algorithm tailored for the radar-aided communication systems by exploiting different parameters that have not been used before, which include range and velocity. The proposed solution provides a more flexible scheduling mechanism for the systems' available resources. We explain in detail how the estimated parameters can aid RRM, including a novel radar-aided communication scheduling mechanism.

The proposed scheduler is evaluated by analyzing its performance with the conventional resource scheduling algorithms. The conventional physical resource block scheduling algorithms are reviewed exhaustively in [66]. The UE scheduling concept based on fairness and reliability has been extensively studied in the literature [67], [68]. PF, RR, and BCQI are the most known scheduling algorithms.

Our scheduler output maximizes the system performance of the communication system by maximizing its performance metrics, including communication data rate, SE, and system throughput. Higher data rates and spectrum efficiency are required in indoor scenarios [69]. The SE should be maximized, for example, if an unmanned aerial vehicle (UAV) covers a high number of targets so the scheduling data can be adequately collected. High system throughput is required due to its high reliability: Transmissions can occur with a probability of 99.999% [70]. This study was published in IEEE Access [71].

1.2.8. Dynamic-structure resource block allocation based scheduling for 5G systems

The time-frequency resources in the static resource block structure (S-RBS) are composed of predetermined resource blocks (RB)s that are shared in an optimized manner. The number of RBs demanded by UEs is not linearly proportional to their traffic demands [72]. The reason behind that is a UE with a higher SINR can use high-order modulation and coding schemes. As a result, the UE can transmit at a higher rate, requiring fewer RBs.

One of the most intriguing targets in communication systems is using more RBs to improve data rate, throughput, SE, and the achievable UE rate. This can be accomplished by increasing bandwidth (BW), which is a valuable resource for a mobile network operator. When more BW is added, the available RBs increase, but utilization decreases [73]. Another approach is to reduce the inactivity timer value, which allows inactive UEs to be released sooner, lowering user perception. These approaches rely on the S-RBS, which is not adaptable enough to accommodate a wide variety of service needs.

The authors of the paper [2] proposed a smart frame structure called dynamic resource block structure (D-RBS). More specifically, the main RB is split into multiple smaller RBs with the same time duration and BW. The UEs are assigned to these small blocks based on their requirements. This D-RBS can handle large fluctuations in data rates and low-latency traffic. The efficiency of small data transfer can be increased by the D-RBS. Specifically, the D-RBS does not need to use a fixed large RB for small data or an aggregation of these small data. This aggregation may increase the latency and complexity of scheduling. However, the usage of longer transmission time intervals (TTI)s is more useful for enhanced mobile broadband (eMBB) UEs because it provides a high data rate with less strict latency requirements.

The resource allocation (RA) algorithm in [2] introduced the D-RBS, which determines the RB assignment and number of RBs for the selected UE. However, [2] does not address the decision of which UE must be served, when UE can use the channel, or which RBs should be scheduled per TTI. Thus, we need to design a scheduling algorithm for efficient RB allocation to ensure the radio interface's quality of service.Based on the necessity of an efficient scheduler with the existing D-RBS based RA algorithm, we propose a new radio resource scheduling (RRS) approach based on the D-RBS.

The proposed scheduling approach differs from the punctured scheduling approach in terms of the used TTI and the allocated resources [74]. The ongoing eMBB transmission has long TTI in the punctured scheduling, where incoming ultra-reliable low-latency communication (URLLC) packet preempts a part of eMBB transmission. This scheduling impacts the decoding procedure of eMBB and leads to potential throughput loss. However, the D-RBS based scheduling does not necessitate packet puncturing since there is satisfactory number of RBs provided by the proposed approach. Another perspective is that the resources in the punctured scheduling are allocated to eMBB UEs at the level of RBs. On the other hand, an improved resource utilization is achieved by the D-RBS due to the flexible UEs' assignments of composite small-sized RBs that are non-contiguous in time and frequency. This study was published in the proceedings of IEEE VTC 2022-Spring conference [75].

CHAPTER 2

2. THEORETICAL PART

This chapter provides a coherent and all-inclusive framework for the many different types of modulation that can be used. The OFDM waveform is emphasized throughout the discussion of the classification of the included modulation options for waveforms in **Section 2.1**. Options for index-based modulation are presented in Section **Section 2.2**. **Section 2.3** offers the number-based modulation possibilities. **Section 2.4** explains the mixed-numerology system. In **Section 2.5**, we describe the wireless channel. Scheduling and radio resource allocation is presented in **Section 2.6**. Finally, some of the related works are presented in **Section 2.7**.

2.1. Classifications Of The Modulation Options For 5G And Beyond Waveforms

The featured modulation options could be integrated with different waveforms with proper adjustments. The OFDM waveform is chosen as a basic waveform in our classification due to its wide use in different standards, technologies, etc. An OFDM frame refers to a number of consecutive OFDM symbols and consists of the M-ary modulation alphabet placed on the time-frequency plane. For the modulation options shown in **Figure 2.1**, it is possible to depict in the time domain the signal that is transferred for an OFDM symbol as

$$\mathrm{x_t} = \frac{1}{\sqrt{K}} \mathrm{F}_N^{-1}\, \mathrm{x}, \tag{2.1}$$

where K represents the number of activated subcarriers, F_N^{-1} is the N-point inverse fast Fourier transform (IFFT) matrix, and x is the frequency-domain (FD) OFDM block of N

subcarriers: $\mathrm{x} = \begin{bmatrix} x(1) & x(2) & \dots & x(N) \end{bmatrix}^T$. **Table 2.1** shows different formations of x for different modulation options.

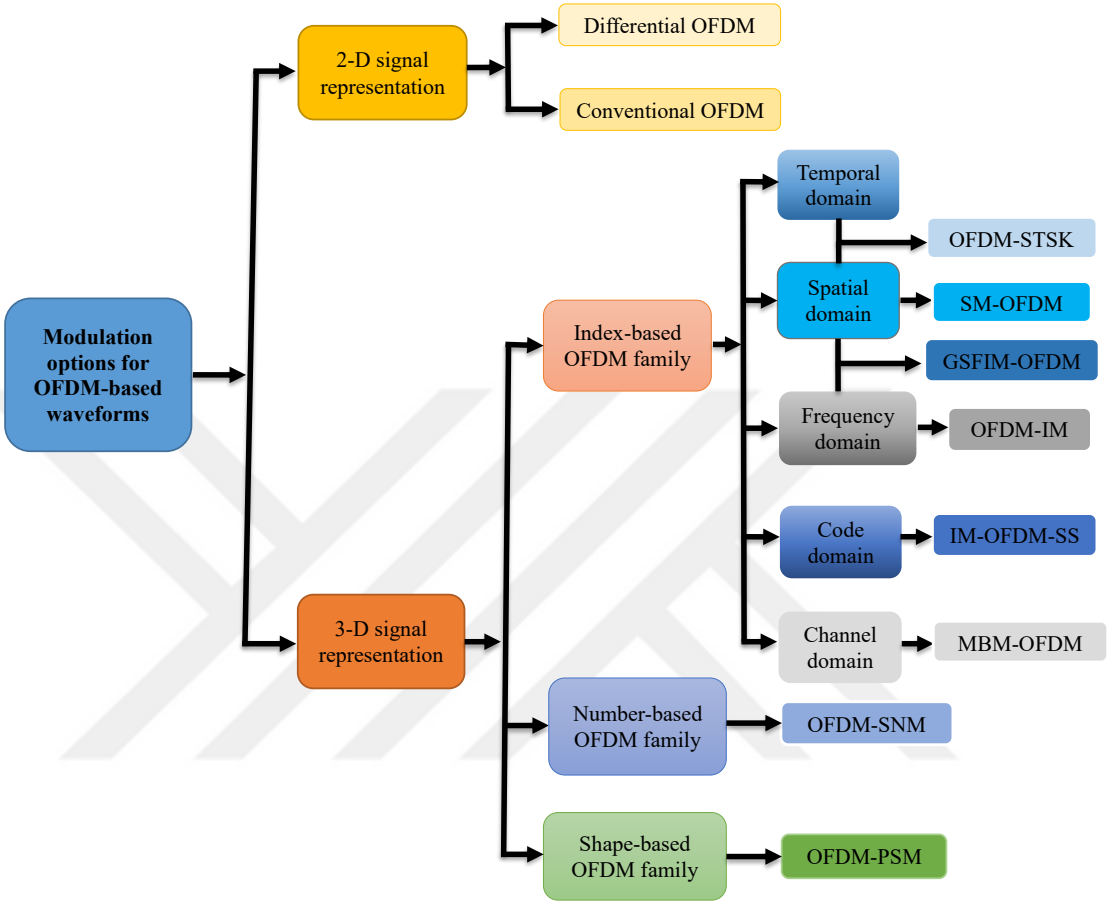

Figure 2.1: Classification of the modulation options for OFDM-based waveform.

Based on the number of dimensions used, OFDM-based waveform modulation techniques can be classified. **Figure 2.1** shows a possible classification where the classical OFDM and OFDM-DM exploit the complex 2-D signal plane, and the remaining modulation options exploit additional dimensions alongside the constellation symbols. These multi-dimensional modulation schemes include index-based [22], number-based [19], and shape-based [20] modulation schemes.

Different domains, such as temporal, frequency, etc., could be utilized separately or jointly for the featured OFDM-based modulation options. Examples of modulation options that exploit combined domains could be:

Table 2.1: The formation of the FD blocks for the featured modulation options.

Modulation option	x
Conventional OFDM [76]	$\mathrm{x} = \begin{bmatrix} s(1) & s(2) & \dots & s(N) \end{bmatrix}^T$, where $s(k) \in S$, S represents the conventional constellations.
OFDM-DM [77]	Different OFDM symbols over the same subcarrier, or different samples inside the same OFDM symbol, carry the information.
SM-OFDM [16]	The FD block of the j-th transmitting antenna: $\mathrm{x} = \begin{bmatrix} x_j(1) & x_j(2) & \dots & x_j(N) \end{bmatrix}^T$, which differs from FD blocks for the transmit antennas whose indices are all integer numbers from 1 to N_T except j.
OFDM-IM [17]	x is built depending on i_g and s_g where $\mathrm{i}_g = \{i_{g,1}, i_{g,2}, \dots, i_{g,a}\}$ and $\mathrm{s}_g = \begin{bmatrix} s_g(1) & s_g(2) & \dots & s_g(a) \end{bmatrix}^T$, where $s_g(\gamma) \in S$. The number of subcarriers that are active in the g-th subblock is fixed.
OFDM-SNM [19]	Similar x formation as in OFDM-IM expect that depending on the data sequence that comes in, the number of active subcarriers in each subblock changes.
OFDM-PSM [20]	The orthogonal HG pulses are modulated by different data symbols $s(k) \in S$.

- OFDM-aided space-time shift keying (OFDM-STSK) [78]: Spatial and temporal domains are exploited in the index dimension.
- Generalized space frequency index modulation-OFDM (GSFIM-OFDM) [79]: Spatial and frequency domains are utilized in the index dimension.
- OFDM-PSM: Time and frequency domains are exploited in the shape dimension.

Moreover, examples of the modulation options that exploit individual domains could be:

- OFDM-IM: Frequency domain is exploited in the index dimension.
- SM-OFDM: Space domain is utilized in the index dimension.
- Index modulated OFDM spread spectrum (IM-OFDM-SS) [80]: Code domain is exploited in the index dimension.
- Media-based modulation (MBM) [81]: Channel domain is utilized in the index dimension.
- OFDM-SNM: Frequency domain is exploited in the number dimension.

The discussions of the highlighted OFDM-based modulation options will be presented in the following subsections.

2.1.1. Conventional and differential digital modulations for OFDM-based waveform

The subcarriers of the conventional OFDM are occupied by conventional constellation symbols [76]. The related main FD block can be built as

$$\mathrm{x} = \begin{bmatrix} s(1) & s(2) & \dots & s(N) \end{bmatrix}^T, \tag{2.2}$$

where $s(k) \in S$. The conventional OFDM transmitter's block diagram can be found in **Figure 2.2**. As noticed from **Figure 2.2**, the basic OFDM system is efficiently synthesized by FFT which simplifies the system complexity, therefore the OFDM transmission scheme has become increasingly prevalent in the development of contemporary standards and systems for wireless communication.

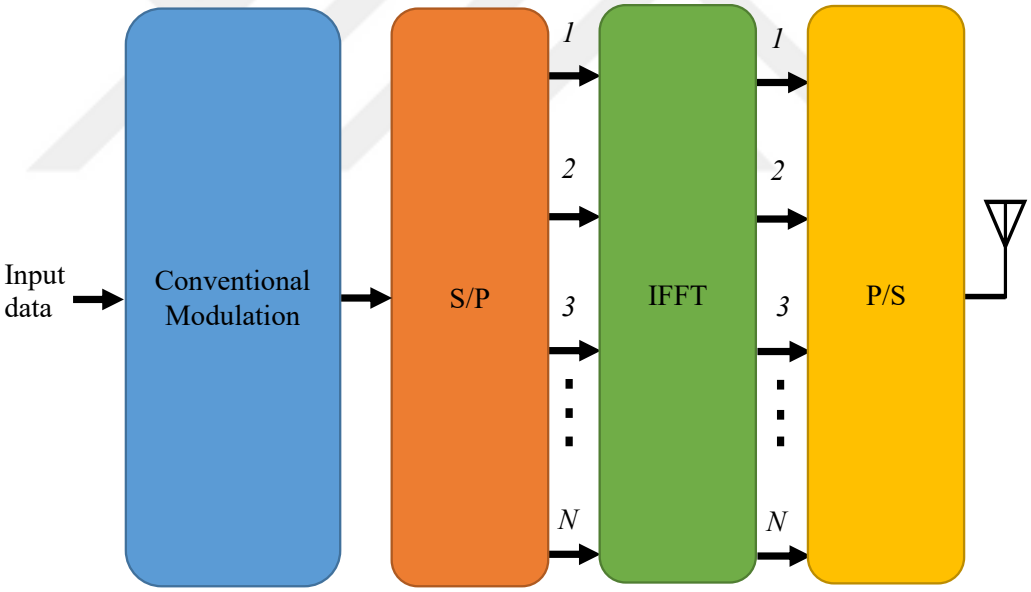

Figure 2.2: The block diagram of the conventional OFDM transmitter.

In the OFDM-differential modulation (OFDM-DM) transmission scheme, the incoming binary data bits are encoded in the difference between the consecutive subcarriers within the same OFDM symbol [82]. This differential encoding is called FD differential modulation. Another way of differential encoding is called time-domain differential modulation, in which the data symbols are conveyed by the difference between the adjacent OFDM symbols over the same OFDM subcarrier [82].

The main difference between the OFDM-DM and its counterpart, i.e., conventional OFDM, in terms of their block diagrams is the type of the modulators and demodulators used. Particularly, differential and conventional modulator/demodulator blocks are used in OFDM-DM and conventional OFDM, respectively. The OFDM-DM scheme enjoys low-complexity detection while avoiding channel estimation and equalization. However, a higher SNR is needed in OFDM-DM to have a similar transmission rate as in the plain OFDM.

2.1.2. Multi-dimensional modulation options for OFDM-based waveform

In the last decade, various transmission mechanisms have been seriously considered by exploiting specific parameters of a given communication system to enhance the data rate at neither increased transmission power nor bandwidth costs. In the literature, novel modulation schemes introduce new constellation diagrams besides the conventional ones with a basic motivation for conveying additional information bits. Several modulation options exploit the third dimension alongside the 2-D signal plan with the major target of sending additional information. The exploited third dimension depends on the application, its requirements, and its capabilities. Examples of these featured modulation schemes are SM-OFDM, OFDM-IM, OFDM-SNM, and OFDM-PSM. The general block diagram of the OFDM-based multidimensional modulation option transmitter is seen in **Figure 2.3**. The function of the FD OFDM block builder is basically forming x based on the used OFDM-based modulation option. Some examples of these options and their x are shown in **Table 2.1**. The detailed descriptions of these multi-dimensional modulation options are presented in the following sections.

2.2. Index-Based Modulation Options

Recently, index-based modulation schemes have witnessed considerable research interest in the literature. In these schemes, extra data is sent by utilizing a third dimension called the index of the medium(s). The generic transmitter for index-based modulation schemes for the OFDM-based waveform is shown in **Figure 2.4**. The medium-based index selection block depends on the medium used for transmitting additional data bits, such as antennas in the SM-OFDM. For further explanation of the transmitter of the index-based

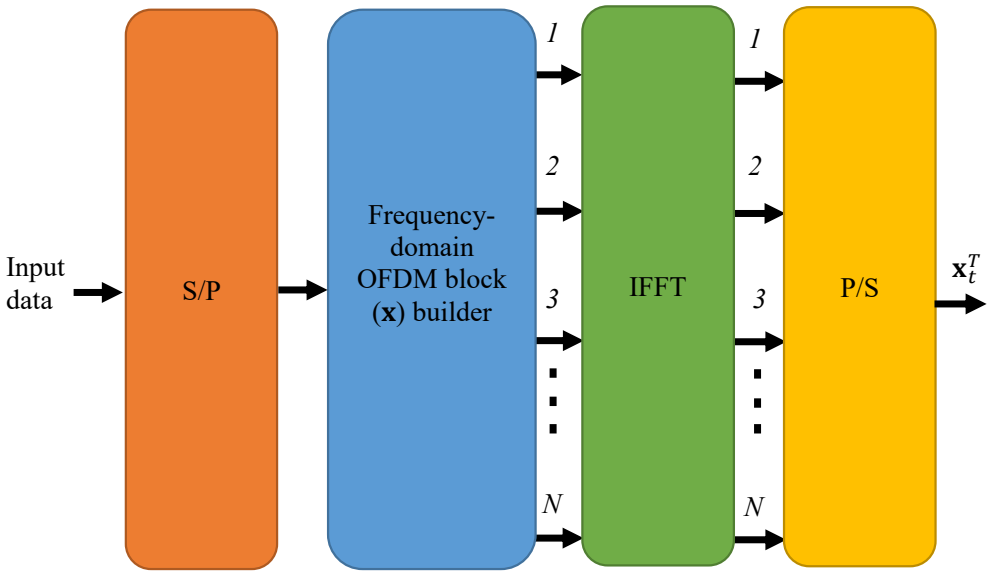

Figure 2.3: The generic transmitter of the OFDM-based multi-dimensional modulation option.

OFDM family, its common members are illustrated as follows.

2.2.1. SM-OFDM scheme

Spatial modulation (SM) is a novel transmission scheme that exploits the indices of building blocks called transmit antennas in the spatial domain to embed extra information bits [83]. In SM, groups of M_c+M_a bits are taken and M_c bits mapped to an information symbol, and M_a bits to the index of specific transmit antenna in such a way that the same data symbol sent by different transmitting antennas conveys extra information, where $M_a \leq \log_2(N_T)$, and N_T is the number of transmitting antennas [84]. In an OFDM system, SM is implemented by assigning a single transmit antenna to each of the OFDM subcarriers, i.e., the corresponding transmit antenna would transmit power on a specific subcarrier only and keep the remaining transmit antennas idle at each transmission instant [16].

The SM-OFDM block structure in FD would be different for different transmit antennas. **Figure 2.5** is a block schematic of the SM-OFDM transmitter [16], [85].

The SM block transfers the binary matrix Q of size $u \times N$ to the matrix W of size $N_T \times N$ for u bits per symbol per subcarrier. The data to be sent in one subcarrier can be represented by the column vectors of Q. Each nonzero element in the W column vector at the location of

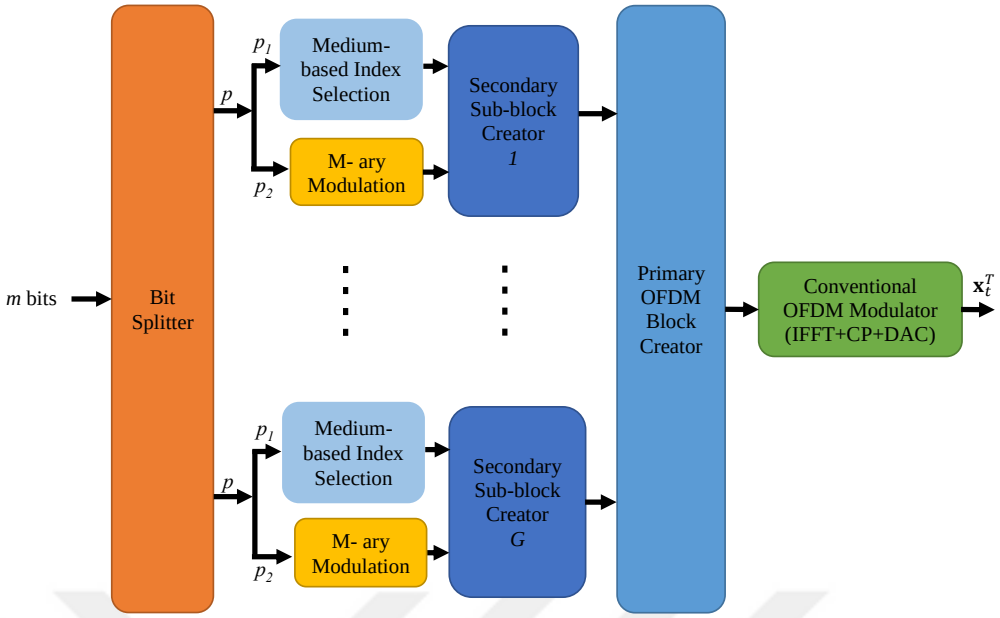

Figure 2.4: The generic transmitter of the index-based modulation options for OFDM-based waveform.

the mapped transmit antenna number represents the symbol conveyed by a subcarrier. The N_T row vectors of W are then modulated using classical OFDM modulators. **Figure 2.6** exhibits the 3-D signal plane of SM-OFDM where only a single antenna is active out of N_T transmit antennas for each subcarrier. A data symbol can be represented as a colored cube along the space axis as shown in **Figure 2.6**.

Example: In **Table 2.2**, a unique SM-OFDM mapper is displayed between Q and W for $u = 2$, $N = 4$, and BPSK. The matrix Q is represented by the possible vector, which is denoted by the vector q. The vector $\mathrm{w} = [w_1\ w_2]$ contain the mapped BPSK symbols (w_1 and w_2) that correspond to the 1st and 2nd transmit antennas, respectively. Moreover, it is not possible to map a single q pattern to two or more transmit antennas.

Table 2.2: Antenna-based index selector with u=2, $N = 4$, and BPSK.

q	w
[0 0]	[-1 0]
[0 1]	[1 0]
[1 0]	[0 -1]
[1 1]	[0 1]

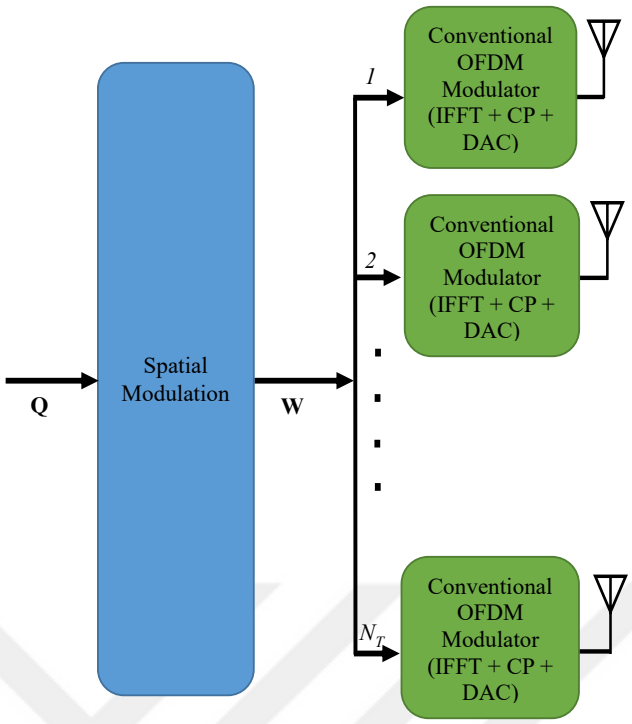

Figure 2.5: The block diagram of the SM-OFDM transmitter.

2.2.2. OFDM-IM scheme

With the inspiration of SM-OFDM, OFDM-IM has been proposed without the need for multiple antennas at the transmitter. Concerning **Figure 2.4**, the medium exploited in the OFDM-IM, as an index-based modulation scheme, is the activated subcarriers.

The OFDM-IM [17], [86] divides the OFDM block into G subblocks with a specific number of available subcarriers. The primary focus of OFDM-IM is on picking A active subcarriers from among all of the other subcarriers that are available and then sending classical constellation symbols over the selected ones. The incoming bit stream (m) are splitted among G subblocks, and p bits enter each OFDM-IM subblock (g) of b available subcarriers and then they are splitted into two parts. The first part comprised of p_1 bits, which controls the selection of active subcarriers' indices of length a in $g = 1, \ldots, G$. Then, the chosen active subcarriers would be sorted in ascending order as

$$\mathrm{i}_g = \{i_{g,1}, i_{g,2}, \ldots, i_{g,a}\}, \tag{2.3}$$

where $i_{g,\gamma} \in [1, \ldots, b]$ for $\gamma = 1, \ldots, a$.

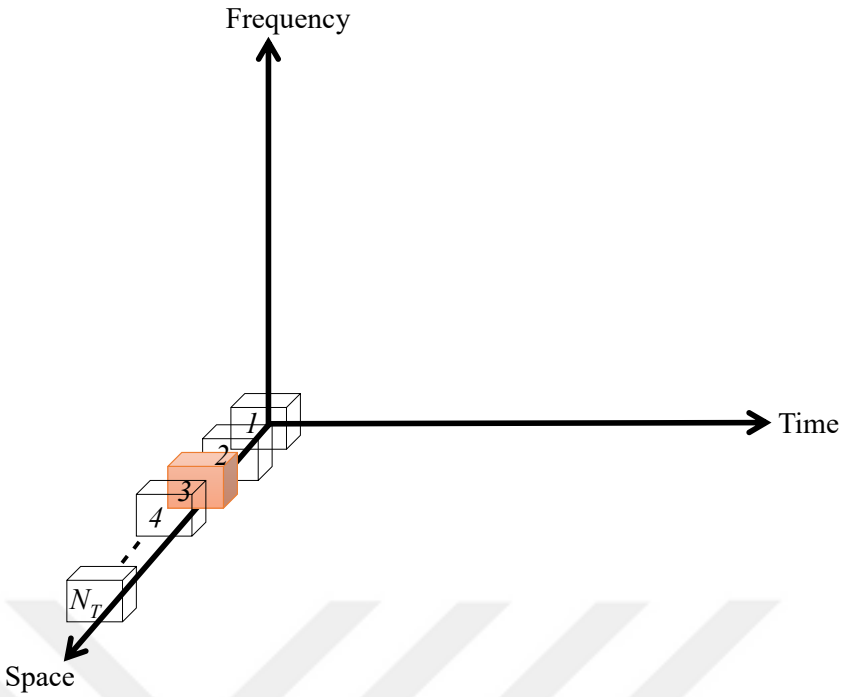

Figure 2.6: The 3-D signal representation of the SM-OFDM transmission scheme.

The second portion of the input bits to the OFDM-IM subblock carries a conventional symbols ($p_2 = a\log_2(M)$ bits). The vector representing the active subcarriers of the g subblock carrying conventional QAM symbols is

$$\mathrm{s}_g = \left[s_g(1) \quad s_g(2) \quad \dots \quad s_g(k)\right]^T, \tag{2.4}$$

where $s_g(\gamma) \in S$, S is the transmitted QAM symbols over $i_{g,\gamma}$. After that, the selected active subcarriers (i_g) and their corresponding data vector (s_g) are concatenated for all G subblocks to build the main FD OFDM-IM block.

Example: Table 2.3 shows an example of a unique mapping between the incoming bits and associated SAP for activation ratio of $a/b = 2/4 = 1/2$. The part of the bit stream that controls the subblock activation is p_1 which equals $p_1 = \log_2(b) = 2$ bits, and the other part of the input bit stream is named as modulation symbol bits: $p_2 = a\ \log_2(M) = 2\ \log_2(M)$. **Table 2.3** shows the possible active indices based on the incoming bit pattern. They could be determined as $\{1, 2\}$, $\{2, 3\}$, $\{3, 4\}$, and $\{1, 4\}$. It is noticed that a fixed activation ratio of 2/4 is assumed in this example.

Table 2.3: Active subcarrier-based index selector with p_1=2 bits and b=4.

Incoming bit stream	SAP
[0 0]	[1 1 0 0]
[0 1]	[0 1 1 0]
[1 0]	[0 0 1 1]
[1 1]	[1 0 0 1]

It should be mentioned that several new enhanced modulation schemes inspired by the conventional OFDM-IM scheme have recently been proposed to enhance its SE. Among these schemes, we mention OFDM with generalized index modulation (OFDM-GIM) [26], OFDM with dual-mode index modulation (OFDM-DMIM) [87], generalized DM-OFDM (GDM-OFDM) [88], OFDM with multi-mode index modulation (OFDM-MMIM) [89].

In OFDM-GIM [26], more degree of freedom in the selection of active subcarriers has been introduced by using different activation ratios for different subblocks within the whole OFDM block to increase throughput. OFDM-DMIM [87] modulates all subcarriers in each subblock by dividing them into two groups and using distinct signal constellation modes for each group to send additional information bits.

The SM-OFDM and OFDM-IM schemes use index modulation in spatial and frequency domains, respectively, although many other domains could be used to communicate additional information alongside classical symbols. The following are four examples of exploiting joint temporal and spatial domains (OFDM-STSK), joint frequency and spatial domains (GSFIM-OFDM), individual code domain (IM-OFDM-SS) and individual channel domain (MBM). More comprehensive classification of index-based modulation schemes could be found in [22].

- **Spatiotemporal domain**: OFDM-aided space time shift keying (OFDM-STSK) [78] is a modulation option in which both temporal as well as spatial domains are jointly utilized. In OFDM-STSK, J space-time codewords are transmitted simultaneously in one OFDM symbol, every OFDM subcarrier carries a column of each space-time codeword. It should be noted that $J = N_c/T$ (N_c is a multiple of T, T is the number of time slots in a STSK symbol).

- **Spectrospatial domain**: GSFIM-OFDM scheme [79] uses both subcarriers (frequency

domain) in addition to the active antennas (spatial domain) to convey additional information bits through their indices, besides conveying bits through conventional M-ary modulation symbols. At any given time, $\mathrm{n_{rf}}$ transmit antennas are active and the remaining n_t-$\mathrm{n_{rf}}$ antennas remain silent. The GSFIM encoder takes $\left\lfloor \log_2 \binom{n_t}{n_{rf}} \right\rfloor$ bits and maps to n_{rf} out of n_t transmit antennas. Therefore, the GSFIM-OFDM scheme is considered as index-based OFDM modulation scheme where the indices of both the active subcarrier and antenna are exploited to transmit additional information bits.

- **Code domain**: Index modulated orthogonal frequency division multiplexing spread spectrum (IM-OFDM-SS) [80] uses spreading codes' indices and M-ary modulated symbols to transmit more information. In this scheme, a selected spreading code is used to spread a data symbol across several OFDM subcarriers to convey additional bits. Extra diversity gain is harvested by using index bits to pick the spreading code from a fixed set. Thus, the IM-OFDM-SS is an index-based OFDM modulation family that uses spreading code indices to convey additional information.

- **Channel domain**: By manipulating the far-field emission pattern of reconfigurable antennas, a technique known as media based modulation (MBM) can be used to take advantage of the channel states domain [81]. The MBM scheme belongs to index-based modulation scheme, by means of selecting the index of the corresponding radiation pattern according to the information bits. It should be noted that MBM integration with OFDM could be regarded as a potential candidate transmission scheme for future wireless systems.

2.3. Number-Based Modulation Options

In the number-based modulation options for an OFDM-based waveform, additional data could be transmitted by utilizing a novel third dimension called the number of transmitting entity (or entities). The generic transmitter for the number-based modulation options for an OFDM-based waveform is shown in **Figure 2.7**. The medium-based number selection block depends on the employed medium in transmitting extra information like active subcarriers as in OFDM-SNM proposed in [19]. OFDM-SNM employs index-independent SAP instead of the index-dependent pattern as in OFDM-IM. OFDM-SNM takes its active subcarrier count from a predetermined input data sequence. The activated subcarriers in

OFDM-SNM are not necessarily adjacent to each other. The new OFDM-SNM technique uses the number of active subcarriers. Thus, OFDM-SNM communicates via constellation symbols and active subcarriers.

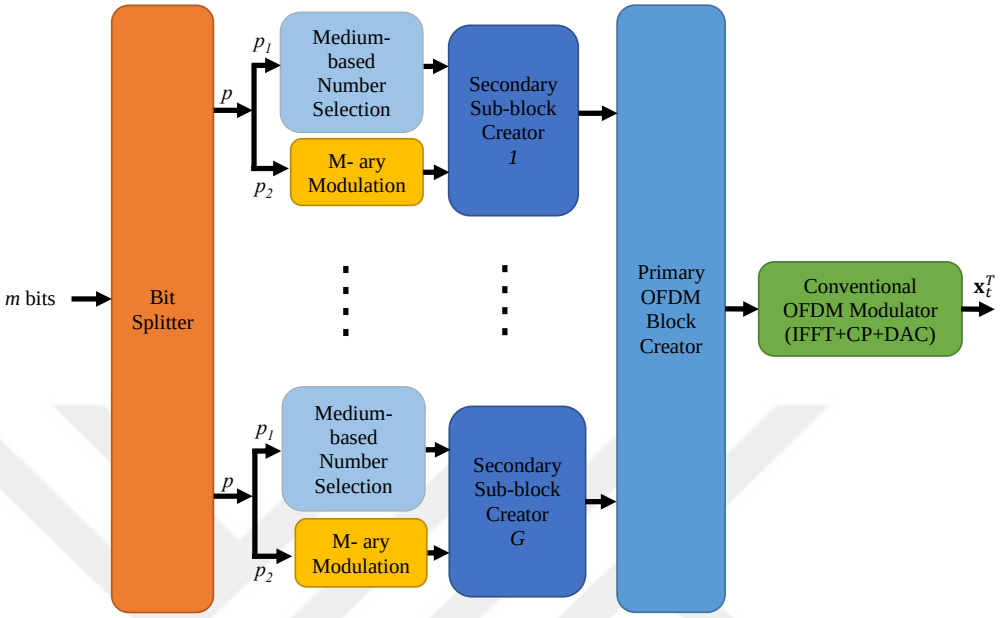

Figure 2.7: The generic transmitter of the number-based modulation options for OFDM-based waveform.

A unique information mapping is observed in the OFDM-SNM scheme. This number-based modulation strategy is based on the variable number of active subcarrier (a) in each subblock of length b in the OFDM-SNM system, unlike OFDM-IM, which is fixed. Based on its $p_1 = \log_2(b)$ bits, each OFDM-SNM subblock has an index-independent number of active subcarriers a out of b. Each subblock's active subcarriers are then mapped onto an M-ary signal constellation that is sent over those subcarriers, hence the amount of $p_2 = a \log_2(M)$ bits varies.

Figure 2.8 presents an example of a 3-D signal representation of OFDM-SNM where the number of adjacent active subcarriers varies in each OFDM-SNM subblock based on the input data bits. In **Figure 2.8**, four possibilities of SAP assignment correspond to OFDM-SNM subblock with a length of 4 subcarriers. The complex QAM symbols would be loaded on the subblock width, i.e. number of active subcarriers, as shown in the colored cubes along the frequency axis.

Example: In **Table 2.4**, we see an actual SAP that maps to a specific combination of bits at the transmitter's input for $b = 4$ and $a \in [1, 2, 3, 4]$. The part of the bit stream that

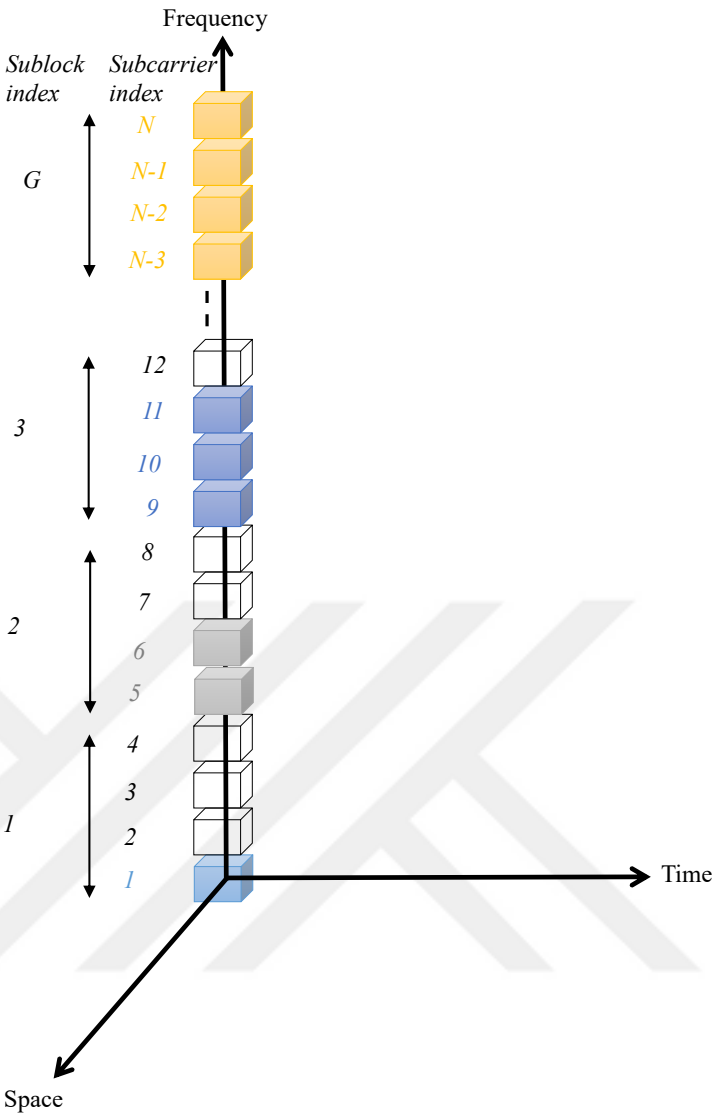

Figure 2.8: 3-D signal plane of the OFDM-SNM scheme.

controls the subblock activation is p_1 which equals $p_1 = \log_2(b) = 2$ bits, and the other part of the incoming stream to the subblock is called modulation symbol bits which is represented by $p_2 = a\ \log_2(M)$. As seen from **Table 2.4**, based on the input information bits to the corresponding subblock, the SAP is firstly loaded with single active subcarrier and then the SAP is loaded with ones until the subblock is filled. The possible sets of active subcarriers in this example are: {1}, {1, 2}, {1, 2, 3}, and {1, 2, 3, 4}.

The authors in [90] proposed an improved OFDM-SNM system that takes advantage of the flexibility provided by the original OFDM-SNM scheme by positioning subcarriers to maximize coding gain in the high SNR region using an adaptive modulation technique. More particularly, instantaneous channel state information (CSI) adaptability is used by

Table 2.4: Active subcarrier-based number selector with p_1=2 bits and b=4.

Incoming bit stream	SAP
[0 0]	[1 0 0 0]
[0 1]	[1 1 0 0]
[1 0]	[1 1 1 0]
[1 1]	[1 1 1 1]

dynamically mapping incoming information bits to subcarriers with substantial channel power gains.

2.4. Mixed-Numerology System

The base numerology adopted in Long Term Evolution (LTE) has $\Delta f_0 = 15$ kHz SCS. A numerology with the subcarrier spacing is defined as [91]

$$\Delta f_k = 2^k \Delta f_0, \tag{2.5}$$

where $k = \{0, 1, 2, 3, ...\}$ is the scaling factor of a given numerology. The IFFT/FFT size of a scalable OFDM numerology can be written as

$$N_k = 2^{-k} N_0, \tag{2.6}$$

where N_0 denotes IFFT/FFT size of the reference numerology. The length of time that a symbol represents in scalable numerology can be stated as

$$T_{OFDM,k} = T_{DATA,k} + T_{CP,k}, \tag{2.7}$$

where data duration $T_{DATA,k} = 1/\Delta f_k$ and CP duration varies for each numerology with $T_{DATA,k}$ as $T_{CP,k} = \alpha T_{DATA,k}$ for $0 < \alpha < 1$. The duration of the OFDM symbol for the reference numerology ($T_{OFDM,0}$) is related to $T_{OFDM,k}$ as

$$T_{OFDM,k} = 2^{-k} T_{OFDM,0}. \tag{2.8}$$

The sampling rate T_s for all used numerologies is considered the same as [91]

$$T_s = \Delta f_k \, N_k = \Delta f_0 \, N_0. \tag{2.9}$$

The time and frequency domain representations of three different numerologies with $4\Delta f_0 = 2\Delta f_1 = \Delta f_2$ are presented in **Figure 2.9**. We assume that users with different numerologies share the system bandwidth equally. Therefore, each subband of different numerologies has the same bandwidth [37].

The vector of modulated symbols for the u-th user, where $u \in \{1, 2, ..., U\}$, in the frequency domain can be expressed by

$$\mathrm{s}_u = [s_u(1) \; s_u(2) \; ... \; s_u(M_k) \; 0 \; ... \; 0]^T_{1\times N_k}, \tag{2.10}$$

where $M_k = 2^{-k} M_0$ is the total number of activated subcarriers for the u-th user (M_0 is the number of activated subcarriers of the reference numerology).

The used numerologies are represented by the set of $\chi = \{\text{Num } 1, \text{Num } 2, ..., \text{Num } U\}$. Here, each user uses distinct numerology with a specific time slot that occupies different subbands of the whole band. After that, the signal in the time domain is found by employing IFFT as

$$\mathrm{x}_u = \frac{1}{\sqrt{N_k}} \mathrm{W}^H_{N_k} \mathrm{s}_u, \tag{2.11}$$

where W_{N_k} represents the inverse discrete Fourier transform (IDFT) matrix with $\mathrm{W}^H_{N_k} \mathrm{W}_{N_k} = N_k \, \mathrm{I}_{N_k}$. Here, I_{N_k} is an $N_k \times N_k$ identity matrix.

Adding the $N_{CP,k}$-length CP to x_u prevents inter-symbol interference. Concatenating multiple CP-added symbols yields the u-th user's CP-OFDM signal ($\mathrm{x}_{CP,u}$). Then, the u-th user sends the $\mathrm{x}_{CP,u}$ signal over a wireless channel with a channel impulse response represented by h_u. This channel-impaired received signal is contaminated with AWGN represented by the vector w. Finally, the noise-contaminated OFDM signal received from U users can be represented as

$$\mathrm{y} = \sum_{u=1}^{U} \mathrm{x}_{CP,u} * \mathrm{h}_u + \mathrm{w}, \tag{2.12}$$

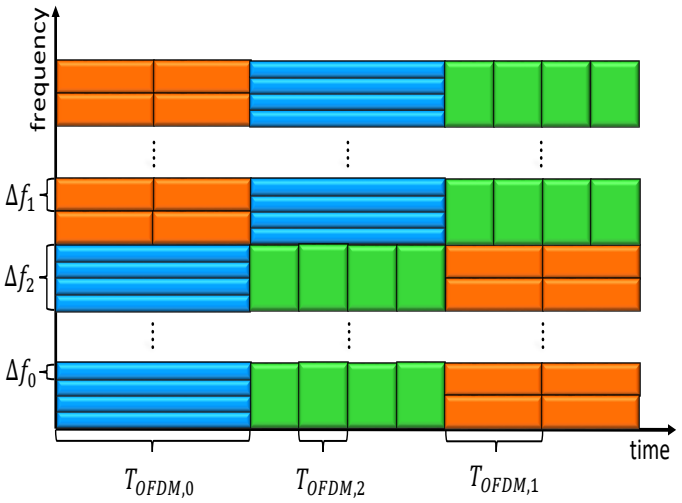

Figure 2.9: Frame structure of mixed-numerology system.

where the received vector y has a length of $N + N_{CP}$ ($N = \max_k \{N_k\}$ and $N_{CP} = \alpha N$).

2.5. Wireless Channel

In a multipath radio environment, different taps of the channel impulse response (CIR) will experience different amounts of pathloss as well as time fluctuations. The CIR could be formulated as [92]

$$h(\tau, t) = \sum_{l=0}^{L-1} \beta_l \, \mu_l(t) \, \delta\left(\tau - \tau_l\right), \tag{2.13}$$

where L represents the total number of channel taps, β_l and τ_l represent pathloss and delay of l-th channel tap, respectively. $\mu_l(t)$ represents the time variation of the l-th channel tap, and $\delta(.)$ is the delta function.

Generally, double-directional CIR is adopted as a fundamental deterministic description of the channel in modern communication systems. This CIR is formulated as [93]

$$h(\tau, t, \psi, \theta) = \sum_{l=0}^{L-1} \beta_l \mu_l(t) \delta\left(\tau - \tau_l\right) \delta\left(\theta - \theta_l\right) \delta\left(\psi - \psi_l\right), \tag{2.14}$$

where θ and ψ represent the angle of departure and angle of arrival, respectively.

The received signal faded by a multipath channel, assuming a noise-free system for simplification, is represented as

$$y(t) = x(t) * h(\tau, t, \psi, \theta), \tag{2.15}$$

where $*$ stands for the convolution operator and $x(t)$ is the transmitted signal.

2.6. Scheduling And Radio Resource Allocation

The general purpose of most traditional schedulers is to exploit channel variations between UEs and, preferably, to schedule transmissions to a UE when channel conditions are favorable. At the very least, most scheduling strategies require information about UE's channel conditions, buffer status and priorities of the different data flows, and the interference situation in neighboring cells.

Medium access control, also known as MAC, is utilized for the reporting of scheduling information. The scheduling strategy is implementation-specific and does not conform to the 3rd Generation Partnership Project (3GPP) specifications.

Different UEs may experience diverse radio conditions at a certain time in the mobile network environment. In many scenarios, system capacity can be increased by the low fairness schemes of conventional scheduling algorithms. These algorithms increase the prioritization of UEs with good channel conditions. On the other hand, UEs with average or bad radio conditions cannot be scheduled. The conventional schedulers enable higher data rates due to a tradeoff between UEs fairness and system capacity. The Mobile Network Operators (MNOs) demand consistent UE and system data rates with the minimum QoS requirements. Besides the UE requirements, network radio resource capacity is an essential issue for the existing mobile network operations, which cover the whole network life cycle management, such as capacity monitoring, optimization, and expansion. More specifically, the MNOs seek more efficient schedulers while considering commercial scheduling methods such as Proportional Fair (PF), Round Robin (RR), and Best Channel Quality Indicator (BCQI) [94]. MNOs need more and more radio resources due to the growing traffic in their current commercial mobile networks. The lack of radio resources affects the user experience of MNOs. The increasing traffic demand requires efficient schedulers in network radio resource usage.

During resource scheduling, base station (BS) distributes fewer RBs to UE transmitting

faster. Higher-SINR UEs can use high-order modulation and coding [72], [95], [96]. SINR is UE vendor-specific, and it is used a lot by MNOs [96]. SINR information is readily available on many commercial radio chipsets [97]. The SINR value for each RB is measured by all UEs and transmitted to the BS. This information is used by BS to make critical scheduling decisions.

2.7. Related Works

Here, the related research of the scope of the work in this thesis are discussed.

2.7.1. Shape-based modulation options

The shape of the transmitting entity (or entities) could be exploited to add another degree of freedom to enhance SE of a given system. One example of these shape-based OFDM modulation schemes is the OFDM with pulse superposition modulation (OFDM-PSM), where data symbols can be carried onto time-frequency shifted versions of a transmit pulse. Several types of pulse can be found in the literature, particularly some of them are commonly used [98]. Different data symbols are carried by different orthogonal, fully overlapping pulses in OFDM-PSM [20]. These pulses are superimposed together within the same time-frequency region to improve the SE while keeping a comparable reliability performance to that of the conventional OFDM. As seen in **Figure 2.10**, four superimposed HG pulses cover approximately twice the time-frequency region as compared to two adjacent Gaussian pulses.

Hence, OFDM-PSM with HG pulses achieves improved SE over the schemes that utilize only single Gaussian transmit pulses. On the other hand, OFDM-PSM has fewer side lobes due to using localized HG pulses instead of the non-localized Sinc pulses as used in classical OFDM. Another integration of the pulse superposition approach is its integration with generalized frequency division multiplexing (GFDM) [99]. This integration results in almost 2.4 much higher than the integration of Gaussian pulses with GFDM [100].

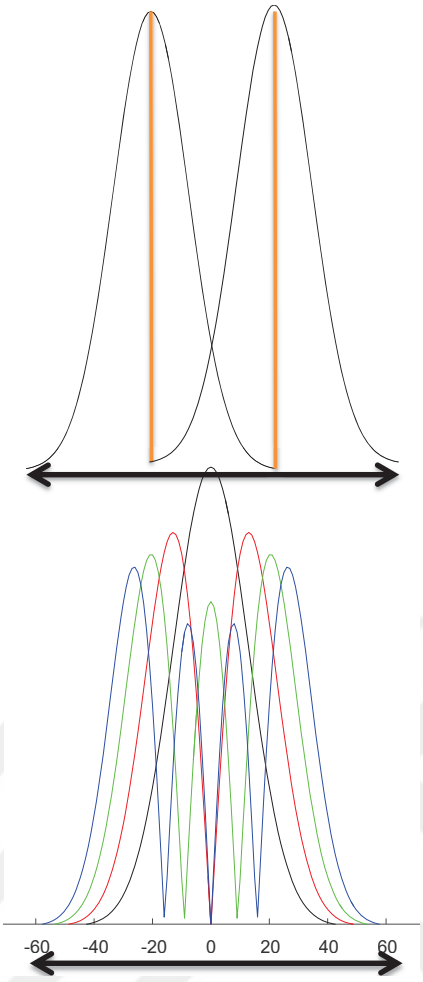

Figure 2.10: Conventional Gaussian transmission (upper part of the figure) vs. pulse superposition modulation using HG pulses (lower part of the figure).

2.7.2. Radio resource management options for radar and communication coexistence

Several physical layer (PHY)-based resource management options for radar and communication coexistence have recently been proposed, including power allocation, spatial beamforming, spectrum sharing with waveform design, and time sharing. **Figure 2.11** illustrates the existing work in PHY and the proposed MAC-based work. The following deficiencies exist in the literature: essential principles and important performance measures linked to resource management are not adequately given [65]. The related radio resource management (RRM) studies for radar and communication coexistence systems are classified according to the resource management issues, i.e., spectrum sharing, power allocation, and interference management. Literature works have not been done on the radar-aided communication system in the MAC layer to the best of our knowledge [65].

However, there has not been extensive discussion or research on the challenges of allocating and scheduling radio resources.

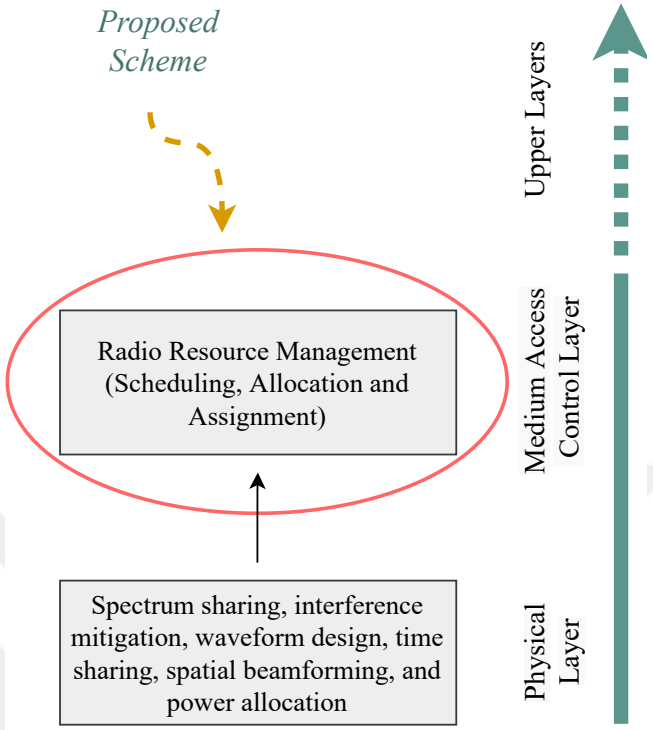

Figure 2.11: Existing PHY-based work in the literature and the proposed MAC-based work.

2.7.3. The conventional scheduling algorithms

Round robin (RR), proportional fair (PF), and best channel quality indicator (BCQI) schedulers are the common scheduling algorithms that power the current RRS solutions [101]. Because it offers a compromise between throughput and fairness, the PF scheduler is used by almost all modern cellular networks. Furthermore, the RR and BCQI schedulers cannot achieve high fairness and throughput at the same time. The dynamic switching between RR and BCQI has been proposed in [102] to find a way for the system to provide as much throughput and fairness as possible at the same time. This dynamic switching mechanism is done based on the operating SNR. In order to maintain the backward compatibility with the current RRS schemes, the proposed approach employs the conventional scheduling algorithms as well as a dynamic switching mechanism between RR and BCQI schedulers.

CHAPTER 3

3. EXPERIMENTAL PART

In this chapter, the proposed OFDM-SNM scheme is discussed in **Section 3.1**. **Section 3.2** and **Section 3.3** presents the proposed OFDM-HNIM and OFDM-SGM schemes, respectively. The proposed floating OFDM-SNM scheme is explained in **Section 3.4**. Performance analysis of the featured modulation options in practical conditions including a comprehensive comparison in terms of SE, reliability, power efficiency (PE), OOBE, and computational complexity is presented in **Section 3.5**.

3.1. The Proposed OFDM-SNM Scheme

The system model of the proposed OFDM-SNM is illustrated in **Subsection 3.1.1**. Performance analysis of the proposed scheme is presented in **Subsection 3.1.2**.

3.1.1. System model

Figure 3.1 depicts the transmitter layout for the proposed OFDM-SNM system. The OFDM-SNM system utilizes a variable amount of information bits, denoted by m_i, to transmit each i_{th} OFDM block. These bits are divided into G groups, each of which has variable $p = p_1 + p_2$ bits. These bits are used to make OFDM subblocks of length $N = N_F/G$, where N_F is the FFT size. Unlike OFDM-IM, where **constant** K out of N number of available subcarriers are used to send information, in our scheme, for each subblock g ($g = 1, 2, \ldots, G$), index-independent variable $K \in [1, 2, \cdots, N]$ out of N subcarriers are activated by a subcarrier number selector according to the corresponding $p_1 = \log_2(N)$ bits, while the remaining $N - K$ subcarriers are inactive. Note that K is not fixed, but rather changing and taking variable values of the number of subcarriers

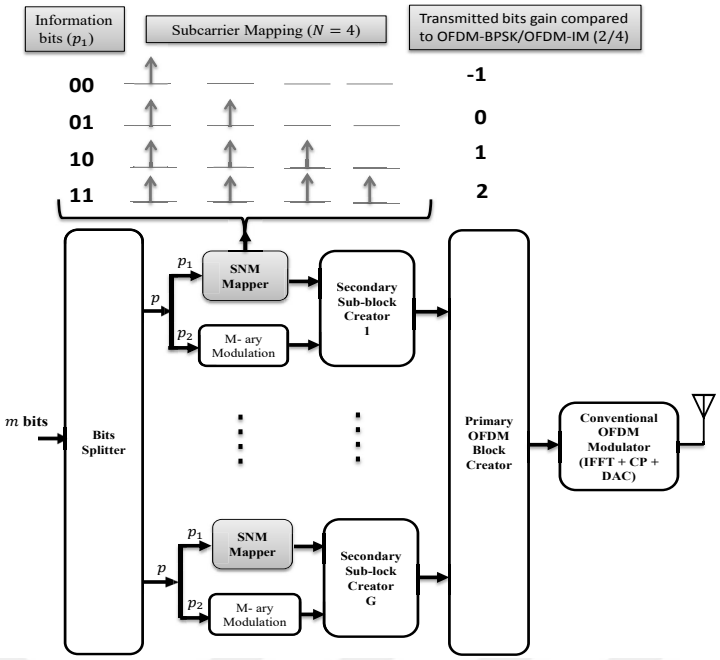

Figure 3.1: OFDM-SNM transmitter structure.

Table 3.1: SNM mapper with p_1=2 bits and N=4.

Information bits	Active subcarriers
[0 0]	[1 0 0 0]
[0 1]	[1 1 0 0]
[1 0]	[1 1 1 0]
[1 1]	[1 1 1 1]

from the bits of incoming data p_1 as shown in **Table 3.1**, which presents the case when $N = 4$, $K \in [1, 2, 3, 4]$ and $p_1 = \log_2(4) = 2$. For each subblock g, the subcarrier on-off activation pattern set can be given as

$$\mathrm{i}_g = \begin{bmatrix} i_1 & i_2 & \cdots & i_K \end{bmatrix}^T, \; g = 1, 2, \ldots, G \tag{3.1}$$

where $i_k \in 1, 0$ for $k = 1, 2, \cdots, K$. **Table 3.1** displays a lookup table that can be used to execute the subcarrier on-off activation pattern technique for smaller N and K values. For each subblock, the remaining $p_2 = K(\log_2(M))$ bits are mapped onto the M-ary signal constellation in order to determine the data symbols that are sent over the activated subcarriers.

After the concatenation of G subblocks, the whole OFDM block is $\mathrm{x_F}$. Now, the remaining steps are performed as done in standard OFDM modulation. After taking IFFT, the signal

can be represented as $\mathrm{x_t} = IFFT(\mathrm{x_F})$. By appending CP of length N_{CP} to the transmitted signal, the resulting signal becomes $\mathrm{x_{CP}} = \left[\mathrm{x_t}(N_F - N_{CP} + 1 : N_F) \quad \mathrm{x_t}\right]$. Now, since we assume AWGN multi-path channel with channel impulse response ($\mathrm{h_t}$), the received time-domain signal is represented as

$$\mathrm{y_t} = \mathrm{x_t} \circledast \mathrm{h_t} + \mathrm{n_t}, \tag{3.2}$$

where $\mathrm{n_t} \sim \mathcal{CN}(0, N_{o,T})$ is the AWGN vector. The operation of the receiver would be the reversal of the transmitter operations, i.e, removing CP, performing FFT and SNM demapping and detection as follows. The received signal after removing the CP is $\mathrm{y_t} = \left[y_0 \quad y_1 \quad \ldots \quad y_{N_F-1}\right]$. After FFT block, $\mathrm{y_F} = FFT(\mathrm{y_t}) = \left[y_F(0) \quad y_F(1) \quad \ldots \quad y_F(N_F - 1)\right]$. A simple one-tap frequency domain equalizer is used to compensate for channel frequency selectivity as $\mathrm{y_{eq}} = \mathrm{y_F}/\mathrm{h_F}$. Then, a threshold-selected energy-based detector extracts the active subcarrier pattern [103]. A threshold-based detector makes the OFDM-SNM receiver low-complex. This detector is much simpler than ML or LLR based detectors [89]. After that, SNM demapper, the transmitter's inversion mapping mechanism, maps active subcarriers to their bits. For constellation symbol detection, the receiver uses each subblock's active subcarriers. SNM demapper and symbol detection bits are combined to generate the estimated subblock bits. The entire OFDM block's data stream is retrieved by repeating the technique for each subblock.

3.1.2. Performance analysis of OFDM-SNM

SE, pairwise error probability, and power efficiency are calculated to evaluate the OFDM-SNM.

3.1.2.1. Spectral Efficiency (SE)

The SE (bits/s/Hz) of the proposed OFDM-SNM scheme can precisely be formulated as

$$\eta_{OFDM-SNM} = \frac{\sum_{g=1}^{G} \left(\log_2(N) + K(g)\log_2(M)\right)}{N_F + N_{CP}}, \tag{3.3}$$

where $K(g)$ is the number of active subcarrier in each subblock of N subcarriers' length. It can be observed that the difference between OFDM-SNM and OFDM-IM is in $K(g)$ parameter. In OFDM-SNM, $K(g)$ varies for each subblock, which is different from OFDM-IM where $K(g)$ is fixed for all subblocks. Thus, the proposed OFDM-SNM improves SE over OFDM-IM as well as conventional OFDM. The amount of improvement over OFDM-IM depends on $K(g)$ values. For instance, if $N = 4$ is selected for both OFDM-SNM and OFDM-IM (with $K = 2$), then the SE gain of OFDM-SNM scheme over OFDM-IM, when BPSK is considered, equals to $\rho = 18/16 = 1.125$.

3.1.2.2. Analytical Bit Error Probability

The activated subcarriers in each sub-block are determined based on the incoming information bits using a mapping process that can basically be represented by code. The reason for this is that there is no information about the exact modulation used in signal constellation, and the known information is that the mapping of the bit information into the number of active subcarriers. Assume there are T time slots which represent the number of bit group, then the transmitted codeword in T time slots $\mathrm{X} = \mathrm{X_{ij}}$, where $i = 1, 2, \cdots, T$ and $j = 1, 2, \cdots, N$. At the receiver, the decoder may decode another codeword $\hat{\mathrm{X}} = \hat{\mathrm{X}}_{\mathrm{ij}}$. Our system model has just those two codewords (X and $\hat{\mathrm{X}}$), so here the analytical BER considers only pairwise error probability ($P(\mathrm{X} \longrightarrow \hat{\mathrm{X}})$). It should be noted that the receiver might cause errors on the two consecutive detection processes, i.e., the number of active subcarriers as well as the M-ary symbols. In the considered model, we assume that the frequency selective channel is fixed within one block and follows Rayleigh distribution. The input-output relationship in the frequency domain can be written in the following form

$$\mathrm{y} = \mathrm{Xh} + \mathrm{n_z}. \tag{3.4}$$

The transmitted sequence X could be detected correctly or erroneously as $\hat{\mathrm{X}}$. An optimal detector for the proposed system can be represented mathematically as

$$P(\mathrm{X} = \mathrm{X}|\mathrm{y}) \geq P(\mathrm{X} = \hat{\mathrm{X}}|\mathrm{y}). \tag{3.5}$$

We assume that $\mathrm{n_z} \sim \mathcal{CN}(0, N_{o,F})$, then the detector is simply ML detector defined as

$$|\mathrm{y} - \mathrm{X}| < |\mathrm{y} - \hat{\mathrm{X}}|. \tag{3.6}$$

The distance from y to X is less than that to $\hat{\mathrm{X}}$, so we can say that X is the nearest neighbor to y. Since we have only two probabilities then the threshold value is assumed to be at the middle point between X and $\hat{\mathrm{X}}$ as $\frac{\mathrm{X}+\hat{\mathrm{X}}}{2}$. So, the probability of choosing X can be computed as

$$\begin{aligned} P(\mathrm{y} < \frac{\mathrm{X}+\hat{\mathrm{X}}}{2} | \mathrm{X} = \mathrm{X}) &= P(\mathrm{z} > \frac{||\mathrm{X} - \hat{\mathrm{X}}||}{2}) \\ &= Q(\frac{||\mathrm{X} - \hat{\mathrm{X}}||}{2\sqrt{N_o/2}}), \end{aligned} \tag{3.7}$$

where $Q(.)$ is the Q-function [104] and $N_o = N_{o,F}$.

Accordingly, the error probability depends only on the distance between the sequences: X and $\hat{\mathrm{X}}$; with the effect of the channel (h), the Q function becomes [105]

$$\begin{aligned} P(\mathrm{y} < \frac{\mathrm{X}+\hat{\mathrm{X}}}{2} | \mathrm{X} = \mathrm{X}) &= Q(\sqrt{\frac{||(\mathrm{X} - \hat{\mathrm{X}})\mathrm{h}||^2}{2N_o}}) \\ &= Q(\sqrt{\frac{\mathrm{h^H}(\mathrm{X} - \hat{\mathrm{X}})^H(\mathrm{X} - \hat{\mathrm{X}})\mathrm{h}}{2N_o}}). \end{aligned} \tag{3.8}$$

Equation (8) can be rewritten as

$$P(\mathrm{y} < \frac{\mathrm{X}+\hat{\mathrm{X}}}{2} | \mathrm{X} = \mathrm{X}) = Q(\sqrt{\frac{\mathrm{h^H A h}}{2N_o}}) = Q(\sqrt{\frac{\delta}{2N_o}}), \tag{3.9}$$

where $\delta = \mathrm{h^H A h} = \mathrm{h^H}(\mathrm{X} - \hat{\mathrm{X}})^H(\mathrm{X} - \hat{\mathrm{X}})\mathrm{h} = ||(\mathrm{X} - \hat{\mathrm{X}})\mathrm{h}||^2$, and the A matrix equals to $(\mathrm{X} - \hat{\mathrm{X}})^H(\mathrm{X} - \hat{\mathrm{X}})$. The channel frequency response $\mathrm{h_F}$ is assumed to be zero-mean Circularly Symmetric Complex Gaussian (CSCG) random variable with unity variance $\mathrm{h_F} \sim \mathcal{CN}(0, 1)$. $\mathrm{h_F}$ can be completely described by its mean and covariance matrix $\mathrm{K} = E[\mathrm{h_F h_F}^H]$, where K is a Hermiation matrix with a dimension of $N < N_F$. So, a submatrix $\mathrm{K_N}$ with size $N \times N$ is sufficient to represent the channel frequency response in each subblock. If we define a complex orthogonal matrix Q where $\mathrm{Q^H Q} = \mathrm{I}$, h as a subset of $\mathrm{h_F}$ can be represented as orthonormal basis $\mathrm{h} = \mathrm{Qu}$, and D as a diagonal matrix with rank $r_1 < N$, where $\mathrm{D} = E[\mathrm{uu^H}] = E[\mathrm{hh^H}]$, and $\mathrm{K_N}$ can be given as

$$\mathrm{K_N} = E[\mathrm{hh^H}] = \mathrm{QDQ^H}. \tag{3.10}$$

The PDF of the orthonormal basis u follows the PDF of h and can be expressed as

$$f(\mathrm{u}) = \frac{exp(-\mathrm{u^H D^{-1} u})}{\pi^{r1} det(\mathrm{D})}. \tag{3.11}$$

The conditional pairwise error probability (CPEP) is the same as **(3.9)** and the PDF of the fading channel is represented in **(3.11)**. After that, by considering what was anticipated for CPEP in relation to the channel, and using the approximation of Q function found in [104], the unconditional pairwise error probability (UPEP) is obtained as

$$P(\mathrm{X} \longrightarrow \hat{\mathrm{X}}) = \frac{1/12}{det(\mathrm{I_N} + q_1 \mathrm{K_N A})} + \frac{1/4}{det(\mathrm{I_N} + q_2 \mathrm{K_N A})}, \tag{3.12}$$

where $q_1 = 1/(4N_{o,F})$ and $q_2 = 1/(3N_{o,F})$. The overall BER is of great interest rather than individual PEP. The Average Bit Error Probability (ABEP) is found as [17]:

$$P_b(E) \approx \frac{1}{p\ n_x} \sum_{\mathrm{X}} \sum_{\hat{\mathrm{X}}} P(\mathrm{X} \longrightarrow \hat{\mathrm{X}})\ e(\mathrm{X}, \hat{\mathrm{X}}), \tag{3.13}$$

where p is the number of information bits that are transmitted with each subblock, n_x represents the number of realizations of X, and $e(\mathrm{X}, \hat{\mathrm{X}})$ is the number of bits of data were incorrectly selected by opting for $\hat{\mathrm{X}}$ rather than X. The BER of OFDM-SNM is demonstrated analytically to be comparable to that of OFDM-IM [17]. This analytical result will be verified by simulation as well.

3.1.2.3. Power Efficiency

Since not all subcarriers are occupied where only active subcarriers carry modulated data, OFDM-SNM approach achieves better power efficiency compared to conventional OFDM. In conventional OFDM, the transmitted power (P_{tx}) is distributed equally among all subcarriers so that the average power per subcarrier equals to (P_{tx}/N_F). The distribution of observing the number of active subcarriers in each subblock is assumed to follow binomial distribution as

$$P(N_{ac} = K) = \binom{N}{K} p_r^K (1 - p_r)^{N-K}, \tag{3.14}$$

where N_{ac} represents the number of active subcarriers which takes values of $K = 1, 2, \cdots, N$. Also, p_r is the probability of the event $(N_{ac} = K)$. By assuming that the total transmitted power allocated to OFDM-SNM block is P_{tx}, and the power is equally distributed to all subblocks, the power consumed by OFDM-SNM scheme can be written as

$$P_c = \frac{P_{tx}}{G\ N} \sum_{g=1}^{G} K(g)\ P(N_{ac} = K(g)), \tag{3.15}$$

where $K(g)$ and $P(N_{ac} = K(g))$ represent the number of active subcarriers and their corresponding probability in the subblock g, respectively. Thus, the average power allocated per subcarrier equals to P_c/N_F.

3.2. The Proposed OFDM-HNIM Scheme

The system model of the proposed OFDM-HNIM scheme is explained in **Subsection 3.2.1**. We provide a performance evaluation of the proposed scheme in terms of SE, ABEP, EE, and computational complexity in **Subsection 3.2.2**.

3.2.1. System model

The block diagram of the proposed OFDM-HNIM transmitter is displayed in **Figure 3.2**. The m incoming bits are partitioned into G subblocks using bits splitter, each subblock of length L subcarriers contains $p = p_1 + p_2 + p_3$ bits. The non-conventional bits, p_1 and p_2, represent the bits conveyed by the SNM and IM modulators, respectively. In each subblock, the SNM and IM mappers can be ordered arbitrary since the hybrid mapper combines both mappings without considering their order. For an easy way to represent the basic OFDM-HNIM system model, we use the p_1 bits to represent the SNM bits, which are used by the SNM mapper to specify the number of active subcarriers in the subblock. The p_2 bits, which are called the IM bits, are used by the IM mapper to specify the subcarrier indices for each subblock. The SAP is then calculated by an appropriate

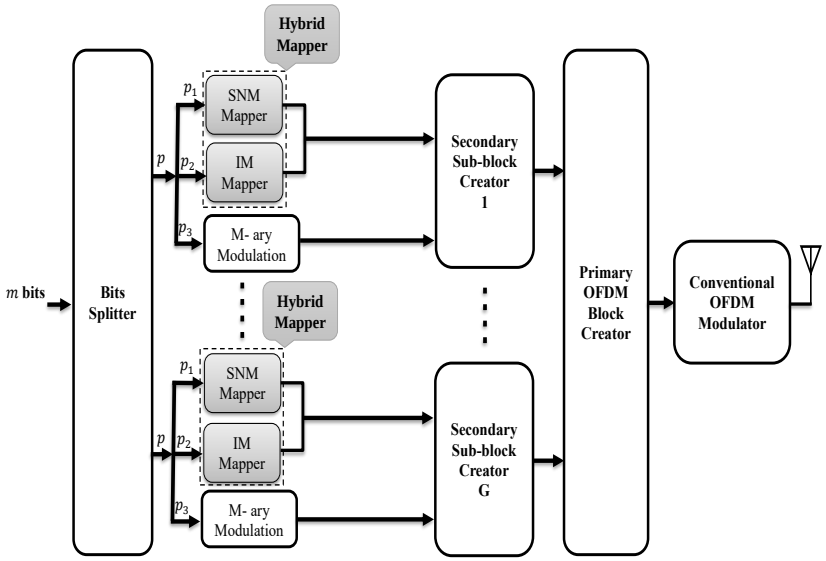

Figure 3.2: The proposed OFDM-HNIM transmitter structure.

mapping strategy employing the hybrid mapper's combined SNM and IM mapping.

The full set of N_F subcarriers that constitutes the OFDM block can be represented by $\mathbb{B} = \{1, 2, \ldots, N_F\}$. Based on the hybrid mapper, specific active subcarriers in each subblock are selected from $\mathbb{B}$, which can be represented by the subset $\mathbb{B}_g \subset \mathbb{B}$, where $g = 1, 2, \ldots, G$ is the index of the subblock. The number of active subcarriers in the g-th subblock ($I(g)$) is an **index and number-dependent variable** that represents the cardinality of $\mathbb{B}_g$ (i.e. $I(g) = |\mathbb{B}_g|$).

The conventional $p_3 = I(g)\log_2(M)$ bits of the g-th subblock correspond to M-ary conventional constellation symbols carried over $I(g)$ active subcarriers. **Table 3.5** presents a bits-to-SAP mapping for small values of $L = 4$ with fixed length of $p_1 = p_2 = \log_2(L) = 2$ bits to simplify the system-level design. The SAP for the g-th subblock can be written as follows:

$$\mathrm{c_g} = \begin{bmatrix} c(1) & c(2) & \cdots & c(L) \end{bmatrix}^T, \tag{3.16}$$

where $c(i) \in \{0, 1\}$ for $i = 1, 2, \cdots, L$.

As shown in **Table 3.5**, a subcarrier in a given index of $\mathrm{c_g}$ is activated with an equal probability of 1/2. The presented codebook ($\mathrm{c_g}$) in **Table 3.5** looks like a classical codebook generated in binary order; however, they are different in the sense that the direct binary mapping does not provide flexibility, whereas, the proposed scheme is an adaptive and

Table 3.2: Look-up table of the proposed OFDM-HNIM scheme with $p_1 = p_2 = 2$ bits.

g	p_1	p_2	c_g	$I(g)$
1	[0 0]	[0 0]	$[1\,0\,0\,0]^T$	1
2	[0 0]	[0 1]	$[0\,1\,0\,0]^T$	1
3	[0 0]	[1 0]	$[0\,0\,1\,0]^T$	1
4	[0 0]	[1 1]	$[0\,0\,0\,1]^T$	1
5	[0 1]	[0 0]	$[1\,1\,0\,0]^T$	2
6	[0 1]	[0 1]	$[1\,0\,1\,0]^T$	2
7	[0 1]	[1 0]	$[1\,0\,0\,1]^T$	2
8	[0 1]	[1 1]	$[0\,1\,0\,1]^T$	2
9	[1 0]	[0 0]	$[1\,1\,1\,0]^T$	3
10	[1 0]	[0 1]	$[1\,0\,1\,1]^T$	3
11	[1 0]	[1 0]	$[1\,1\,0\,1]^T$	3
12	[1 0]	[1 1]	$[0\,1\,1\,1]^T$	3
13	[1 1]	[0 0]	$[0\,0\,0\,0]^T$	0
14	[1 1]	[0 1]	$[0\,0\,1\,1]^T$	2
15	[1 1]	[1 0]	$[0\,1\,1\,0]^T$	2
16	[1 1]	[1 1]	$[1\,1\,1\,1]^T$	4

flexible transmission technique, whose mapping blocks can be employed based on the requirements of the used application. For example, SNM and IM mapping blocks are proper mappers for throughput-aware, especially at low-order modulation, and EE-aware applications, respectively [10]. Therefore, the proposed hybrid mapper is appropriate for both throughput-aware and EE-aware applications.

It should be noted that there would be similar SAP when $g = 13, 14, 15, 16$ as expected from their SNM mapping, due to setting a fixed length of p_2 data code. To solve this ambiguity in mapping, extra bits could be transmitted to a receiver to differentiate between these exceptional cases. However, this solution is not spectrally efficient due to sending additional non-data bits. Moreover, the expected SNM mapping leads to a nonuniform subcarrier activation, which results in unfair protection of transmitted bits, thus hindering the OFDM-SNM and OFDM-IM relevant schemes from attaining their ultimate error performance.

The problem of unbalanced activation of subcarriers in the OFDM-SNM and OFDM-IM schemes is avoided in the proposed mapping process, which is represented in **Table 3.5**, by having an equiprobable probability of subcarrier activation without relying on the channel status [106]. To avoid ambiguity and extra bits signaling at the ML detector as well as

satisfying the equiprobable subcarrier activation (ESA) requirement [106], the aforementioned exceptional cases are assigned unique SAPs where their corresponding $I(g)$ values are mostly different from their expected SNM mapping.

However, the zero-active subcarrier dilemma, where all subcarriers are switched off and their corresponding data symbols cannot be transmitted, can be seen in **Table 3.5** at $g = 13$, which corresponds to $\mathrm{c_g} = [0\,0\,0\,0]^T$. This dilemma could lead to difficulty in higher layer design, especially the synchronization process, which is the key for OFDM-based systems to reduce ICI and/or inter symbol interference (ISI) [107], [108]. One efficient solution to such a dilemma could be done by exploiting the lexicographic ordering principle and implementing the codebook optimization method as in [109], where the codebooks are optimized in such a way that the subcarriers are activated based on their corresponding instantaneous CSI. The novel codebook design in [109] does not involve optimizing the power usage, unlike the forward error correction method that introduces more computational complexity at the receiver [110].

As shown in **Table 3.5**, the equally probable bit sequence enables easier detection and flexible designs of higher layer protocols unlike the dual-mode transmission protocol [108], where the bit sequence of variable length is modulated.

Control signaling is not required in [109] unlike the method in [111] where the always-active control subcarrier used for control signaling transmission. Therefore, the lexicographic-based codebook design in [109] provides an efficient solution to the observed dilemma as compared to the existing solutions [108], [110], [111]. In this work, we focus on the basic idea and system model of the proposed OFDM-HNIM, whereas employing the novel design in [109] to the proposed scheme could be considered as a future work for improving the OFDM-HNIM system.

By considering the SAP ($\mathrm{c_g}$) for the g-th subblock, the OFDM subblock can be formed as

$$\mathrm{x_F^g} = \left[x_F^g(1) \quad x_F^g(2) \; \cdots \; x_F^g(L)\right]^T, \tag{3.17}$$

where $x_F^g(i) \in \{0, \mathcal{S}\}$ for $i = 1, 2, \cdots, L$.

The OFDM block of N_F subcarriers is built based on the chain of G subblocks and given as

$$\mathrm{x_F} = \begin{bmatrix} x_F(1) & x_F(2) & \cdots & x_F(N_F) \end{bmatrix}^T, \tag{3.18}$$

where $x_F(k) \in \{0, \mathcal{S}\}$ for $k = 1, 2, \cdots, N_F$.

The remaining steps are done as in the classical OFDM system. By performing N_F-inverse fast Fourier transform (IFFT) to $\mathrm{x_F}$, the output vector is $\mathrm{x_t}$ with dimension $N_F \times 1$. To combat ISI effects, cyclic prefix (CP), of length N_{CP} longer than the channel impulse response (CIR) length v, is appended to the beginning of $\mathrm{x_t}$, the resultant is the transmitted signal represented by

$$\mathrm{x_{CP}} = \begin{bmatrix} \mathrm{x_t}(N_F - N_{CP} + 1 : N_F) & \mathrm{x_t} \end{bmatrix}^T, \tag{3.19}$$

It is assumed that $\mathrm{x_{CP}}$ passes to a slowly time-varying multipath Rayleigh fading channel modeled by a CIR $\mathrm{h_t} = [h_t(1)\, h_t(2) \cdots h_t(v)]^T$, whose elements (i.e. $h_t(\sigma)$, $1 \leq \sigma \leq v$) are a circularly symmetric complex Gaussian random variable with the distribution $\mathcal{CN}(0, \frac{1}{v})$ [107]. Then, this channel-impaired received signal is contaminated with additive white Gaussian noise (AWGN) with noise variance of $N_{o,T}$ in the time domain.

The receiver part of the proposed OFDM-HNIM system is the reversal of the transmitter part, which includes CP removal, FFT processing, hybrid demapping, and detection. The frequency-domain received signal vector of dimension $N_F \times 1$ after taking off CP from the received signal and applying FFT can be written as

$$\mathrm{y_F} = \mathrm{X_F h_F} + \mathrm{n_F}, \tag{3.20}$$

where $\mathrm{X_F}$ is an $N_F \times N_F$ diagonal matrix whose prime-diagonal elements are denoted by $x_F(1), x_F(2), \ldots, x_F(N_F)$. $\mathrm{h_F}$ is the $N_F \times 1$ frequency-domain channel vector following the distribution of $\mathcal{CN}(0, \mathrm{I_{N_F}})$, where $\mathrm{I_{N_F}}$ denotes the identity matrix with dimension $N_F \times N_F$. It should be noted that $\mathrm{h_F} = \mathrm{W_{N_F} h_t^0}$, where $\mathrm{W_{N_F}}$ is the N_F-point discrete Fourier transform (DFT) with $\mathrm{W_{N_F}^H W_{N_F}} = N_F \mathrm{I_{N_F}}$, and $\mathrm{h_t^0}$ is the zero-padded version of $\mathrm{h_t}$ with length N_F (i.e. $\mathrm{h_t^0} = [\mathrm{h_t}, 0, ..., 0]^T$) [107]. $\mathrm{n_F} \sim \mathcal{CN}(0, N_{o,F})$ is the AWGN vector in the frequency domain with zero-mean complex Gaussian distribution of variance $N_{o,F}$. The frequency selectivity of the multipath channel is then compensated for via a one-tap

frequency domain equalizer, as $\mathrm{y_{eq}} = \mathrm{y_F}/\mathrm{h_F}$ shows. Next, a detector is used to pull out the SAP.

The demapping procedure is relevant to the remaining processes of the OFDM-HNIM receiver. To be more specific, the bits that are communicated by the index as well as the number of activated subcarriers for each subblock are approximated based on the SAP that was received through the use of the hybrid demapper. To regenerate p_1 and p_2, a mapping (look-up) table similar to **Table 3.5** is employed at the receiver, but the operation carried out on it is the opposite of what was done at the transmitter. Based on subblock SAP, symbols are detected. Finally, the subblock bits are integrated from hybrid demapping and conventional QAM detection. The OFDM block data sequence is retrieved by conducting equivalent techniques on all subblocks. Different detectors, including the optimal ML, ML-based, and LLR, which can be used in this process, are explained below.

In the proposed hybrid scheme, the detection of the number and position of active subcarriers as well as the traditional QAM symbols can be implemented subblock by subblock with no additional performance cost since the encoding operations for all subblocks are independent. We could employ the ML detector in each subblock to jointly estimate its active subcarriers and traditional symbols as follows:

$$(\hat{\mathrm{s}}_\mathrm{g}, \hat{\mathbb{B}}_g) = \arg\min_{\mathrm{s_g}, \mathbb{B}_g} ||\mathrm{y}_\mathrm{F}^\mathrm{g} - \mathrm{x}_\mathrm{F}^\mathrm{g}\mathrm{h}_\mathrm{F}^\mathrm{g}||^2, \tag{3.21}$$

where $\mathrm{s_g}$ and $\hat{\mathrm{s}}_\mathrm{g}$ represent the conventional transmitted and estimated symbols conveyed by the active subcarriers of the g-th subblock, respectively, $\mathbb{B}_g$ and $\hat{\mathbb{B}}_g$ are the set of active subcarriers of the g-th subblock specified by the transmitter and the ML receiver, respectively.

This work studies two different low-complexity approaches for ML-based detection, namely, perfect subcarrier activation pattern estimation (PSAPE), and imperfect SAP estimation (ISAPE). The former ignores the errors due to the incorrect detection of received SAP's subcarriers, while the latter is prone to errors. Particularly, in the case of correct detection of SAP, p_1 and p_2 are detected correctly, while the detection of p_3 is not certain, but depends on the quality of QAM detection. However, in the case of incorrect SAP detection, all subblock bits are erroneous due to the demodulation of some unmodulated

subcarriers.

For further reduction in the computational complexity of the proposed OFDM-HNIM scheme, an LLR detector is employed with logarithmic ratios $\lambda(\alpha)$, where $\alpha = 1, 2, \cdots, N_F$, is calculated for the OFDM block, assuming BPSK modulation is used for simplification [107].

$$\lambda(\alpha) = \max(a, b) + \ln(1 + \exp(-|b - a|)) + \frac{\left|\mathrm{y}_{\mathrm{F}}^{\mathrm{g}}(\alpha)\right|^2}{N_{o,F}}, \tag{3.22}$$

where

$$a = -\frac{\left|\mathrm{y}_{\mathrm{F}}^{\mathrm{g}}(\alpha) - \mathrm{h}_{\mathrm{F}}^{\mathrm{g}}(\alpha)\right|^2}{N_{o,F}}, \tag{3.23}$$

and

$$b = -\frac{\left|\mathrm{y}_{\mathrm{F}}^{\mathrm{g}}(\alpha) + \mathrm{h}_{\mathrm{F}}^{\mathrm{g}}(\alpha)\right|^2}{N_{o,F}}. \tag{3.24}$$

The subcarrier with a larger logarithmic ratio implies that it is more probable that this subcarrier carries a constellation symbol. The proposed LLR detector decides on specific active subcarriers that have maximum LLR values. Then, these selected active subcarriers map to p_1 and p_2 bits and the symbols carried over these active subcarriers would be demodulated to acquire the p_3 bits.

3.2.2. Performance evaluation of the proposed OFDM-HNIM scheme

Here, the evaluation of the hybrid system performance is performed based on key metrics such as SE, average bit error probability, energy efficiency, and computational complexity.

3.2.2.1. Spectral Efficiency

The achievable rate of the proposed OFDM-HNIM scheme can be calculated based on the mutual information between the channel input and the channel output averaged over the subcarriers [112]. Because the data formation in OFDM-HNIM is performed in a sub-block level, whose structure is repeated for all the other consecutive subblocks, the performance evaluation is performed on a subblock basis while considering that the subblocks experience independent, different channel realizations. Therefore, the mutual information over the OFDM block should be calculated for each subblock as shown in **(3.25)**, which

presents the achievable rate of the OFDM-HNIM scheme,

$$R_h = \frac{(\mathrm{x}_\mathrm{F}^\mathrm{g})}{L} = \frac{(\mathrm{x}_\mathrm{F}^\mathrm{g})}{L} + \frac{(\mathrm{x}_\mathrm{F}^\mathrm{g}|\mathrm{y}_\mathrm{F}^\mathrm{g})}{L}, \tag{3.25}$$

where $(\mathrm{x}_\mathrm{F}^\mathrm{g})$ represents the mutual information of the channel input of the g-th subblock $(\mathrm{x}_\mathrm{F}^\mathrm{g})$, $(\mathrm{x}_\mathrm{F}^\mathrm{g})$ is the marginal entropy of $\mathrm{x}_\mathrm{F}^\mathrm{g}$ and $(\mathrm{x}_\mathrm{F}^\mathrm{g}|\mathrm{y}_\mathrm{F}^\mathrm{g})$ is the conditional entropy of $\mathrm{x}_\mathrm{F}^\mathrm{g}$ and the channel output of the g-th subblock $(\mathrm{y}_\mathrm{F}^\mathrm{g})$.

The achievable rate formula in **(3.25)** can be written in terms of probability density functions (PDFs) of the channel input, channel, and channel output as follows [113]:

$$\begin{aligned} R_h = \eta_h - \frac{1}{2^p L} \sum_{j=1}^{2^p} E_{\mathrm{h}_\mathrm{F}^\mathrm{g}} \Bigg\{ \int f(\mathrm{y}_\mathrm{F}^\mathrm{g}|{\mathrm{x}_\mathrm{F}}^{g(j)}, \mathrm{h}_\mathrm{F}^\mathrm{g}) \\ \times \log_2 \left(\frac{f({\mathrm{x}_\mathrm{F}}^{g(j)}, \mathrm{y}_\mathrm{F}^\mathrm{g}|\mathrm{h}_\mathrm{F}^\mathrm{g})}{f(\mathrm{y}_\mathrm{F}^\mathrm{g}|\mathrm{h}_\mathrm{F}^\mathrm{g})} \right) d\mathrm{y}_\mathrm{F}^\mathrm{g} \Bigg\}, \end{aligned} \tag{3.26}$$

where $f(\mathrm{y}_\mathrm{F}^\mathrm{g}|\mathrm{h}_\mathrm{F}^\mathrm{g}) = \frac{1}{2^p} \sum_{j=1}^{2^p} f(\mathrm{y}_\mathrm{F}^\mathrm{g}|{\mathrm{x}_\mathrm{F}}^{g(j)}, \mathrm{h}_\mathrm{F}^\mathrm{g})$, and ${\mathrm{x}_\mathrm{F}}^{g(j)}$ is the j-th realization of $\mathrm{x}_\mathrm{F}^\mathrm{g}$. Furthermore, **(3.26)** can be simplified to the following in the analogy with [112], [113]:

$$R_h \approx \eta_h - \frac{1}{2^p L} \sum_{j=1}^{2^p} \log_2 \sum_{w=1}^{2^p} \frac{1}{det(\mathrm{I}_\mathrm{L} + \mathrm{K}_\mathrm{L} \mathrm{U}_{j,w})}, \tag{3.27}$$

where η_h is the SE of the hybrid scheme, and it can be found in **(3.28)**, $\mathrm{K}_\mathrm{L} = E[\mathrm{h}_\mathrm{F}^\mathrm{g}(\mathrm{h}_\mathrm{F}^\mathrm{g})^H]$ is the covariance matrix of $\mathrm{h}_\mathrm{F}^\mathrm{g}$, I_L represents the identity matrix with dimensions $L \times L$, and $\mathrm{U}_{j,w} = \frac{({\mathrm{x}_\mathrm{F}}^{g(j)} - {\mathrm{x}_\mathrm{F}}^{g(w)})^H ({\mathrm{x}_\mathrm{F}}^{g(j)} - {\mathrm{x}_\mathrm{F}}^{g(w)})}{2N_{o,F}}$. This analytical result will be verified by simulation as well.

The SE of the proposed OFDM-HNIM scheme is:

$$\eta_h = \frac{\sum_{g=1}^{G} \left(\log_2(L) + \left\lfloor \log_2 \binom{L}{I(g)} \right\rfloor + I(g) \log_2(M) \right)}{N_F + N_{CP}}. \tag{3.28}$$

Because two parts of the incoming bits are used for non-conventional mapping in the hybrid scheme compared to only one part in the OFDM-SNM and OFDM-IM schemes, the hybrid scheme improves the SE over the OFDM-IM and OFDM-SNM transmission

schemes. For example, **Table 3.3** shows the SE of the proposed hybrid scheme and its competitive schemes including OFDM-SNM, OFDM-IM, and conventional OFDM, assuming $N_F = 64$ with $N_{CP} = 8$, and BPSK modulation is employed.[1] For convenient comparisons, we consider a fixed length of p_2 bits that enter the IM mapper of the OFDM-HNIM scheme. Also, we set the subblock size (L) to either 4 ($G = N_F/L = 64/4 = 16$), or 8 ($G = 64/8 = 8$). For the system settings shown in **Table 3.3**, the proposed hybrid scheme outperforms its counterparts in terms of SE. Moreover, the SE becomes much more significant in the hybrid scheme as the subblock length increases. This SE trend cannot be achieved by the conventional OFDM-SNM and OFDM-IM schemes, in which SE is degraded as subblock size rises.

Table 3.3: SE of the featured OFDM-based modulation schemes with BPSK.

OFDM modulation option	L	$G\,p_1$	$G\,p_2$	$G\,p_3$	$G\,p$	SE gain
Proposed OFDM-HNIM	4	32	32	32	96	1.333
	8	24	24	216	264	3.6667
OFDM-SNM [19]	4	32	40	N/A	72	1
	8	24	36	N/A	60	0.8333
OFDM-IM [107]	4	32	32	N/A	64	0.8889
	8	24	24	N/A	48	0.6667
Conventional OFDM	4	N/A	N/A	N/A	72	1
	8	N/A	N/A	N/A	72	1

Figure 3.3 shows the number of transmitted bits per OFDM symbol with 64 subcarriers for the featured OFDM-based modulation options at a fixed subblock size of 8. It can be observed from **Figure 3.3** that the OFDM-HNIM scheme outperforms the conventional OFDM-SNM and OFDM-IM schemes at different modulation orders.

Mathematically, we can deduce the values of M and L that satisfy the condition where the SE of the proposed scheme improves over that of the conventional OFDM. The SE of the hybrid scheme can be calculated from **(3.28)** with an average number of active subcarriers of $I_{avg} = \left\lfloor \frac{L+1}{2} \right\rfloor$ over the OFDM subblock:

$$\bar{\eta}_h = \frac{N_F \left(\log_2(L) + \left\lfloor \log_2 \binom{L}{I_{avg}} \right\rfloor + I_{avg} \log_2(M) \right)}{L(N_F + N_{CP})}. \tag{3.29}$$

[1] The phrase N/A, as shown in **Table 3.3**, refers to not applicable.

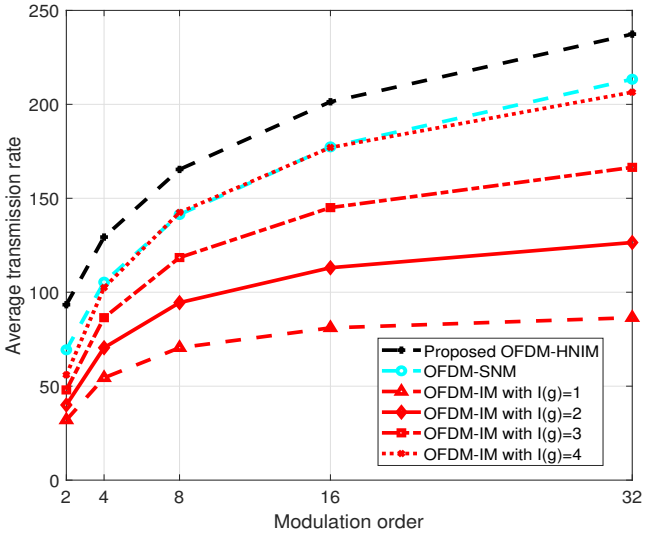

Figure 3.3: Average transmission rate measured in terms of the total number of transmitted bits per OFDM symbol with 64 subcarriers for the featured OFDM-based modulation options as a function of M when the subblock size (L) is set to 8

By comparing **(3.29)** to the SE of the conventional OFDM, which is represented by

$$\bar{\eta}_{OFDM} = \frac{N_F \log_2(M)}{N_F + N_{CP}}, \tag{3.30}$$

we can observe the trend in the SE for the hybrid scheme and conventional OFDM as M and L vary. Then, we can set the inequality that results from considering the SE of the hybrid scheme greater than that of the conventional OFDM as follows:

$$\log_2(L) + \left\lfloor \log_2 \binom{L}{I_{avg}} \right\rfloor + I_{avg} \log_2(M) \geq L \log_2(M). \tag{3.31}$$

Since classical OFDM does not use subblock-based mapping, the average transmission rate per OFDM symbol with 64 subcarriers does not rely on subblock size, as shown in **Figure 3.4**. The hybrid scheme outperforms ordinary OFDM at low modulation orders, especially when $M = 2$ or $M = 4$, for varied subblock sizes. As M rises, the proposed method is less likely to have a higher average transmission rate than standard OFDM, and this degradation increases as subblock size increases. As subblock size increases, more probable bits experience deep fading and become harder for the receiver to identify.

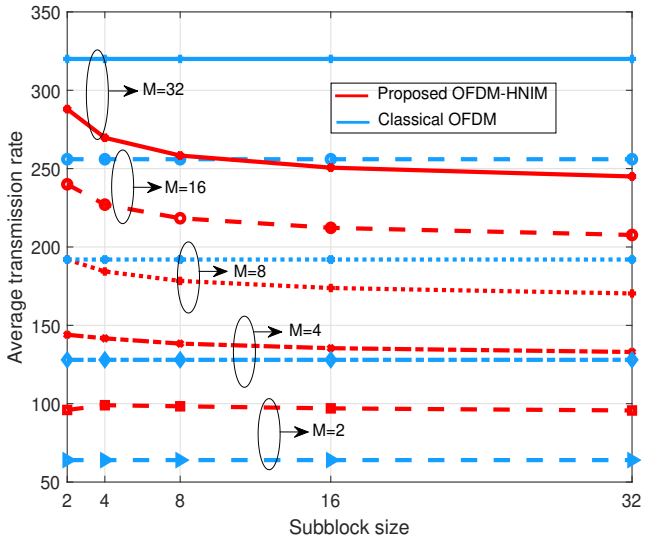

Figure 3.4: Average transmission rate measured in terms of the total number of transmitted bits per OFDM symbol with 64 subcarriers for the proposed hybrid scheme (OFDM-HNIM) and plain OFDM as a function of the subblock size (L).

3.2.2.2. Average Bit Error Probability

The transmission bits in the number and index of activated subcarriers and traditional constellation symbols should be used to detect the hybrid scheme block [108]. The block error rate, also known as the BLER, is the first thing to be determined, followed by the average BER, which is based on the average BLER [109], [114]. The BLER is shown as a function of the pairwise error probability (PEP). The PEP is calculated in two steps; first, when determining the conditional PEP, it is necessary to take into account the influence of the channel ($\mathrm{h_t}$), then the unconditional PEP is computed by getting rid of the channel effect. The conditional PEP can be represented using the Q-function [105]

$$P(\mathrm{c_g} \longrightarrow \hat{\mathrm{c}}_{\hat{\mathrm{g}}} | \mathrm{h_t}) = Q\left(\sqrt{\frac{P_t}{N_{o,F}} || \mathrm{h_t} (\frac{\mathrm{c_g}}{\sqrt{I(g)}} - \frac{\hat{\mathrm{c}}_{\hat{\mathrm{g}}}}{\sqrt{I(\hat{g})}}) ||^2}\right), \tag{3.32}$$

where P_t represents the total transmit power, $I(g)$ and $I(\hat{g})$ represent the number of active subcarriers in the g-th transmitted and $\hat{g}$-th detected, received subblock, respectively, $\mathrm{c_g}$ and $\hat{\mathrm{c}}_{\hat{\mathrm{g}}}$ are the transmitted and detected SAPs of the g-th and $\hat{g}$-th subblocks, respectively. The conditional PEP shown in **(3.41)** can be approximated by using the exponential approximation of the Q-function as [104], [115]

$$Q(x) \approx \sum_{j=1}^{2} \rho_j \exp(-q_j x^2), \tag{3.33}$$

where $\rho_1 = 1/12$ and $\rho_2 = 1/4$, $q_1 = 1/2$ and $q_2 = 2/3$. The new formula of the conditional PEP becomes [90]

$$P(\mathrm{c_g} \longrightarrow \hat{\mathrm{c}}_{\hat{\mathrm{g}}} | \mathrm{h_t}) = \sum_{j=1}^{2} \rho_j \prod_{l=1}^{L} \exp\left(\frac{-q_j P_t}{N_{o,F}} V(l) \Delta(l, g, \hat{g}) \right), \tag{3.34}$$

where $V(l) = |h_t(l)|^2$ and $\Delta(l, g, \hat{g}) = \left| \frac{\mathrm{c_g}(l)}{\sqrt{I(g)}} - \frac{\hat{\mathrm{c}}_{\hat{\mathrm{g}}}(l)}{\sqrt{I(\hat{g})}} \right|^2$.

The unconditional PEP can be found by averaging the conditional PEP over the channel as [116], [117]

$$P(\mathrm{c_g} \longrightarrow \hat{\mathrm{c}}_{\hat{\mathrm{g}}}) = \sum_{\hat{\mathrm{c}}_{\hat{\mathrm{g}}} \neq \mathrm{c_g}} E_{\mathrm{h_t}} \left\{ P(\mathrm{c_g} \longrightarrow \hat{\mathrm{c}}_{\hat{\mathrm{g}}}) | \mathrm{h_t}) \right\}. \tag{3.35}$$

Assuming equiprobable information bits, the upper bound of ABEP of the hybrid system could be obtained as [107], [118]

$$P_b(E) = \frac{1}{p_g \, n_x} \sum_{g=1}^{G} \sum_{\hat{\mathrm{c}}_{\hat{\mathrm{g}}} \neq \mathrm{c_g}} P(\mathrm{c_g} \longrightarrow \hat{\mathrm{c}}_{\hat{\mathrm{g}}}) e(\mathrm{c_g}, \hat{\mathrm{c}}_{\hat{\mathrm{g}}}), \tag{3.36}$$

where p_g represents the vector length of the information bits that correspond to the g-th subblock, n_x represents the number of possible realizations of the transmitted sequence, and $e(\mathrm{c_g}, \hat{\mathrm{c}}_{\hat{\mathrm{g}}})$ denotes errors in information bits due to erroneously choosing $\hat{\mathrm{c}}_{\hat{\mathrm{g}}}$ rather than $\mathrm{c_g}$ [107]. This derived theoretical BER result will be verified by simulations as well.

3.2.2.3. Energy Efficiency

The energy efficiency (EE) implies how efficiently energy is consumed in a given system. The EE of the proposed OFDM-HNIM scheme is analyzed in terms of the energy saving factor (ESF) achieved by not activating all of the available subcarriers in the OFDM block. The evaluation of ESF for the featured schemes is discussed below.

The SE and EE ratios of the featured OFDM-based modulation options can be shown in **Figure 4.11**. The symbols s1, s2, s3, s4, s5 correspond to the proposed OFDM-HNIM scheme, OFDM-SNM, OFDM-IM with $AR = 0.25$, OFDM-IM with $AR = 0.5$, and conventional OFDM, respectively.

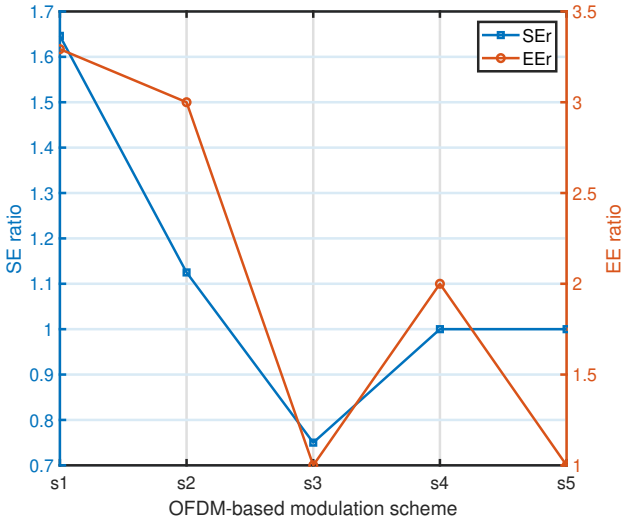

Figure 3.5: The SE and EE ratios of the featured OFDM-based modulation options. The symbols s1, s2, s3, s4, s5 correspond to the proposed OFDM-HNIM scheme, OFDM-SNM, OFDM-IM with $AR = 0.25$, OFDM-IM with $AR = 0.5$, and conventional OFDM, respectively.

One main aspect of the overall energy saving is the saving in signal transmission [14]. For the considered OFDM-based modulation options, we define the EE based on the ratio of saved energy under a given total transmit power (P_t) in a single OFDM symbol. We assume equiprobable subcarrier activation [106] for a convenient comparison between the proposed OFDM-HNIM scheme and its competitive schemes. Moreover, the average number of active subcarriers is considered in our analysis of EE. The number of activated subcarriers in an OFDM block impacts both SE and EE, and their ratios relation for the traditional OFDM as a reference scheme [119], can be defined as [14]

$$EE_r = \frac{SE_r}{1 - ESF}, \tag{3.37}$$

where EE_r and SE_r represent the EE and SE ratios of the scheme of interest, and ESF represents the saved energy by activating N_a subcarriers out of N_v available subcarriers

$$ESF = 1 - \frac{N_a}{N_v}. \tag{3.38}$$

As seen from **(3.38)**, as N_a decreases, ESF increases and more energy could be saved. Maximizing SE and EE are generally two conflicting objectives as can be seen from **(3.37)** [120]. Moreover, the term ($I_{avg} \log_2(M)$) in **(3.29)** characterizes the SE and EE trade-off by using high I_{avg} and M values to achieve high SE, more energy needed to be spent to

attain such a SE.

For example, the proposed OFDM-HNIM scheme with half of the available subcarriers are activated on average is the equivalent case of the OFDM-IM scheme with a subcarrier activation ratio of half ($AR = 0.5$). The energy saving resulting from the OFDM-HNIM and OFDM-IM with $AR = 0.5$ is limited to the half of the OFDM symbol ($ESF = 0.5$). In other words, the active subcarriers of the OFDM-HNIM scheme gain higher power as compared to the individual subcarriers of the classical OFDM under the same transmitted power. Hence, the receiver design of the proposed OFDM-HNIM scheme would only differentiate between the active set with higher power and the inactive set regardless of the exact amplitude and phase of each subcarrier.

It is well-known that the conventional OFDM is not an EE scheme since most of the available subcarriers are usually used for data transmission, which results in very low ESF. **Figure 4.11** shows the SE_r and EE_r of the featured OFDM modulation schemes under BPSK. It is clear from **Figure 4.11** that the proposed OFDM-HNIM scheme provides higher SE_r and EE_r as compared to the OFDM-SNM, OFDM-IM with low AR, and the classical OFDM.

3.2.2.4. Complexity Analysis

The computational complexity performances of the proposed detectors of the OFDM-HNIM scheme are discussed here. The computational complexity of the optimal ML detector of the proposed scheme in terms of complex multiplications is of order $\sim O(G\,M^{L/2})$ per bit detected in each OFDM block, which becomes impractical for large values of G, L, and M, due to its exponentially increasing complexity.

The average number of calculations per subcarrier is used as a performance parameter to evaluate the computational complexity of the various proposed detectors. **Table 3.6** presents the complexity comparison results for the featured OFDM-based modulation schemes. As seen in **Table 3.6**, the computational complexity of the optimal ML detector is highly susceptible to G, L, and M; however, the complexity of the proposed ML-based detectors is only determined by G , and much lower than the optimal ML detector, and there is much reduction of complexity in order of M by employing LLR detector. Moreover, **Table 3.6** shows the comparison between the detection complexity of the proposed

hybrid scheme with that of its counterparts schemes such as OFDM-SNM, OFDM-IM, and plain OFDM. The proposed OFDM-HNIM along with the LLR detector is considered as a simple, not sophisticated scheme with similar complexity order to that in OFDM-IM and conventional OFDM.

Table 3.4: Complexity comparison between different detectors for the featured OFDM-based modulation schemes.

OFDM modulation option	Detector type	Complexity order
Proposed OFDM-HNIM	Optimal ML	$\sim O(G\,M^{L/2})$
	PSAPE	$\sim O(G)$
	ISAPE	$\sim O(G)$
	LLR	$\sim O(M)$
OFDM-SNM [19]	ML	$\sim O(L, I(g), M)$
OFDM-IM [107]	Near optimal LLR	$\sim O(M)$
Conventional OFDM	ML	$\sim O(M)$

3.3. The Proposed OFDM-SGM Scheme

The system model of the OFDM-SGM scheme is illustrated in **Subsection 3.3.1**. Performance evaluation of the OFDM-SGM in terms of ABEP and computational complexity is presented in **Subsection 3.3.2**.

3.3.1. System model

The transmitter architecture of the OFDM-SGM is depicted in **Figure 3.2**. The m source bits are split into G groups using the bits splitter module, each group includes $p = p_1 + p_2$ bits that form an OFDM-SGM subblock with a length of $L = N/G$, where N is the FFT size. The gap selecting bits (p_1) specify the number of gaps between active subcarriers in every subblock in which the subcarrier activation pattern (SAP) is formed using a proper mapping method.

The gap mapper places the active subcarriers in each subblock g ($g = 1, 2, \ldots, G$) from the set $\Lambda = \{1, 2, \cdots, L/2 - (\log_2(L/2) - 1), L/2, L\}$. The number of activated subcarriers in the g-th subblock can be represented by the **gap-dependent variable** $I(g)$. This variable is determined based on the p_1 incoming bits that enter the gap mapper. **Table 3.5** shows the proposed mapping for $L = 4$ with $p_1 = \log_2(L) = 2$. As shown in **Table 3.5**, the

assignment of zero, one, two, and three gaps between active subcarriers correspond to p_1 of [0 0], [0 1], [1 0], and [1 1], respectively. The SAP in each subblock can be formulated as $\mathrm{c}_g = \begin{bmatrix} c_1 & c_2 & \cdots & c_L \end{bmatrix}^T$, where $c_i \in \{0, 1\}$ for $i = 1, 2, \cdots, L$. In each subblock, $p_2 = I(g)\log_2(M)$ data symbol bits are available depending on the SAP. Particularly, these p_2 bits are mapped to standard constellations conveyed by the active subcarriers.

Table 3.5: SGM mapping with p_1=2 bits and L=4.

p_1	c_g
[0 0]	$[1\,1\,1\,1]^T$
[0 1]	$[1\,0\,1\,0]^T$
[1 0]	$[1\,0\,0\,1]^T$
[1 1]	$[1\,0\,0\,0]^T$

The OFDM-SGM subblock can be represented based on c_g as x_F^g. Then, the OFDM-SGM block is formed by concatenating G subblocks as $\mathrm{x}_F = \begin{bmatrix} x_F(1) & x_F(2) & \ldots & x_F(N) \end{bmatrix}^T$. The remaining steps are performed as in the plain OFDM transmission process, including IFFT and CP addition. By applying IFFT to x_F, the resultant signal is x_t. By adding N_{CP} CP samples to x_t, the output vector can be written as $\mathrm{x}_{CP} = \begin{bmatrix} \mathrm{x}_t(N - N_{CP} + 1 : N) & \mathrm{x}_t \end{bmatrix}^T$. This CP appended signal would be faded by a wireless channel with impulse response h_t, along with an AWGN with a variance of $N_{o,T}$ in the time-domain.

CP removal, FFT operation, gap demapping, and detection constitute the operations that performed at the OFDM-SGM receiver. The frequency-domain received signal vector of dimension $N \times 1$ after the CP removal and after applying FFT can be written as

$$\mathrm{y}_F = \mathrm{X}_F \mathrm{h}_F + \mathrm{n}_F, \tag{3.39}$$

where X_F is a diagonal matrix with dimension $N \times N$, and its elements on the main diagonal are represented by $x_F(1), x_F(2), \ldots, x_F(N)$. h_F is the channel vector in the frequency domain with a size of $N \times 1$, and it follows the distribution of $\mathcal{CN}(0, \mathrm{I}_N)$, where I_N represents the identity matrix with size $N \times N$. The frequency-domain channel vector is related with its time representation as $\mathrm{h}_F = \mathrm{W}_N \mathrm{h}_t^0$, where W_N represents the DFT matrix of dimension $N \times N$ with $\mathrm{W}_N^H \mathrm{W}_N = N\mathrm{I}_N$, and $\mathrm{h}_t^0 = [\mathrm{h}_t, 0, ..., 0]^T$ denotes the zero-padded version of h_t with length N. $\mathrm{n}_F \sim \mathcal{CN}(0, N_{o,F})$ is the frequency-domain AWGN vector [107].

Thereafter, a one-tap frequency domain equalizer is applied to compensate for the frequency selectivity of the multi-path channel. A maximum likelihood (ML) detection would detect the SAP. For detection of the data code p_1, a similar **Table 3.5** is used at the receiver.

Subsequently, the gap demapper module is used to get the SAP, and then the gap bits could be estimated in each subblock. Then, M-ary signal constellation detection is done depending on the received SAP in each subblock. At the final stage, the detected bits from the gap demapping and classical symbols detection jointly form the latest estimated subblock bits. The recovered data sequence is obtained for the whole block by performing similar steps to all subblocks.

To reduce the detection complexity of the employed optimal ML, we adopt two low-complexity detectors, namely, perfect SAP estimation (PSAPE), and imperfect SAP estimation (ISAPE). The PSAPE detector neglects the errors caused by the wrong detection of subcarriers in the received SAP, whereas, the detection in ISAPE is error-prone. In the both detectors, the demodulation stage of the classical constellation symbols would be unsuccessful to extract p_2 bits correctly when an erroneous SAP detection happens. This occurs because of the demodulation of some incorrectly detected subcarriers. So, the transmitted p_1 and p_2 bits are erroneous when the detected SAP is wrong. On the other hand, if SAP is correctly detected, then p_1 is correct but it is not certain that p_2 is correctly estimated.

The PSAPE detector is taken into account for the conducted simulations due to its low complexity compared to that of the ISAPE. It is worthy to note that the performance comparison between PSAPE and ISAPE detectors is presented as well. A log-likelihood ratio (LLR) detector is also implemented for the proposed scheme to reduce its computational complexity. Assuming BPSK is adopted in the proposed scheme, the LLR values can be represented as [107]

$$\lambda(\alpha) = \max(a, b) + \ln(1 + \exp(-|b - a|)) + \frac{|\mathrm{y}_F(\alpha)|^2}{N_{o,F}}, \tag{3.40}$$

where $a = \frac{-|\mathrm{y}_F(\alpha) - \mathrm{h}_F(\alpha)|^2}{N_{o,F}}$ and $b = \frac{-|\mathrm{y}_F(\alpha) + \mathrm{h}_F(\alpha)|^2}{N_{o,F}}$.

This LLR detector decides on specific active subcarriers that have maximum LLR values. Then, these selected active subcarriers would be mapped to p_1 bits, and the symbols carried over these active subcarriers would be demodulated to get the p_2 bits.

3.3.2. Performance evaluation of the proposed OFDM-SGM

Here, the assessment of the proposed scheme is done based on some key metrics like ABEP and the complexity associated with the detectors.

3.3.2.1. Average Bit Error Probability

The ABEP should be calculated based on the evaluation of pairwise error probability (PEP) since the transmission bits are carried over the gap dimension as well as the conventional symbols [19]. The CPEP could be expressed by the Q-function [105]

$$P(\mathrm{c}_g \longrightarrow \hat{\mathrm{c}}_{\hat{g}}|\mathrm{h}_t) = Q\left(\sqrt{\frac{P_t}{N_{o,F}}||\mathrm{h}_t\Delta||^2}\right), \tag{3.41}$$

where P_t is the total transmitted power, $\Delta = \frac{\mathrm{c}_g}{\sqrt{I(g)}} - \frac{\hat{\mathrm{c}}_{\hat{g}}}{\sqrt{I(\hat{g})}}$. $I(g)$ and $I(\hat{g})$ represent the number of activated subcarriers in the g-th and $\hat{g}$-th OFDM-SGM subblock, respectively, c_g and $\hat{\mathrm{c}}_{\hat{g}}$ are transmitted and detected sequences. The formula of CPEP in **(3.41)** can be approximated using the Q-function as [104]

$$Q(x) \approx \sum_{j=1}^{2} \rho_j \exp(-\eta_j x^2), \tag{3.42}$$

where $\rho_1 = 1/12$ and $\rho_2 = 1/4$, $\eta_1 = 1/2$ and $\eta_2 = 2/3$. Using **(3.42)**, the CPEP can be formulated as [90]

$$P(\mathrm{c}_g \longrightarrow \hat{\mathrm{c}}_{\hat{g}}|\mathrm{h}_t) = \sum_{j=1}^{2} \rho_j \prod_{l=1}^{L} \exp(\frac{-\eta_j P_t}{N_{o,F}} U(l)|\Delta(l)|^2), \tag{3.43}$$

where $U(l) = |h_t(l)|^2$, $|\Delta(l)|^2 = |\frac{\mathrm{c}_g(l)}{\sqrt{I(g)}} - \frac{\hat{\mathrm{c}}_{\hat{g}}(l)}{\sqrt{I(\hat{g})}}|^2$.

The unconditional PEP (UPEP) can be calculated by averaging CPEP over h_t as [117]

$$P(\mathrm{c}_g \longrightarrow \hat{\mathrm{c}}_{\hat{g}}) = \sum_{\hat{\mathrm{c}}_{\hat{g}} \neq \mathrm{c}_g} E_{\mathrm{h}_t}\left\{P(\mathrm{c}_g \longrightarrow \hat{\mathrm{c}}_{\hat{g}})|\mathrm{h}_t)\right\}. \tag{3.44}$$

Furthermore, a more approximative Q-function expression in [121] could be used for a tighter upper bound of BER as

$$Q(x) \approx 0.168e^{-0.876x^2} + 0.144e^{-0.525x^2} + 0.002e^{-0.603x^2} \tag{3.45}$$

By using the spectral theorem [122] and **(3.45)**, **(3.44)** can be simplified to [107]

$$\begin{aligned} P(\mathrm{c}_g \longrightarrow \hat{\mathrm{c}}_{\hat{g}}) \approx & \frac{1}{1/0.168 \det\left(\mathrm{I}_L + \frac{0.876}{2N_{o,F}}\mathrm{K}_L\mathrm{A}\right)} + \\ & \frac{1}{1/0.144 \det\left(\mathrm{I}_L + \frac{0.525}{2N_{o,F}}\mathrm{K}_L\mathrm{A}\right)} + \\ & \frac{1}{1/0.002 \det\left(\mathrm{I}_L + \frac{0.603}{2N_{o,F}}\mathrm{K}_L\mathrm{A}\right)}, \end{aligned} \tag{3.46}$$

where I_L represents $L \times L$ identity matrix, $\mathrm{K}_L = E\left\{\mathrm{h}_t\mathrm{h}_t^H\right\}$, $\mathrm{A} = \left(\mathrm{c}_g - \hat{\mathrm{c}}_{\hat{g}}\right)^H \left(\mathrm{c}_g - \hat{\mathrm{c}}_{\hat{g}}\right)$.

Considering all UPEP events and assuming information bits are equiprobable, the upper bound for ABEP in the OFDM-SGM could be attained [107]

$$P_b(E) = \frac{1}{p_g\, n_x} \sum_{g=1}^{G} \sum_{\hat{\mathrm{c}}_{\hat{g}} \neq \mathrm{c}_g} P(\mathrm{c}_g \longrightarrow \hat{\mathrm{c}}_{\hat{g}}) e(\mathrm{c}_g, \hat{\mathrm{c}}_{\hat{g}}), \tag{3.47}$$

where p_g is the length of the vector that constitutes data bits corresponding to an OFDM-SGM subblock, n_x is the number of legitimate realizations of the transmitted sequence, and $e(\mathrm{c}_g, \hat{\mathrm{c}}_{\hat{g}})$ shows how many bits are different between c_g and $\hat{\mathrm{c}}_{\hat{g}}$. The aforementioned theoretical analysis for the error performance of OFDM-SGM is verified with its corresponding simulation one, as shown in **Section 4.3**.

3.3.2.2. Complexity analysis

The complexities of the considered OFDM-based modulation options are presented in **Table 3.6**. As observed from **Table 3.6**, the complexity of the ML is critical to G, L, and M; however, the complexity of the PSAPE and ISAPE detectors is only determined by G, which is significant reduction in comparison to ML. Furthermore, **Table 3.6** presents the

comparison between different detectors for OFDM-SGM with its counterparts. OFDM-SGM with an LLR detector has equivalent complexity performance to OFDM-IM and classical OFDM. Thus, LLR detectors are best for realistic OFDM-SGM systems.

Table 3.6: Complexity comparison between different detectors for the proposed scheme and its counterparts.

Modulation Scheme	**Detector type**	**Complexity order**
Proposed OFDM-SGM	Optimal ML	$\sim \mathcal{O}(G\,M^{L/2})$
	PSAPE	$\sim \mathcal{O}(G)$
	ISAPE	$\sim \mathcal{O}(G)$
	LLR	$\sim \mathcal{O}(M)$
OFDM-SNM	ML	$\sim \mathcal{O}(L, I(g), M)$
OFDM-IM	Near optimal LLR	$\sim \mathcal{O}(M)$
Conventional OFDM	ML	$\sim \mathcal{O}(M)$

3.4. The Proposed Floating OFDM-SNM For PAPR And OOBE Reduction

The proposed floating OFDM-SNM scheme is illustrated in **Subsection 3.4.1**. The proposed PAPR and OOBE reduction techniques for the floating OFDM-SNM are introduced in **Subsection 3.4.2** and **Subsection 3.4.3**, respectively.

3.4.1. System model

Here, the system model of the conventional OFDM-SNM is revisited, and its enhanced version, called floating OFDM-SNM, is presented. We consider an OFDM block with a total number of N_F subcarriers. These N_F available subcarriers are divided into G groups with each containing two data codes: p_1 determines the number of active subcarriers and p_2 carriers the bits that are mapped to conventional symbols over the activated subcarriers. Hence, $p = p_1 + p_2$ bits are sent over each OFDM-SNM subblock. The incoming information bits are mapped to q active subcarriers based on a successive SAP. **Table 3.7** shows an example of a simple look-up table for the classical OFDM-SNM with $p_1 = 2$ bits and a subblock length of 4 ($N = 4$). Further details about the mapping process of the conventional OFDM-SNM can be found in [123].

In this work, we propose an enhanced version of the conventional OFDM-SNM by enabling flexible SAP, i.e., not necessarily successive SAP, in which this floated SAP is

Table 3.7: Classical SNM mapper with p_1=2 bits and N=4.

Information bits	SAP
[0 0]	[1 0 0 0]
[0 1]	[1 1 0 0]
[1 0]	[1 1 1 0]
[1 1]	[1 1 1 1]

Table 3.8: Floating SNM mapper with p_1=2 bits and N=4.

Information bits	SAP
[0 0]	[1 0 0 0]
	[0 1 0 0]
	[0 0 1 0]
	[0 0 0 1]
[0 1]	[1 1 0 0]
	[1 0 1 0]
	[1 0 0 1]
	[0 1 1 0]
	[0 1 0 1]
	[0 0 1 1]
[1 0]	[1 1 1 0]
	[1 1 0 1]
	[1 0 1 1]
	[0 1 1 1]
[1 1]	[1 1 1 1]

designed for specific purposes such as reducing the PAPR or OOBE of the conventional OFDM-SNM. **Table 3.8** shows one example of bits-to-SAP mapping, where successive SAP is not maintained as proposed in [123]. Instead, flexible SAP is introduced to enhance the performance of the successive-based SAP in the conventional OFDM-SNM.

After this mapping procedure, the resultant signal in the frequency domain represented by X would pass through a serial to parallel (S/P) converter. After that, IFFT is applied to acquire OFDM samples in the time domain as

$$x(n) = \sum_{k=0}^{N_F-1} X(k) e^{\frac{j2\pi nk}{N_F}}, \tag{3.48}$$

where the time-domain samples' indices are represented by $n = 0, 1, ..., N_F$. After that, the transmitted signal is sent over a frequency-selective Rayleigh fading channel with

complex Gaussian distribution path gains, which are represented by

$$h(n) = \sum_{l=0}^{L-1} h(l)\delta(n-l), \tag{3.49}$$

where L represents the number of channel taps. The received faded signal could be formulated as

$$y(n) = \sum_{l=0}^{L-1} h(l)x(n-l) + w(n), \tag{3.50}$$

where $w(n)$ is the complex Gaussian noise with zero mean and variance $N_{o,T}$. The received signal in the frequency domain could be found as

$$Y(k) = X(k)H(k) + W(k), \tag{3.51}$$

where $H(k)$ and $W(k)$ represent the frequency response of the channel and noise, respectively. To prevent inter-symbol interference, a CP with length l_{CP} is appended to the transmitted signal. It is worth noting that the receiver of the proposed scheme is similar to that of the conventional OFDM-SNM receiver [123].

3.4.2. Proposed floating OFDM-SNM for PAPR reduction

The PAPR for the transmitted OFDM signal $x[n]$ is computed by dividing the maximum instantaneous power by the average power, as shown in the following:

$$PAPR(x[n]) = \frac{\max_n |x[n]|^2}{E[|x[n]|^2]}. \tag{3.52}$$

Here, we propose a PAPR reduction technique by intelligently changing the location of active subcarriers among the data symbols. This smart shifting of the activated subcarriers does not require any arithmetic operation. **Figure 3.6** shows the systematic structure of the proposed PAPR reduction technique for the floating OFDM-SNM. The PAPR is computed after performing the IFFT process, as shown in **Figure 3.6**. These PAPR values are stored with specific SAPs that constitute a specific floating OFDM-SNM block. It should be noted that the location of active subcarriers is not known by the floating OFDM-SNM receiver.

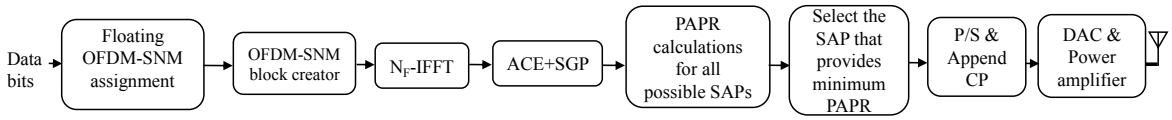

Figure 3.6: The proposed PAPR reduction method for the floating OFDM-SNM.

The ACE and SGP methods in [33] employed to OFDM-IM, could be also used for the proposed scheme to provide a further reduction in its PAPR. The reason behind this direct application of ACE/SGP is the similarity in the general shape of the OFDM-IM and OFDM-SNM blocks. The typical steps performed for the ACE algorithm with SGP are listed as follows:

1. Apply IFFT to the OFDM-SNM signal in the frequency domain (X) to form the time-domain signal, $x^i[n]$. Set $i = 0$.

2. Apply clipping to $x^i[n]$ based on a clipping threshold amplitude (A) as $|x^i[n]| > A$, and the clipped signal can be represented as follows:

$$c[n] = \begin{cases} 0, & \text{if } |x[n]| \leq A \\ Ae^{j\theta[n]} - x[n], & \text{if } |x[n]| > A \end{cases} \quad \textbf{(3.53)}$$

   where $\theta[n]$ is the angle of the n_{th} sample of $x[n]$.

3. Apply FFT operation to (c) to obtain the clipped signal C in the frequency domain.

4. Keep the components of C that correspond to the inactive subcarriers in X, unchanged, and set the remaining C components to zero.

5. Apply FFT to the updated C to get c.

6. Determine a step size (μ) as

$$x^{i+1}[n] = x^i[n] + \mu * c. \quad \textbf{(3.54)}$$

7. If the maximum iteration count (J) has not been reached, update, and go to Step 2. Otherwise, halt the process.

Different SAPs arrangements, corresponding to the same data bits' sequence, are generated using the floating OFDM-SNM assignment block, as shown in **Figure 3.6**, and the

one which provides the minimum PAPR is selected for transmission. Mathematically, we can find the peak power for a given SAP as follows:

$$PP = max_{0 \le n \le N_F - 1} |x[n]|^2. \quad \textbf{(3.55)}$$

The PAPR vector contains all $N! \times N$ possible SAPs that can be represented as

$$VPP = [PP_1\, PP_2 ... PP_{N! \times N}]. \quad \textbf{(3.56)}$$

The SAP, that provides minimum PAPR in the floating OFDM-SNM signal, can be found as

$$IP_{min} = \arg\min_{v} [VPP(v)], \quad \textbf{(3.57)}$$

where $v = 1, 2, ..., N! \times N$ is the index of a possible SAP, and IP_{min} represents the index of the SAP that provides the minimum PAPR among all possible SAPs.

The complementary cumulative distribution function (CCDF) is used to measure the PAPR performance, which represents the probability that the PAPR of the considered floating OFDM-SNM signal's envelope exceeds a specified γ threshold within the floating OFDM-SNM symbol. Thus, the CCDF formula can be written as

$$CCDF = \Pr\{PAPR > \gamma\}. \quad \textbf{(3.58)}$$

As an analogy to OFDM, the CCDF of the floating OFDM-SNM could be expressed as in [124] for a sufficient number of subcarriers, assuming that the OFDM samples are mutually independent, the CCDF expression could be formulated as

$$CCDF = 1 - (1 - e^{-\gamma})^{\alpha N_F}, \quad \textbf{(3.59)}$$

where α denotes the oversampling factor.

3.4.3. Proposed floating OFDM-SNM for OOBE minimization

The OOBE is the minimum value of the power spectrum for the OFDM signal, and it can be formulated as [34]

$$OOBE = \min X_F; \quad 0 \le k \le N_F - 1 \tag{3.60}$$

where $X_F = \frac{1}{T}\|X(k)\|_2^2$ represents the power spectrum of the OFDM signal with T symbol duration.

The proposed floating OFDM-SNM for OOBE reduction is displayed in **Figure 3.7**. As can be observed from **Figure 3.7** that OOBE calculations for all the possible SAPs arrangements are performed, and the SAPs arrangement with minimum OOBE would be chosen for transmission as follows.

The OOB vector, containing all possible $N! \times N$ SAPs, can be represented as

$$VOB = [OOBE_1\, OOBE_2 ... OOBE_{N!\times N}]. \tag{3.61}$$

The SAP, providing minimum OOBE in the floating OFDM-SNM signal, can be found as

$$IO_{min} = \arg\min_{v}[VOB(v)], \tag{3.62}$$

where IO_{min} represents the index of the SAP that provides the minimum OOBE.

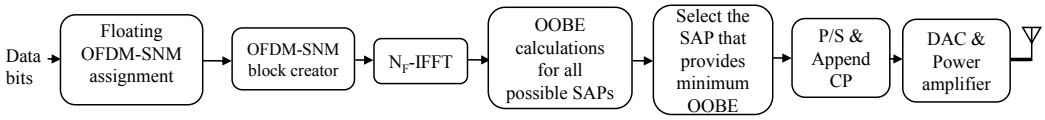

Figure 3.7: The proposed OOBE reduction method for the proposed floating OFDM-SNM.

3.5. Performance Evaluation And Comparison Of Modulation Options In Practical Conditions

Reliability, SE, power efficiency (PE), out-of-band (OOB) leakage, and computational complexity are the performance measures used to evaluate the OFDM-based modulation techniques. Monte Carlo simulations are conducted to evaluate their performances, and the simulation parameters used can be shown in **Table 3.9**. Point-to-point transmission with a single user is considered to have a fair comparison between the featured modulation schemes. It is assumed that the transmitter and receiver have a single antenna. The multi-antenna transmission scheme discussed in **Subsection 2.2.1**, i.e. SM-OFDM would be analyzed with its counterparts including the famous ones such as Vertical Bell Labs Layered Space-Time (V-BLAST) [125] and Alamouti-Coded [126] OFDM systems.

A Rayleigh fading channel is used in the conducted simulations, and the CSI is available at the receiver. SNR is defined as $\rho = E_b/N_{o,T}$, where E_b is the average transmitted energy per bit, and $N_{o,T}$ is the time-domain noise variance. The SNR region in the considered simulations is between 0 dB and 30 dB for practical purposes, however, similar realization trends have been noticed for other possible SNR values.

Table 3.9: Simulation parameters.

Modulation type	BPSK
FFT size (N)	64
CP Guard Interval (samples)	8
Number of subblocks in each OFDM symbol	16
Number of available subcarriers in each subblock	4
Multipath channel delay samples locations	[0 3 5 6 8]
Multipath channel tap power profile (dBm)	[0 -8 -17 -21 -25]

3.5.1. Spectral efficiency

The SE is important for data rate requirements, user communication, and traffic density. The SE (η) in (bits/s/Hz) of the featured modulation options for an OFDM-based waveform can be formulated as

$$\eta_{Plain\ OFDM} = \frac{N \log_2(M)}{N + N_{CP}}, \tag{3.63}$$

$$\eta_{OFDM-IM} = \frac{N\left(\log_2(M^a) + \lfloor \log_2 \binom{b}{a} \rfloor\right)}{(N + N_{CP})b}, \tag{3.64}$$

$$\eta_{OFDM-SNM} = \frac{\sum_{g=1}^{G} (\log_2(b) + a(g) \log_2(M))}{N + N_{CP}}, \tag{3.65}$$

where N_{CP} is the CP or guard length, a represents the number of activated subcarriers in an OFDM-IM subblock with a length of b. $a(g)$ is the number of turned on subcarriers in an OFDM-SNM subblock with length of b, G represents the number of subblocks that constitute the OFDM-SNM block.

As can be seen in **Figure 3.8**, the relative loss in throughput is higher in OFDM-DM compared to classical OFDM [82]. $a(g)$ varies in each subblock of the OFDM-SNM scheme, while it is fixed for all OFDM-IM subblocks. The SE improvement of OFDM-SNM over OFDM-IM holds just when subblock length is low as implemented in the considered deployment option in the simulations. However, the SE improvement does not hold anymore for more general cases.

As M increases, it is less likely to have enhanced SE of OFDM-SNM as compared to the plain OFDM [90]. In addition to that, the average SE of OFDM-SNM could be higher than that of OFDM-IM when [90]

$$a \leq \frac{b+1}{2}. \tag{3.66}$$

The selected M based on **(3.66)** could be formulated as [90]

$$M \geq \left(b / \binom{b}{a}\right)^{\frac{1}{a - \frac{b+1}{2}}}. \tag{3.67}$$

As the number of transmit antennas increases, the SE of SM-OFDM increases in a logarithmic way as

$$\eta_{SM-OFDM} = \frac{N \log_2(N_T) + \log_2(M)}{N + N_{CP}}. \tag{3.68}$$

The SE of OFDM-PSM with HG pulses is superior to the transmission scheme that uses only Gaussian pulses as the transmit pulse.

Figure 3.8 shows that the achievable rate of the OFDM-SNM scheme outperforms its counterparts for the given simulation parameters in **Table 3.9**.

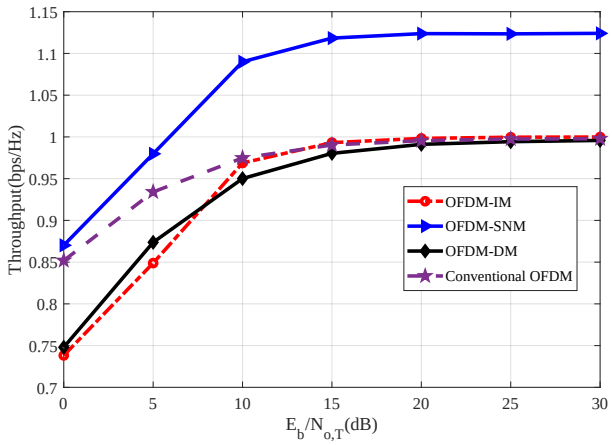

Figure 3.8: Throughput of the featured OFDM-based modulation options.

Furthermore, throughput performances of the OFDM-DM and OFDM-IM converge to that of classical OFDM at high SNR values. Moreover, the plain OFDM scheme outperforms OFDM-DM by almost 2.9 dB [82]. It is worthy to mention that changing some parameters, such as subblock size and activation ratio, in a given modulation scheme results in achieving diverse transmission rates.

3.5.2. Reliability

The BER performance of the featured OFDM-based modulation schemes is depicted in **Figure 3.9**, OFDM-SNM and OFDM-IM have almost similar reliability performance which is superior to the classical OFDM in the high SNR region.

The OFDM-DM transmission scheme has the worst BER performance at high SNR values. Furthermore, OFDM-PSM has almost the same reliability performance to conventional

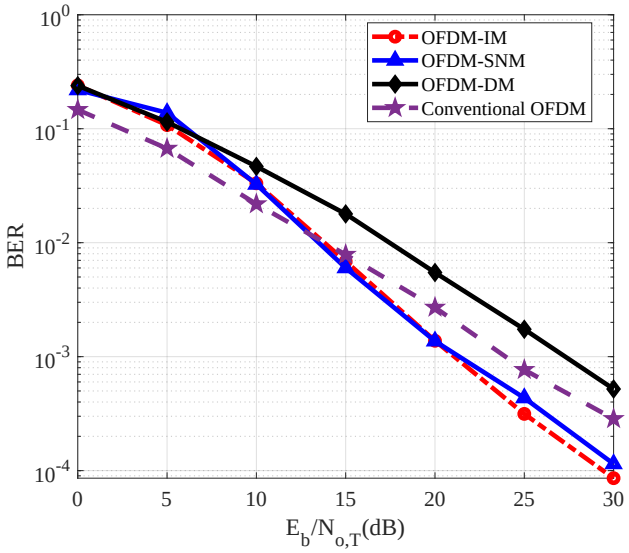

Figure 3.9: BER of the featured OFDM-based modulation options.

OFDM [100]. The SM-OFDM scheme has superior reliability performance as compared to the popular V-BLAST and Alamouti-coded OFDM systems at low SE. Even though, at high SE, its reliability performance would rely on a trade-off between the spatial constellation size ($N_T \times N_R$) and signal constellation size (M) [85].

3.5.3. PAPR and power efficiency

The power efficiency (PE) analysis of modulation schemes is critical to be considered in the system design. Peak-to-average power ratio (PAPR) of a given waveform is defined as the ratio of maximum power to average power. High PAPR is a common drawback in the multicarrier waveforms. This high PAPR performance of the OFDM transmission scheme causes non-linearity problems as the transmitted signal passed through the high power amplifier (HPA). Thus, an efficiency reduction would be expected at the HPA. This phenomenon happens due to having a constructive combination between the modulated subcarriers with independent phases.

The number of available subcarriers (N) and their corresponding pulse shapes are the major factors of PAPR performance in the OFDM-based waveforms. The total transmitted power (P_t) is distributed fairly among subcarriers with (P_t/N) average power allocated for each subcarrier. As demonstrated in [10], the featured modulation options, including OFDM-SNM, OFDM-IM [127], OFDM-DM, and traditional OFDM, have almost the same high PAPR performance. It is assumed that OFDM symbols are uncorrelated to each

other within each block.

Although the number of active subcarriers in some transmission schemes such as OFDM-SNM and OFDM-IM is less than that used in the classical OFDM, their PAPR performances remain high and comparable to the plain OFDM. This is due to the sparsity nature of the activated subcarriers in OFDM-SNM or OFDM-IM. The PAPR of OFDM-PSM is also high as in the conventional OFDM, due to the superimposed pulses within the same time-frequency region that results in a significant increase of the peak power of the transmitted signal. For a large number of subcarriers, the SM-OFDM attains similar PAPR performance compared to the V-BLAST OFDM system [128].

Besides the PAPR as one way to assess the PE of a given modulation scheme, there could be another way to evaluate the PE by considering the inactive subcarriers. A reduction in power consumption is expected in some modulation schemes, such as OFDM-SNM and OFDM-IM, which have some inactive subcarriers of zero power while its active subcarriers only carry data symbols. The average power per active subcarrier in OFDM-IM is $\frac{P_t}{aN}$. Observing a active subcarriers in the OFDM-SNM subblock of b available subcarriers follows a binomial distribution of N_c as a random variable

$$\mathrm{P}(N_c = a) = \binom{b}{a} \mathrm{p}^a (1 - \mathrm{p})^{b-a}. \tag{3.69}$$

It is assumed that the allocated power to the OFDM-SNM block (P_t) is equally distributed to its subblocks. Therefore, a fair comparison between OFDM-SNM and its competitive schemes is possible. The power consumed in OFDM-SNM could be formulated as [19]

$$P_c = \frac{P_t}{G\ b} \sum_{g=1}^{G} a(g)\ \mathrm{P}(N_c = a(g)), \tag{3.70}$$

where $a(g)$ is the number of activated subcarriers in the g-th subblock. Thus, the average power assigned for each subcarrier is

The SM-OFDM scheme is considered as an energy-efficient transmission scheme since the power consumed at its transmitter does not depend on the number of transmit antennas [129]. **Figure 3.10** shows the PE that can be achieved due to not sending on all OFDM

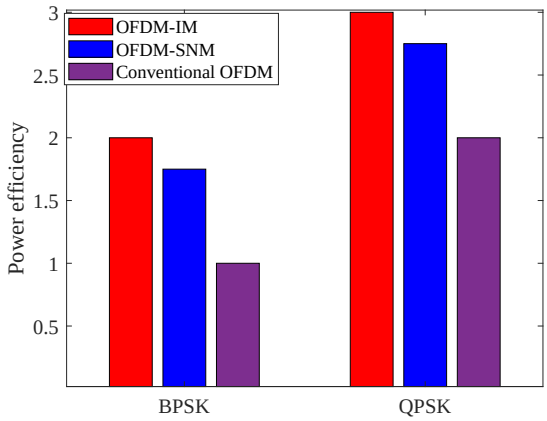

Figure 3.10: PE of OFDM-IM, OFDM-SNM, and conventional OFDM.

subcarriers of some featured OFDM modulation schemes such as OFDM-IM, OFDM-SNM, and classical OFDM under BPSK and QPSK. For a fair comparison between the aforementioned schemes, an average of unit transmit power per subcarrier is assumed. In **Figure 3.10**, this PE value is calculated as

$$P_{eff} = \frac{N_b}{K_a \, P_S}, \tag{3.71}$$

where K_a represents the average number of active subcarriers, P_S is power assigned for each subcarrier which is assumed to be unity, N_b is the total number of bits per block, which is computed as

$$N_b = K_a \, N_s \, N_a, \tag{3.72}$$

where N_s is the number of bits corresponding to M-ary complex symbols employed on each active subcarrier, N_a is the number of extra transmitted bits by a transmitting entity (or entities) like index modulus observed in OFDM-IM or number modulus in OFDM-SNM. It is observed from **Figure 3.10** that the OFDM-IM obtains enhanced PE over OFDM-SNM and plain OFDM due to the less average number of active subcarriers in OFDM-IM compared to its counterparts.

3.5.4. Out-of-band leakage

Frequency localization is advantageous for efficient spectrum utilization and multiplexing of various 5G services on single carrier using diverse waveform numerologies. In OFDM, side-lobes are observed due to the multiple subcarriers of Sinc-shaped. Particularly, larger side-lobes lead to high OOB leakage, which is one of the major setbacks in the OFDM system [13]. Therefore, it is required to have new modulation options with considerable low levels of OOB leakage.

As proved in [10], the OOBE leakage is almost the same for the featured modulation schemes including OFDM-SNM, OFDM-IM [130], OFDM-DM, and classical OFDM. Particularly, the sparse distribution of the activated subcarriers in the OFDM-SNM and OFDM-IM transmission blocks causes this high OOBE leakage. Moreover, the OOB leakage of SM-OFDM reaches a minimal level due to activating single transmitting antenna once at a time which considerably lowers the interference between the transmitting antennas. Exploiting localized pulses such as HG pulses in OFDM-PSM contributes to having less OOBE leakage as compared to the non-localized pulses used in the plain OFDM.

3.5.5. Computational complexity

The baseband complexity is critical at the UE, particularly at the receiver side. Also, a low baseband complexity speeds the processing and allows low latency applications. The assessment tool used in the complexity analysis is the required number of complex operations in each subcarrier. Channel estimation or equalization operations are not considered in the analysis. Moreover, perfect synchronization is assumed in the analyzed transmission schemes. The classical OFDM is considered as an efficient scheme in terms of computational complexity due to the employed IFFT and FFT process to the OFDM system. The conventional OFDM and OFDM-DM are considered as low-complex schemes and their computational complexities rely on the employed modulation order. Moreover, the OFDM-IM scheme with near-optimal log-likelihood ratio detector has comparable complexity to the conventional and differential transmission schemes for OFDM waveform. On the other hand, the complexity of the OFDM-SNM scheme can be seen in its subcarrier activation process in each subblock as well as the used modulation order.

$$\tilde{C}_{CP}(k,i) = \frac{\left|\sum_{j=1}^{N_{CP,k}} y\left[n_s + j\right]^* y\left[n_s + N_k + j\right]\right|}{\sqrt{\sum_{j=1}^{N_{CP,k}} \left|y\left[n_s + j\right]\right|^2}\sqrt{\sum_{j=1}^{N_{CP,k}} \left|y\left[n_s + N_k + j\right]\right|^2}} \tag{3.73}$$

The evaluation of the computational complexity of the OFDM-PSM is based on the number of polyphase components (R) of the filter, length of filter (U), HG function order (D), and the used modulation order (M) [100]. As the modulation order, number of transmitting and receiving antennas (N_T, N_R) increase, the SM-OFDM complexity increases [131]. The SM-OFDM transmission could be handled by only a single RF chain and a switch since a single transmit antenna activated at each time instant. Moreover, the number of mapped bits in the SM-OFDM scheme are limited in case of using a small number of antennas in a wireless device.

3.6. Blind Numerology Identification For Mixed Numerologies

We discuss the proposed identification algorithms based on the characteristics of numerology transmission. The autocorrelation method is commonly used in the literature for signal detection. We adopted a CP correlation method based on the periodicities brought by the CP signals in different numerologies. This approach is built based on the fact that the maximum point of the time-domain metric corresponds to the starting point of an OFDM symbol. For each numerology, we can independently obtain different timing metrics.

We assume that the receiver has no prior information about numerology parameters. More specifically, SCS, data/CP durations are not known at the receiver. Therefore, we employ our method with all possible numerology parameters. To identify the candidate numerology for the u-th user, the received composite OFDM signal (y) is correlated with all possible CP signals in y. The absolute values of the normalized correlation of y for the u-th user at the position $i = n_s \mod (N_k + N_{CP,k})$ are calculated by (9), where $n_s = 0, 1, ..., N + N_{CP} - 1$ represents the sample index.

We consider finding the first two highest peaks in the first OFDM symbol of each numerology as

$$i_{p1} = \arg\max_{i_1} \left\{ \tilde{C}_{CP}(k, i_1) \right\},$$
$$i_{p2} = \arg\max_{i_2} \left\{ \tilde{C}_{CP}(k, i_2) \right\}, \quad \textbf{(3.74)}$$

where $i_1 = 0, 1, ..., (N_k + N_{CP,k})/2 - 1$ and $i_2 = (N_k + N_{CP,k})/2, (N_k + N_{CP,k})/2 + 1..., (N_k + N_{CP,k}) - 1$. Afterward, the calculated distance between the peaks of the candidate numerology can be found as follows:

$$\Delta f_{\hat{k}} = |i_{p2} - i_{p1}|. \quad \textbf{(3.75)}$$

If $\Delta f_{\hat{k}}$ corresponds to the numerology with Δf_k whose order is defined in the set χ, then a correct identification of numerology type as $\Delta f_{\hat{k}}$ is achieved. The proposed time-domain identification algorithm is summarized in Algorithm **3.1**.

Algorithm 3.1 The proposed time-domain identification algorithm

1: $\tilde{C}_{CP}(k, i) \leftarrow$ Correlate the CP signal for the u-th user in y.
2: $i_{p1}, i_{p2} \leftarrow$ Evaluate the positions of the first two highest correlation peaks as in (10).
3: $\Delta f_{\hat{k}} = |i_{p2} - i_{p1}| \leftarrow$ Estimate the FFT size of the candidate numerology.
4: **if** $\Delta f_{\hat{k}} \in \chi$ **then**
5: Correct identification of numerology type.
6: **else**
7: Incorrect identification of numerology type.
8: **end if**

The frequency-domain offers reliable results about signals in the communication systems. After identifying the numerology in the time domain using Algorithm 1, we can detect its location by exploiting its characteristics in the frequency domain. The time-domain samples are transferred to their corresponding frequency-domain ones.

The CP of the numerology, whose type is identified in the time domain, is removed from y, and the resultant signal given as y_k. Afterward, the FFT operation with a length of N_k is employed to y_k to get the subband signal of the u-th user in the frequency domain ($\mathrm{y}_{F,u}$). The location of the candidate numerology is detected by observing the lowest amplitude variation in the absolute response of $\mathrm{y}_{F,u}$ (i.e. $|\mathrm{y}_{F,u}|$) for the U subbands. More specifically, the variation coefficient (V_u) is calculated for each subband as

$$V_u = \sigma/\mu$$
$$= \frac{\frac{1}{N_k-1}\sum_u \left||\mathrm{y}_{F,u}| - \frac{1}{N_k}\sum_u |\mathrm{y}_{F,u}|\right|^2}{\frac{1}{N_k}\sum_u |\mathrm{y}_{F,u}|}, \tag{3.76}$$

where σ and μ represent the sample variance and mean over a specific band in $|\mathrm{y}_{F,u}|$ with a length of N_k. The location of the candidate numerology is estimated based on the obtained V_u values as

$$\hat{u} = \arg\min_u \{V_u\}. \tag{3.77}$$

From (13), the numerology of the $\hat{u}$-th user subband is identified as Δf_k. Since the FFT operation is employed based on N_k, the $\hat{u}$-th user subband with the minimum V_u value identifies the numerology for the u-th user subband as $\Delta f_k^{\hat{u}}$. If there is no mismatch between numerologies of the users as $\Delta f_k^{\hat{u}} = \Delta f_k^u, \forall u$, then a correct identification of numerology location is achieved. Otherwise, an incorrect identification occurs, and it introduces extra bit errors besides the error bits in the detection of the conventional symbols in the classical mixed-numerology system. The step-by-step procedure of the proposed frequency-domain algorithm can be summarized, as shown in Algorithm **3.2**.

Algorithm 3.2 The proposed frequency-domain identification algorithm

1: $\mathrm{y}_k \leftarrow$ Remove the CP signal part of the candidate numerology from y.
2: $\mathrm{y}_{F,u} \leftarrow$ Employ FFT with length N_k to y_k.
3: $|\mathrm{y}_{F,u}| \leftarrow$ Find the amplitude response of $\mathrm{y}_{F,u}$.
4: $V_u \leftarrow$ Find the variation coefficient for each band in $|\mathrm{y}_{F,u}|$.
5: $\hat{u} = \arg\min_u \{V_u\} \leftarrow$ Estimate the location of the candidate numerology.
6: **if** $\Delta f_k^{\hat{u}} = \Delta f_k^u, \forall u$ **then**
7: Correct identification of numerology location.
8: **else**
9: Incorrect identification of numerology location.
10: **end if**

To evaluate the robustness of the proposed method, its BER performance is compared with the theoretical results of the conventional OFDM that are formulated for binary phase shift keying (BPSK) transmissions over AWGN and Rayleigh fading channels as [132]

$$P_b = \frac{1}{2}\mathrm{Q}(\sqrt{2SNR}) \tag{3.78}$$

and

$$P_b = \frac{1}{2}\left(1 - \sqrt{\frac{SNR}{SNR+1}}\right), \tag{3.79}$$

where $Q(.)$ is the standard Q-function [104] and $SNR = E_b/N_{o,T}$ (E_b and $N_{o,T}$ represent the bit energy and the noise variance in the time domain, respectively).

The computational complexity is evaluated per detected numerology for the proposed method and the non-blind identification approach. The autocorrelation method adopted in Algorithm 1 (step 1) involves $N_{CP,k}$ multiplications and additions for a limited number of lags. The maximum operation used in step 2 of Algorithm 1 has a complexity order of $O(N_k + N_{CP,k})$. Step 3 in Algorithm 1 requires constant time complexity. The complexity of the conditional operation (step 4 to 8 in Algorithm 1) is based on U. The FFT, variation coefficients calculations, minimum, and conditional operations are performed in Algorithm 2. The complexity order of FFT is $O(N_k \log_2 N_k)$ [133], and $U \times M_k$ additions/subtractions are needed to find the variation coefficients for the whole used band. Minimum and conditional operations have a complexity of the order $O(U)$. Thus, the overall complexity level of the proposed method is linear-logarithmic.

3.7. Identification Of The Number Of Wireless Channel Taps Using Deep Neural Networks

In the following **Subsection 3.7.1**, we will discuss the underlying system model and present a summary of it. Then, we present the datasets generation and simulation setup in **Subsection 3.7.2**.

3.7.1. System model

With different wireless environments, the number of channel taps (L) varies due to different propagation paths. Therefore, it is necessary to identify L in the CIR since it is usually unknown in practical scenarios.

The k-th observation ($k = 1, 2, ..., K$) of the j-th channel class ($j = 1, 2, ..., J$) can be represented as

$$\mathrm{r}_j^{(k)} = \left[\mathrm{x}^{(k)}\ \mathrm{y}^{(k)}\right]_j^T, \tag{3.80}$$

where $(.)^T$ is the transpose operation, $\mathrm{x}^{(k)}$ and $\mathrm{y}^{(k)}$ represent the k-th instance of $x(t)$ and $y(t)$ for the j-th class of channels that is characterized by a specific number of taps.

Our problem is focused on finding a maximally sparse vector c of length M such that $\mathrm{r}_j^{(k)}$ with length N can be represented by the fewest number of features in a feasible region. The m-th value of c is related to the m-th value of h as

$$\mathrm{c}_m = \begin{cases} 0 & \text{if } h_m = 0 \\ 1 & \text{if } h_m \neq 0 \end{cases} \tag{3.81}$$

where $m = 1, 2, ..., M$.

In general, the aforementioned problem is considered an optimization problem given by [1] as

$$\begin{aligned} \min_{\mathrm{c}} \quad & \|\mathrm{c}\|_0 \\ \text{s.t.} \quad & \mathrm{r}_j^{(k)} = \mathrm{W}\mathrm{c} \end{aligned} \tag{3.82}$$

where $||\mathrm{c}||_0$ denotes l^0 norm, which counts the non-zero elements in c, reflects the number of channel taps. W is a known, overcomplete dictionary of feature vectors with size $N \times M$ where $M > N$. These vectors provide an indirect measurement for CIR [134]. If there is a strong coherence between columns of W, then the sparse recovery estimation shown in (6) could be significantly poor. It has been proven that the existing DNNs can efficiently deal with coherent dictionaries and adversarial restricted isometry property constant [1].

Inspired by the featured characteristics offered by the DNN in [1], we employ a similar DNN, and its detailed structure can be found in **Figure 3.11**.

To improve the performance of the used network, we incorporate some modifications by introducing two Dropout layers to the DNN proposed in [1]. These Dropout layers offer regularization to avoid overfitting.

The adopted DNN includes fully-connected layers with non-linear transformation functions. In particular, the feed-forward design comprises fully-connected layers with 300 neurons and batch normalization. The batch normalization is incorporated in the designed DNN to provide a reasonable initialization. Simple Rectilinear units (ReLU) tend to promote sparse features by deactivating weights with negative values. The used non-linear

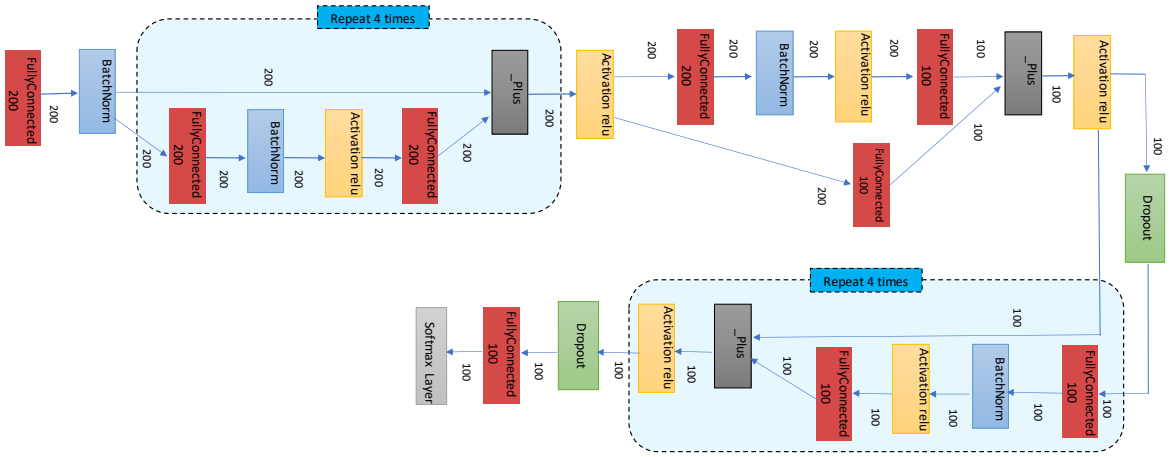

Figure 3.11: Basic network structure [1].

unit is

$$f(u) = u\,\mathrm{sign}(\max\{|u| - \alpha, 0\}), \tag{3.83}$$

where sign(.) represents the sign function and α denotes the shrinkage parameter.

Also, a final softmax layer is included, which yields a vector p of length J. For the loss function, we used the cross-entropy loss function, which is defined as

$$CE = -\sum_{j=1}^{J} g_j \log\left(p_j\right), \tag{3.84}$$

where g_j represents the ground truth for the j-th class of channels for a given observation, and $p_j \in [0, 1]$ provides an assessment of the likelihood that the subject channel belongs to the j-th class.

3.7.2. Methodology

Here, the datasets generation and simulation setup are presented.

3.7.2.1. Training Data Generation

Here, we import the measurement-based channel datasets from the NYUSIM simulator [135]. This simulator is an open-source 5G and 6G channel model software. The existing channel simulators, such as Quasi Deterministic Radio channel Generator

(QuaDRiGa) [136], have not been developed based on extensive propagation measurements at centimeter-wave to mmWave bands in diverse scenarios for 5G wireless systems. However, NYUSIM has been built based on extensive field measurements at mmWave bands in different outdoor environments, including urban microcell, urban macrocell, and rural macrocell environments. Another feature found in NYUSIM is that it can recreate wideband power delay profiles/CIRs and channel statistics for a broad set of frequencies, beamwidths, bandwidths, wireless channel scenarios, etc. [135]. Moreover, the NYUSIM simulator generates a realistic three-dimensional statistical spatial CIRs as represented in (2).

3.7.2.2. Simulation setup

The parameters of the conducted simulations are chosen to be similar to that of the default simulation setup in [135] for the spatial channel model using NYUSIM. The selected parameters are suitable in 3GPP and other standard bodies as well as industrial/academic simulations.

The transmitted signals with an arbitrary size of 1000×1 are sent through different wideband frequency-selective channels with the generated CIR of a length corresponding to the number of multipath components. Then, the complex-valued received signals with their corresponding number of channel taps are used as the training dataset. The samples of both the sent signal and the received signal are assigned to the DNN's inputs. On the other hand, the output is equal to the number of wireless channel taps. The received signal corresponding to the largest CIR is of length 1499, where real values are concatenated with its imaginary values. The dataset includes several channel realizations, consisting of 222 different channel classes in terms of the number of channel taps.

The DNN is implemented and trained using the Keras framework on Google Colaboratory service graphical processing unit (GPU). The training process is performed until a stop criterion is satisfied. The hyper-parameters selection is critical to the performance of DNN and they are determined empirically. The batch size is 128 and the learning rate follows a scheduler. The initial value of learning rate is 0.001 and decreases by a factor of 0.8 when the training accuracy forms a plateau for 18 epochs. Our DNN is trained with Adam optimizer [137] due to its computational efficiency, fast, and smooth convergence. The generated dataset size is 30K observations which are divided into 70% training data, 15%

validation data, and 15% test data.

The developed DNN is also compared with the existing SWISS algorithm [49]. **Table 3.10** shows the simulation parameters of the SWISS algorithm. It is proven in [49] that choosing a proper threshold (η) becomes a more difficult problem as the number of paths increases, which limits the achievable accuracy performance of the SWISS algorithm.

Table 3.10: The considered parameters for the SWISS algorithm.

Threshold (η)	0.995
Number of pilots	128
Pilot energy	1
Modulation type	BPSK
Number of OFDM subcarriers	512
Number of OFDM symbols	2
Root-finding method	Newton's method [138]
Initial guess in Newton's method	1
Number of iterations in Newton's method	10
Error tolerance in Newton's method	0.001

3.8. Radar-Aided Communication Scheduling Algorithm For 5G And Beyond Networks

We provide a summary of the fundamental system model in **Subsection 3.8.1**. Then, we present the radar and communication models in **Subsection 3.8.2** and **Subsection 3.8.3**.

3.8.1. System model

We investigate a radar echo-based scenario where a radar echo is reflected from the radar target [65]. In this scenario, the echo is exploited to obtain different scheduling parameters, such as target(s) range, velocity, and SINR information.

We consider a mmWave vehicle-to-infrastructure (V2I) communication system, e.g., supported through 5G cellular network, where mmWave BSs serve as infrastructure for V2I communications. A monostatic radar system is collocated on the BS, which receives the radar echos from the surrounding targets, as illustrated in **Figure 3.12**. When a moving target is detected by the radar, the raw echo signal is sent to the communication module at the BS. Side information derived from radar mounted on the infrastructure operating in a

given mmWave band is used to schedule the available resources of the vehicular communication system [94]. The objective of the considered system is to schedule the available resources in the BS relying on information extracted from the radar echo.

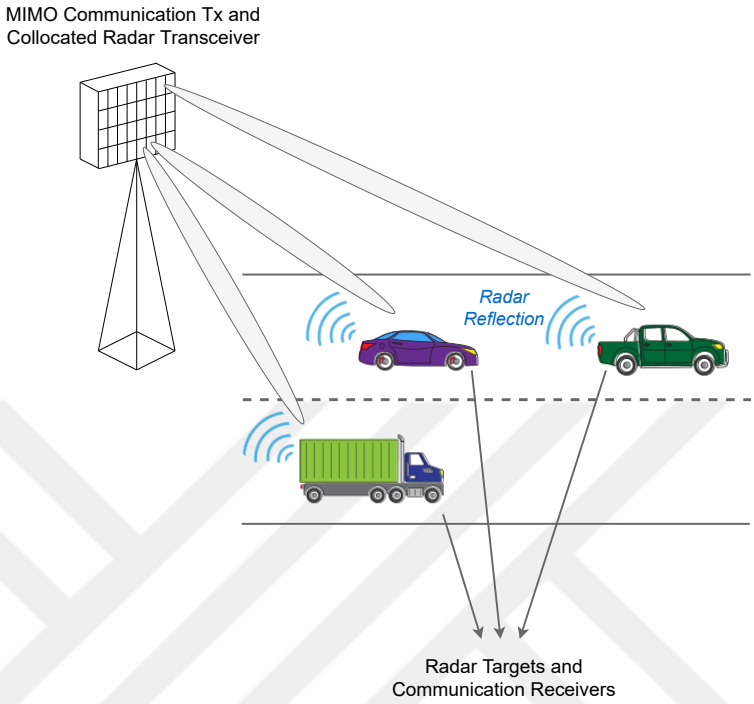

Figure 3.12: The system model where the radar information at the BS is leveraged to schedule the resources of multiple mobile users.

The system under consideration in this study comprises of a BS and multiple mobile users which act as radar targets and also as communication receivers. The BS has two major components: (i) A phased array-equipped mmWave communication terminal to communicate with the mobile users, and (ii) a collocated radar system using frequency modulated continuous wave (FMCW) signal. Next two subsections briefly cover the radar and communication component system and signal models. [94].

3.8.2. Radar model

An FMCW radar signal is used by BS in the system under consideration. This radar was designed to collect data about the surroundings through sensing it. FMCW radars transmit chirp signals whose frequency varies continually. The FMCW radar transmits a linear chirp signal that starts at f_c and linearly ramps up to $f_c + \mu t$, as shown by [94]

$$s_{\text{chirp}}^{\text{tx}}(t) = \begin{cases} \sin\left(2\pi\left[f_c t + \frac{\mu}{2}t^2\right]\right) & \text{if } 0 \le t \le T_c \\ 0 & \text{otherwise} \end{cases} \tag{3.85}$$

where $\mu = B/T_c$ is the slope of the linear chirp signal and B and T_c are its bandwidth and duration.

A single radar measurement is obtained from the frame of duration T_f. A chirp waves are sent in each frame, with T_s of time between each one. No more signals are sent until the end of the frame after the last chirp is transmitted. An expression for the radar frame's transmitted signal is [94]

$$s_{\text{frame}}^{\text{tx}}(t) = \sqrt{\mathcal{E}_t}\sum_{a=0}^{A-1} s_{\text{chirp}}^{\text{tx}}\left(t - a\left(T_c + T_s\right)\right), \quad 0 \le t \le T_f \tag{3.86}$$

where $\sqrt{\mathcal{E}_t}$ is the transmitter gain. The signal that is sent out is echoed by the target(s) in the environment, and the radar picks up the echo(s).

At the receiver, an in-phase and quadrature sample are made by mixing the send and receive signals in a quadrature mixer. Following that, the combined signals are applied to a low-pass filter. The result is a signal called the intermediate frequency (IF) signal, which shows the difference in frequency and phase between the signal being sent and the signal being received. If there is only one thing in the environment, the single chirp's receive IF signal can be written as [94]

$$s_{\text{chirp}}^{\text{rx}}(t) = \sqrt{\mathcal{E}_t\mathcal{E}_r}\exp\left(j2\pi\left[\mu\tau t + f_c\tau - \frac{\mu}{2}\tau^2\right]\right), \tag{3.87}$$

where $\sqrt{\mathcal{E}_r}$ is the channel gain of the object, which depends on the path loss and radar cross section, $\tau = 2d/c$ is the round-trip delay of the reflected signal through the object, where d represents the distance between the object and the radar, and c denotes the speed of light.

The receive IF signal, s_{chirp} is then sampled at the sampling rate of the analog to digital converter (ADC), f_s, producing S samples for each chirp. Finally, the ADC samples from each frame are collected. For an FMCW radar with M_r receive antennas, each having the described RF receive chain, the resulting measurements of one frame can be denoted by

$\mathrm{X} \in \mathbb{C}^{M_r \times S \times A}$. Given X, important parameters for the proposed scheduler, including the range and velocity of moving target(s) in the surroundings, are extracted. Once the IF signal is obtained by the correlation of the transmitted and received echo, the parameters are extracted through a range-Doppler matrix that is obtained by the 2D FFT method over each coherent processing interval [139]. It should be noted that the investigation of this method is not given in our work since it is out of the scope of the proposed MAC-based scheduler. After the radar information is extracted, they are fed into the communication module. In the following subsection, the communication model is described.

3.8.3. Communication model

The considered BS employs a mmWave OFDM-based transmitter with M_A antennas which is used to communicate with multiple single-antenna mobile users. Adopting a narrowband channel model with P paths, the channel between the k-th user and the BS can be expressed as [140]

$$\mathrm{h_k} = \sum_{p=0}^{P-1} \alpha_p \mathrm{a}\left(\phi_p, \theta_p\right), \tag{3.88}$$

where α_p denotes the complex gain, $\mathrm{a}\left(\phi_p, \theta_p\right)$ is the array response vector of the BS, and ϕ_p, θ_p represent transmit azimuth and elevation angles of the p-th path at BS. In the downlink, the BS transmits the data symbol s_d to the user via the beamforming vector $\mathrm{f} \in \mathbb{C}^{M_A}$. The receive signal at the k-th user can be written as

$$y_k = \sqrt{\mathcal{E}_c}\mathrm{h_k}^H \mathrm{f} s_d + n, \tag{3.89}$$

where $n \sim \mathcal{CN}\left(0, \sigma^2\right)$ is the additive white Gaussian noise (AWGN) with a variance of σ^2, and $\sqrt{\mathcal{E}_c}$ is the transmitter gain of the BS. The signal-to-noise ratio (SNR) measured at the k-th user can be written as

$$SNR_k = \frac{\mathcal{E}_c |\mathrm{h_k}^H \mathrm{f}| P_{s_d}}{\sigma^2}, \tag{3.90}$$

where $P_{s_d} = \mathbb{E}[|s_d|^2]$ is the average power of s_d. SINR quantity should be measured as a pertinent indicator of the system's merit due to the unwanted signal that is picked up from other interfering BSs. The SINR, expressed in dB, measured at the target user is calculated as the SNR received from the intended BS minus the sum of power received

from all other concurrently active BSs.

In the conventional communication CSI acquisition process, a known pilot signal is transmitted, and the communication beams are adjusted based on this signal [141]. The FMCW radar signal being a known signal, is used in the considered system to estimate the CSI for the communication users rather than transmitting additional pilots. As a result, pilot transmission overhead is reduced [139]. Furthermore, the radar measurements are leveraged to optimize the communication scheduler's performance. Based on the classical SINR measurements and the information gathered about the users from the echo signal, namely range (g_k) and velocity (v_k), the BS allocates its available resources to the users. The next section contains more information on the proposed multi-user scheduling scheme.

3.8.4. Proposed scheme

A new scheduling algorithm is proposed in this work based on the range, velocity, and SINR information collected from the radar echo signal reflected from a target. The positions and velocities of vehicles are estimated. With the assistance of the radar, it is much easier to detect and track moving vehicles. As shown in the field measurements in [142], the accuracy of position information provided by radar is higher than that provided by the Global Positioning System (GPS), resulting in a larger reduction in communication overhead when leveraging position information provided by a radar sensor than when leveraging GPS-based position. Based on the considered scheduling inputs, we set the following scheduling rules:

- UEs near the BS are prioritized due to low path loss; UEs in the center of the cell have a better channel quality indicator (CQI) and modulation scheme than UEs on the cell edge due to their proximity to the BS.
- Low-speed UEs are also prioritized due to their invariant channel conditions.
- UEs with better SINR are also prioritized due to their high power.

Figure 3.13 shows the scheduling priorities for a bad SINR scenario. Regarding the range parameter, the conventional relationship between signal strength and range in free space is that the power of radio signals decreases with the square of the distance (d). The SNR decreases with d due to path loss, so range knowledge can be utilized to estimate the

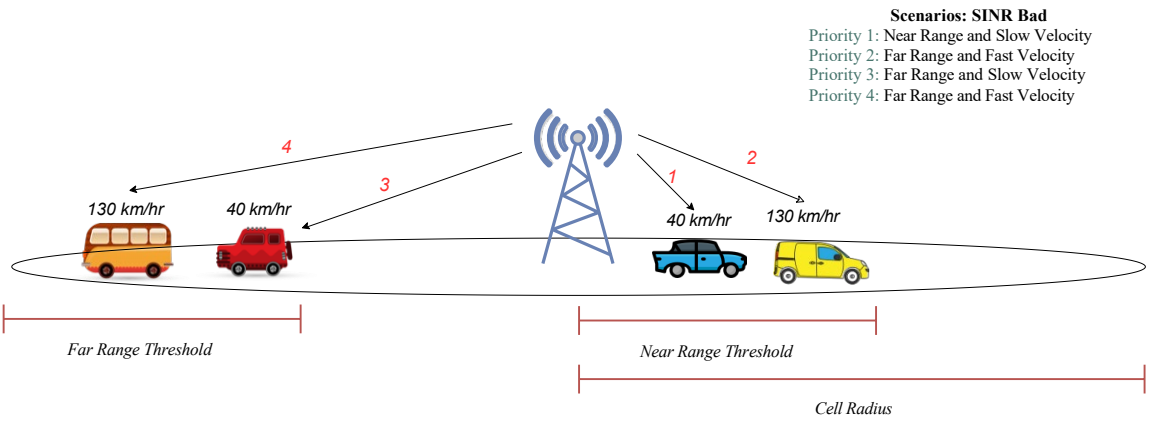

Figure 3.13: Scheduling priorities for bad SINR scenario.

received power and interference level. It should be noted that SINR should be high to receive the packet correctly. For example, the minimum required SINR could be 0 dB.

The range and velocity of the target can be extracted from the echo signal. The radar receiver uses different signal detection algorithms, e.g., correlation based methods [143]. Based on the considered coexistence communication and radar use cases, it is found that range and velocity are the critical metrics to be measured. **Figure 3.14** shows the proposed radar aided communication scheduler. We consider a DL transmission from BS to UE in a typical radar aided communication system.

Table 3.11: Use cases proposed by Hexa-X [3] along with selected performance metrics, based on [4]–[8].

Use cases	Range	Velocity
Smart city	< 200m	< 50 km/h
Health care	0.1 10 m	< 1 m/s
Transport cobots	< 200 m	< 100 km/h
Industrial cobots	< 200 m	< 30 km/h
Public safety/security	< 200 m	< 50 km/h
Mixed reality, gaming	< 10 m	< 10 km/h

The scheduling inputs are collected by the echo signal from the target. These inputs include range, velocity, and SINR information. The considered inputs are imported from the considered applications and use cases. Some numerical values of the considered inputs can be shown in **Table 3.11** [144]. It should be noted that the velocity metric, shown in **Table 3.11**, refers to the maximal (relative) velocity that should be supported.

Based on the considered scheduling inputs, we set proper scheduling rules. The range-based scheduling rule is set where UE near the BS is prioritized due to low path loss. The velocity-based scheduling rule is set where low-speed UEs are prioritized due to their invariant channel conditions. The SINR-based scheduling rule is set where UEs with better SINR are also prioritized due to their high power. We consider a scenario where multiple BSs and UEs exist in the communication network. In this case, SINR is measured since the interfering BSs cause interference to the desired UE served by its serving BS [145]. For simplicity, equal radar and communication transmit powers are assumed.

The estimated range and velocity from the considered system, as well as some of the assumptions made in the proposed scheme, are described further. Basically, the mutual distance between k-th UE and b-th BS, d_{bk} (km), can be found as [146]

$$d_{bk} = \sqrt{\left(m_{k,x_2} - m_{b,x_1}\right)^2 + \left(m_{k,y_2} - m_{b,y_1}\right)^2}, \tag{3.91}$$

where m_{k,x_2} and m_{k,y_2} represent the position of k-th UE in the x and y axis, respectively, and m_{b,x_1}, m_{b,y_1} denote the position of b-th BS in the x and y axis, respectively. Then, the path loss (dB) can be calculated as [147]

$$PL_{bk} = 32.45 + 20\log_{10}(d_{bk}) + 20\log_{10}(f_c), \tag{3.92}$$

where f_c represents the carrier frequency in MHz. The received power (dB) can be represented as

$$P_{bk}^{Rx} = P_{bk}^{Tx} - PL_{bk}, \tag{3.93}$$

where P_{bk}^{Tx} (dB) represents the transmitted power from b-th BS to k-th UE. Then, the SNR (dB) can be evaluated as follows:

$$SNR_k = P_{bk}^{Rx} - BN_0, \tag{3.94}$$

where N_0 is the power spectral density (PSD) of AWGN, and B represents the system bandwidth. The quality of the radio link between b-th BS and k-th UE can be measured by considering the interference effects caused by interfering BSs as

$$SINR_k = SNR_k - \sum_{v \in \mathbb{V}} P_{vk}^{Rx}, \tag{3.95}$$

where $\mathbb{V}$ is the set of interfering BSs and P_{vk}^{Rx} (dB) is the interference power received from the v-th interfering BS.

The goal of the proposed approach is to schedule BS transmissions so that the range (g_k), velocity (v_k), and SINR ($SINR_k$) are higher than specific threshold values g_{Th}, v_{Th}, and $SINR_{Th}$ for every UE k that can receive a transmission from a scheduled BS:

$$\begin{aligned} g_k &\geq g_{Th} \\ v_k &\geq v_{Th} \\ SINR_k &\geq SINR_{Th}. \end{aligned} \tag{3.96}$$

According to the SINR formulated in (**3.95**), the data rate of k-th UE can be expressed as

$$r_k = B \ \log_2(SINR_k) \tag{3.97}$$

The domain knowledge offered by the considered system provides a high reduction in communication overhead to extract g_k and v_k fed to the communication modules, thus enhancing SE (η). Furthermore, the accuracy in estimating g_k and v_k is proportional to the system throughput (ζ). Our scheduler maximizes r_k, η, and ζ. The decision variables that control the considered scheduler outputs are g_k, v_k, and $SINR_k$. The formulation of the objective function is shown as

$$\begin{aligned} \max_{g_k, v_k, SINR_k} \quad & r_k + \eta + \zeta \\ \text{s.t.} \quad & g_k \geq g_{Th} \\ & v_k \geq v_{Th} \\ & SINR_k \geq SINR_{Th} \end{aligned} \tag{3.98}$$

The values g_k^{opt}, v_k^{opt}, and $SINR_k^{opt}$ are optimally chosen using the classical trial and error method [148] to maximize the considered scheduling outputs. The employed trial and error method continues until the stopping criterion is satisfied. The selected values of the

considered scheduler outputs correspond to the optimal factors at the i-th TTI. Mathematically, the optimal solutions can be found as

$$\beta_{r_k} = \arg\max_i r_k^i \tag{3.99}$$

$$\beta_{\eta} = \arg\max_i \eta^i \tag{3.100}$$

$$\beta_{\zeta} = \arg\max_i \zeta^i \tag{3.101}$$

Algorithm 1 shows the step-by-step proposed radar-aided communication scheduling algorithm.

Algorithm 3.3 Radar-aided Communication Scheduling Algorithm

Input: The scheduling inputs.
Output: The scheduling outputs.
While stop criterion is not satisfied in i**-th** TTI

A. Pre-Processing
   1: **Acquiring scheduling inputs for all UEs:** $g_k, v_k, SINR_k$.
   2: **Acquiring the threshold values for the scheduling inputs:** $g_{Th}, v_{Th}, SINR_{Th}$.

B. Setting the scheduling rules
   3: **Check** if $g_k \geq g_{Th}$.
   4: **Check** if $v_k \geq v_{Th}$.
   5: **Check** if $SINR_k \geq SINR_{Th}$.
   6: **Else**
   7: **Go to Step 1**

C. Forming the optimization problem
   8: **Find** $\max_{g_k, v_k, SINR_k} r_k + \eta + \zeta$.

D. Finding the final output
   9: **Find** g_k^{opt}, v_k^{opt}, and $SINR_k^{opt}$
   10: **Set** $\beta_{r_k} = \arg\max_i r_k^i$
   11: **Set** $\beta_{\eta} = \arg\max_i \eta^i$
   12: **Set** $\beta_{\zeta} = \arg\max_i \zeta^i$

End

3.9. Dynamic-Structure Resource Block Allocation Based Scheduling For 5G Systems

Here, we introduce the proposed approach and system model. The system model of the D-RBS has been discussed in [2]. Using the same system model as shown in **Section 3.9**, we assumed that the used RBs in the considered D-RBS and S-RBS scenarios span by TTI of T (s) and BW of W (Hz). In the S-RBS, the size of the RBs is constant. As illustrated in **Figure 3.15a**, the considered S-RBS contains 8 RBs: 2 RBs with TTI of 1 ms and BW of 15 kHz, 2 RBs with TTI of 0.5 ms and BW of 30 kHz, and 4 RBs with TTI of 0.25 ms and BW of 60 kHz. On the other hand, the RB in the D-RBS is divided into small-sized RBs with time duration T_i (s) and frequency size W_i (Hz), where $T_i < T$ and $W_i < W$. The small-sized RBs of D-RBS have equal dimensions in the time and frequency domains, as shown in **Figure 3.15b**, with $T_i = 0.25$ ms and $W_i = 15$ kHz. Furthermore, different-sized RBs comprised of these small-sized RBs are assigned to UEs. The considered D-RBS offers 8×4 RBs, assigned to UEs that are flexibly multiplexed over some small RBs that may be non-contiguous in time and frequency.

As shown in **Figure 3.16**, the small-sized RBs are assigned to UEs requesting specific services. To guarantee meeting the requirements of the services, specific constraints should be set as follows [2]; In order to satisfy the extremely high peak data rate requirements of eMBB service, the minimum data rate constraints of k-th UE, that requests the eMBB service at b-th gNB, is represented by $R_{bk}^{min,e}$. On the other hand, massive machine type communication (mMTC) UEs require fixed, typically low, data rate and packet error probability on the order of 10^{-1} [149]. Thus, the maximum data rate constraints of k-th UE that requests mMTC service should be equal to $R_{bk}^{min,m}$. Moreover, the packet error probability of k-th UE requesting mMTC service in the i-th small-sized RB (ϵ_k^i) has a maximum value of $\epsilon_{bk}^{max,i}$. Due to the delay limitation of URLLC UEs, each URLLC UE should be assigned to only one column of small RBs. This could be done by the binary-valued factor that determines the association of the small-sized RB i to k-th UE in b-th gNB is s_{bk}^i, i.e., $s_{bk}^i = 1$ when b-th gNB allocates the i-th small-sized RB to k-th UE, otherwise, $s_{bk}^i = 0$.

After determining the D-RBS and its associated decision rules, a specific topology for the proposed approach is established. More specifically, the cellular topology with 7 gNBs is constructed in a single ring hexagonal structure, as shown in **Figure 3.17**. Static UEs are

distributed randomly across the region of interest, which is around 7×7 km in size. The mutual distance between k-th UE and b-th gNB, d_{bk} (km), can be found as follows [146]:

$$d_{bk} = \sqrt{\left(m_{k,x} - m_{b,x}\right)^2 + \left(m_{k,y} - m_{b,y}\right)^2}, \tag{3.102}$$

where $m_{k,x}$ and $m_{k,y}$ represent the position of k-th UE in x and y axises, respectively, and $m_{b,x}$, $m_{b,y}$ denote the position of b-th gNB in x and y axises, respectively. Then, the pathloss (dB) can be calculated as [147]

$$PL_{bk} = 32.45 + 20\log_{10}(d_{bk}) + 20\log_{10}(f_c), \tag{3.103}$$

where f_c represents the carrier frequency in MHz. The received power (dB) can be represented as

$$P_{bk}^{Rx} = P_{bk}^{Tx} - PL_{bk}, \tag{3.104}$$

where P_{bk}^{Tx} (dB) represents the transmitted power from b-th gNB to k-th UE. Then, the SNR (dB) can be evaluated as follows:

$$SNR_k = P_{bk}^{Rx} - WN_0, \tag{3.105}$$

where N_0 is the power spectral density (dBm/Hz) of the additive white Gaussian noise (AWGN). The quality of the radio link between b-th gNB and k-th UE can be measured by considering the interference effects coming from the interfering gNBs as

$$SINR_k = SNR_k - \sum_{v \in \mathbb{V}} P_{vk}^{Rx}, \tag{3.106}$$

where $\mathbb{V}$ is the set of interfering gNBs and P_{vk}^{Rx} (dB) is the interference power received from the v-th interfering gNB.

The transmission rate of k-th UE, R_k (bits/s), on any small-sized RB can be formulated based on the $SINR_k$ as

$$R_k = W \times \log_2\left(1 + SINR_k\right). \tag{3.107}$$

The UE α_{BCQI} in the BCQI scheduler is selected as [150]

$$\alpha_{BCQI} = \arg\max_{k} R_k. \tag{3.108}$$

On the other hand, the PF scheduler decides on the selected UE α_{PF} as

$$\alpha_{PF} = \arg\max_{k} \frac{R_k}{\overline{R_k}}, \tag{3.109}$$

where $\overline{R_k}$ represents the average transmission rate of k-th UE over a given time period. This interval should be short enough to avoid the effect of long-term differences in channel conditions while also being lengthy enough to account for short-term quality variations. It should be noted that the RR scheduler's transmission rate is low due to the fact that it serves all UEs regardless of their channel conditions.

The D-RBS based switching mechanism between RR and BCQI schedulers is examined in addition to using D-RBS based conventional schedulers. The dynamic process in [102] is proposed for throughput and fairness balancing by sensing the SNR to switch between RR and BCQI and get the best assignment of RBs in the considered system. A practical assumption is considered where CSI of UEs is acquired. The SNR of each accessed UE is measured, and a threshold value of -10 dB is chosen since the BCQI achieves good throughput at high SNR. The RB occupancy for each TTI is examined in relation to the remained RBs (N_{RBr}) out of the available RBs (N_{RBn}).

The steps of the proposed approach are summarized as follows; 1) The existing D-RBS scheme is employed. 2) The conventional schedulers, including RR, PF, and BCQI are adopted based on the D-RBS. 3) The D-RBS based switching mechanism between RR and BCQI scheduling algorithms is employed. 4) To evaluate the performance of the proposed approach, data rate, system throughput, and SE are used.

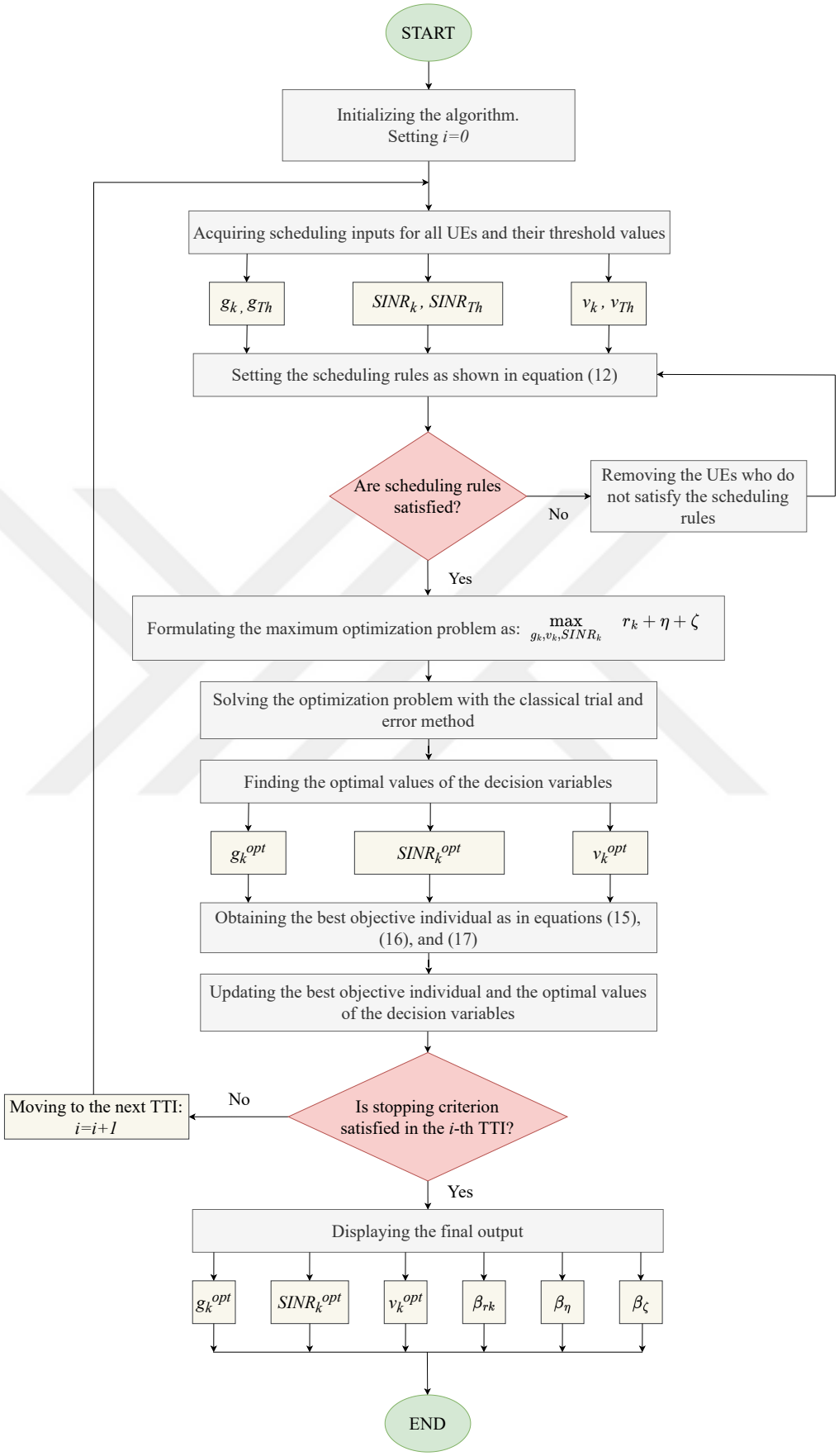

Figure 3.14: The proposed scheduling algorithm.

a): S-RBS. **b):** D-RBS.

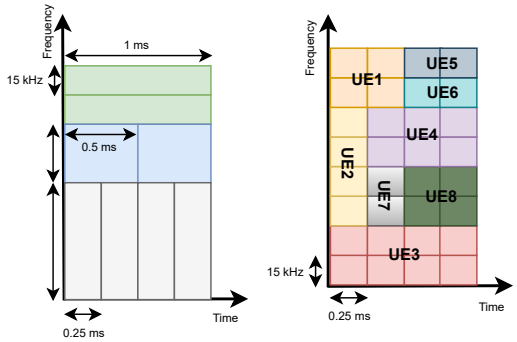

Figure 3.15: The S-RBS and D-RBS schemes [2].

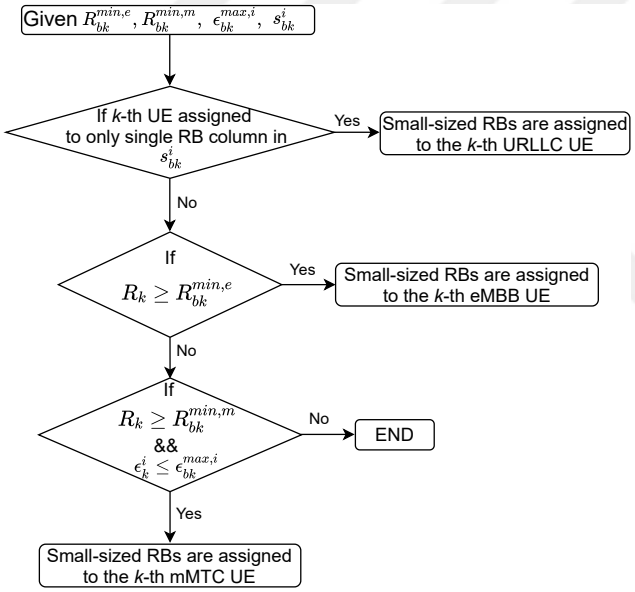

Figure 3.16: D-RBS decision rules for UEs requesting 5G services.

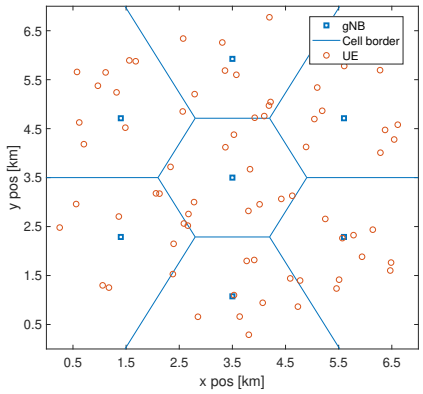

Figure 3.17: Simulation network layout.

CHAPTER 4

4. RESULTS AND DISCUSSION

4.1. The OFDM With Subcarrier Modulation

Simulation results are carried out in this section 4.1.

The BER and throughput performances of OFDM-SNM system are simulated and compared with both standard OFDM and OFDM-IM. The simulation parameters used are shown in **Table 4.1**. It is assumed that the multi-path channel is Rayleigh distributed. **Figure 4.1** shows BER vs. $E_b/N_{o,T}$ of the OFDM-SNM system compared to its competitive systems such as conventional OFDM, OFDM-IM [17] (with $K = 2$ and $N = 4$) and OFDM-GIM [26] (with $N = 4$ and $K = [1, 2, 3]$). As seen from **Figure 4.1**, both OFDM-SNM and OFDM-IM have similar BER performance which is better than that of classical OFDM for high SNR values (SNR > 10 *dB*). Also, it is observed that the BER can be improved further when interleaving is adopted [151].

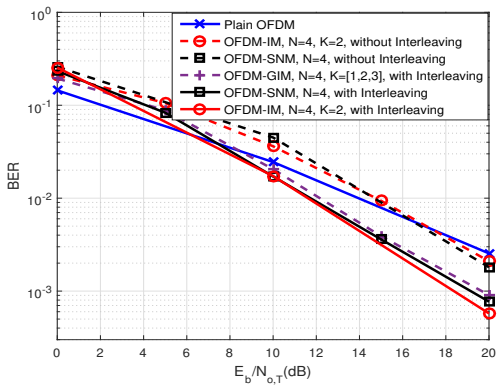

Figure 4.1: BER of OFDM-SNM compared to conventional schemes.

Figure 4.2 demonstrates that the throughput performance of the OFDM-SNM (in both cases when CP is included and excluded from the throughput calculation) is better than

Table 4.1: Simulation parameters.

Modulation type	BPSK ($M = 2$)
IFFT/FFT size (N_F)	64
CP Guard Interval (samples)	8
Number of subblocks in each OFDM symbol (G)	16
Number of available subcarriers in each subblock (N)	4
Number of bits mapped to each subblock (p_1)	2
Multipath channel delay samples locations	[0 3 5 6 8]
Multipath channel tap power profile (dBm)	[0 -8 -17 -21 -25]

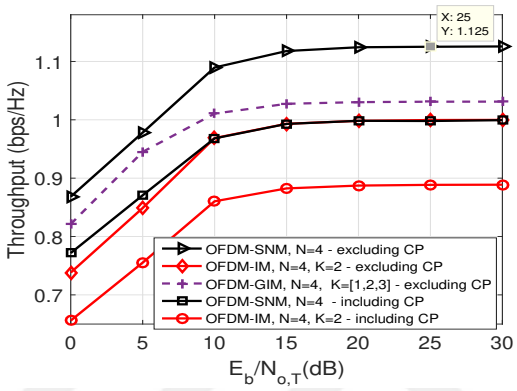

Figure 4.2: Throughput of OFDM-SNM compared to conventional schemes.

that of OFDM-IM by a factor of 1.125 and than that of OFDM-GIM by a factor of 1.1 at equivalent BER performances.

4.2. The OFDM With Hybrid Number And Index Modulation

Simulation results are carried out in this section 4.2. Throughput, BER, and PAPR performance metrics of the hybrid scheme are compared to those of OFDM-GIM. We assume that the number of allowed active subcarriers of the OFDM-GIM is one, two, or three out of four available subcarriers in each subblock [26]. The proposed scheme is also compared with the OFDM-IM, OFDM-SNM, and conventional OFDM.

It is assumed that FFT size is $N_F = 64$, subblock length is $L = 4$, and $p_1 = p_2 = \log_2(L) = 2$ bits for each subblock. The modulation used in simulations is BPSK. A Rayleigh fading frequency-selective channel with an impulse response of length 9 and normalized power delay profile given by $\varrho = [0.8407, 0, 0, 0.1332, 0, 0.0168, 0.0067, 0, 0.0027]$ mW is considered [152]. We assume here that the CP length (N_{CP}) is longer than the effective CIR,

and there is no Doppler effect. For a fair comparison, the same SNR ($E_b/N_{o,T}$) level is assumed for all schemes, where E_b is the bit energy. The number of iterations in the conducted Monte Carlo simulations is 8000. The proposed OFDM-HNIM scheme is evaluated under ideal channel conditions and imperfect CSI to assess its robustness.

4.2.1. Performance of the proposed OFDM-HNIM scheme under ideal channel conditions

Figure 4.3 and **Figure 4.4** shows the throughput performance of the OFDM-HNIM scheme compared to its competitive schemes under different modulation types. In the conducted simulations, the throughput is calculated by multiplying the SE for a given modulation scheme with BER subtracted from one. At very high SNR, the possible rates or SEs for all the schemes reach their maximum values. These SE values are dependent on the mapping between incoming bits, SAPs, and conventional symbols. As demonstrated in **Figure 4.3**, the hybrid scheme's SE is 1.33 bits/s/Hz with SE gains of 0.44, 0.33, and 0.3 compared to OFDM-IM, conventional OFDM, OFDM-SNM, and OFDM GIM, respectively, at BPSK modulation. The reason behind the superiority of the hybrid scheme over other schemes using BPSK modulation is due to the low noise and interference effects in lower-order modulation in addition to the additional data transmitted by indices and the number of active subcarriers. This illustrates that OFDM-HNIM has better SE than OFDM-IM and OFDM-SNM, which solely use subcarrier indices or numbers to send additional data bits.

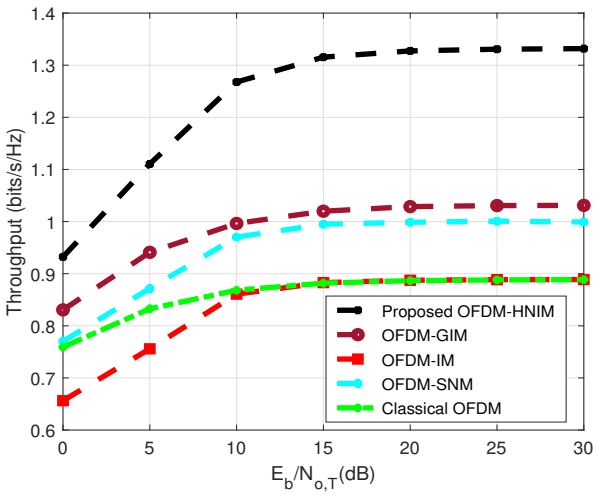

Figure 4.3: Throughput performance over the available OFDM subcarriers of the proposed scheme and its competitive schemes under BPSK.

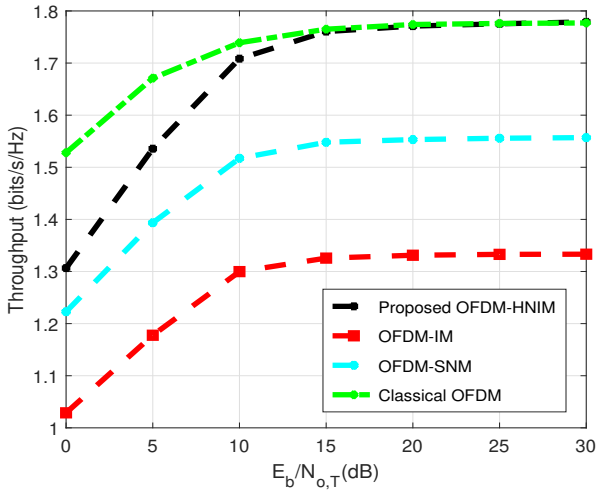

Figure 4.4: Throughput performance over the available OFDM subcarriers of the OFDM-HNIM scheme and its competitive schemes under QPSK.

The throughput performances of the featured OFDM-based schemes under QPSK are shown in **Figure 4.4**, where SE superiority of the OFDM-HNIM scheme also seen over the OFDM-IM and OFDM-SNM schemes. However, the classical OFDM outperforms the OFDM-HNIM in terms of throughput under QPSK at low SNR values due to the sparse distribution of active subcarriers in the proposed hybrid scheme, OFDM-SNM, and OFDM-IM schemes.

Figure 4.5 shows the BER performance of the featured OFDM-based modulation options under BPSK. The transmitters of the investigated schemes have the same total power, and the inactive subcarriers' power is evenly transferred to the active ones. The hybrid system's ISAPE-based detector had a lower BER than the PSAPE detector due to three error sources.

As shown in **Figure 4.5**, using the LLR detector with the proposed OFDM-HNIM scheme provides the best performance in the SNR range of interest. Employing PSAPE and ISAPE detectors, on the other hand, results in non-competitive BER performance, especially in the high SNR region. This is due to the weaker protection offered to the number and index-modulated bits compared to conventionally modulated ones, leaving them prone to a higher number of errors. Moreover, due to the high ratio of number and index-modulated bits, their impact on BER is magnified. Furthermore, **Figure 4.5** shows reasonable theoretical ABEP results to that using computer simulations as SNR increases, which proves the correctness of the theoretical analysis.

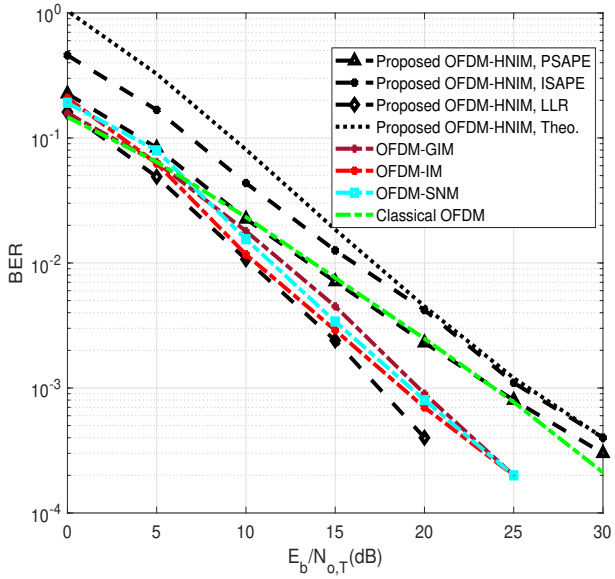

Figure 4.5: BER of the proposed scheme, OFDM-GIM, OFDM-IM, OFDM-SNM, and classical OFDM under frequency-selective Rayleigh channel with BPSK.

To have a fair comparison between the proposed scheme and its competitive schemes under equivalent SE, their BER performances are simulated under the same SE. Particularly, the BER performance of the proposed scheme is compared to OFDM-IM and conventional OFDM, at equivalent SE of 1.78 bits/s/Hz, as shown in **Figure 4.6**. To attain this SE, the active subcarriers of each subblock of the proposed scheme are modulated by QPSK. While the active subcarriers, of the OFDM-IM and conventional OFDM, are loaded with 8-QAM and QPSK, respectively.

As shown in **Figure 4.6**, the proposed OFDM-HNIM significantly outperforms OFDM-IM and conventional OFDM schemes in terms of BER under equivalent SE of 1.78 bits/s/Hz. Particularly, the OFDM-HNIM scheme has much better BER performance over OFDM-IM at the low SNR region, but this considerable improvement degrades slightly for high SNR values. The reason behind this SNR-loss in OFDM-IM compared to the hybrid scheme at low SNR values is that the effective power per subcarrier in OFDM-HNIM is more than that of OFDM-IM due to having higher EE. This results in making the sensitivity of OFDM-IM to both noise and interference to achieve the same SE much higher as compared to the OFDM-HNIM scheme.

Figure 4.7 presents the complementary cumulative distribution functions (CCDFs) of the PAPR of the proposed OFDM-HNIM scheme compared to its counterparts. **Figure 4.7**

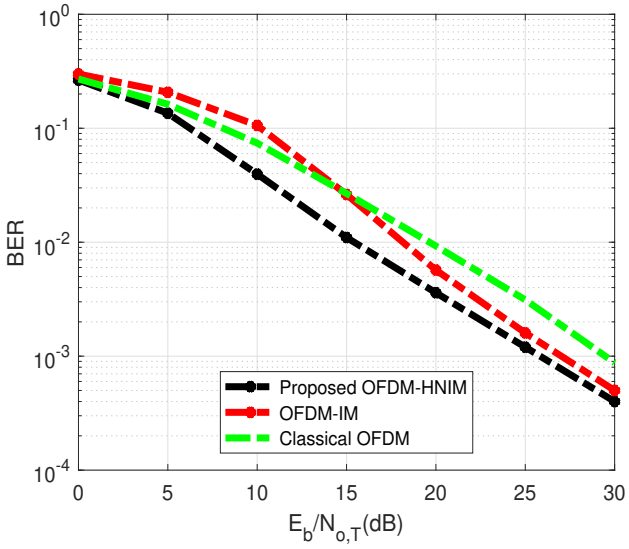

Figure 4.6: BER of the proposed scheme, OFDM-IM, and classical OFDM under frequency-selective Rayleigh channel with SE of 1.78 bits/s/Hz.

shows that the PAPR performances of these featured OFDM modulation options are high and almost the same as plain OFDM [10], [153]. The reason behind this high PAPR performance of the proposed OFDM-HNIM scheme is the sparsity nature of active subcarriers in OFDM-HNIM, which is also a problem in the conventional OFDM-SNM and OFDM-IM schemes. This inherent feature of having some inactive subcarriers in OFDM-HNIM, OFDM-SNM, and OFDM-IM schemes can be exploited to reduce the PAPR by designing a proper mapping while ensuring that the PAPR level is minimal. The proposed PAPR reduction techniques for conventional OFDM [154] may not be directly applied to non-conventional OFDM modulation schemes such as the OFDM-HNIM scheme. The reason behind this is having unique features and characteristics for different OFDM modulation options [10]. Therefore, we need proper, effective PAPR reduction methods to reduce the PAPR of the proposed OFDM-HNIM scheme, which is left for future works.

4.2.2. Performance of the proposed OFDM-HNIM scheme under imperfect channel estimation

The subcarrier activation in the proposed scheme, OFDM-SNM, and OFDM-IM schemes is dependent on the non-conventional bits, i.e. index and number bits for the proposed OFDM-HNIM scheme, and index bits for the OFDM-IM scheme. Therefore, channel estimation techniques developed for conventional OFDM cannot be applied directly to

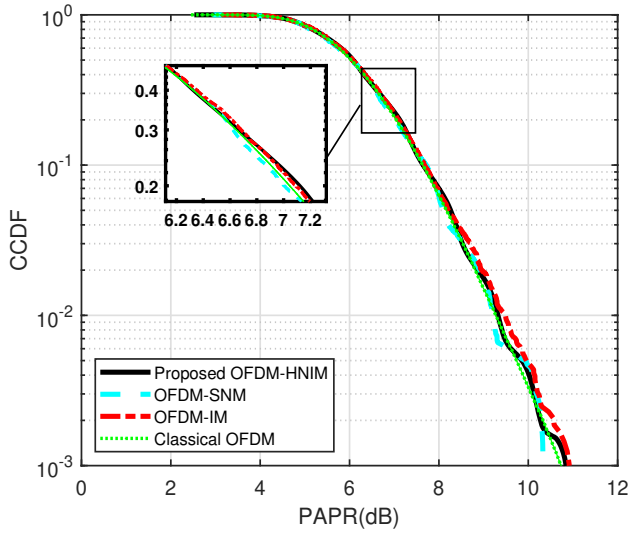

Figure 4.7: PAPR performances of the featured OFDM modulation options.

these schemes [155]. Some channel estimation methods for OFDM-IM have been proposed in [155] based on its subcarrier activation process. Particularly, pilot symbols are inserted in the frequency domain based on the active subcarriers for tracking the channel variation. After that, the existing interpolation algorithms, such as piecewise linear interpolation (PLI) [156], are applied to estimate the channel frequency response at data symbols. Based on the general principle of subcarrier activation in OFDM-HNIM and OFDM IM, the developed channel estimation techniques for OFDM-IM [155] could be applied to OFDM-HNIM.

It is assumed that the channel estimation process is performed before data transmission. The estimate version of the channel can be represented by an error vector added to the CIR vector ($\mathrm{h_t}$) as

$$\widetilde{\mathrm{h_t}} = \mathrm{h_t} + \boldsymbol{\epsilon}, \tag{4.1}$$

where $\boldsymbol{\epsilon} \sim \mathcal{CN}(0, \beta)$ represents the channel estimation error vector, which is independent of $\mathrm{h_t}$. **Figure 4.8** shows the BER performance of our proposed scheme compared to its counterparts under low channel estimation quality, particularly when $\beta = 1$. It is clearly shown that our scheme is robust against channel estimation errors, especially in the high SNR regime. Moreover, the effect of channel estimation error on the proposed scheme is investigated under different channel estimation qualities with $\beta = 0.01$, $\beta = 0.1$, and $\beta = 1$. For comparison purposes, the performance of the perfect channel estimation case

($\beta = 0$) is also included. **Figure 4.9** shows that the BER performance gets better as the channel estimation quality enhances (i.e., low values of β). Particularly, the proposed scheme is resistant to channel estimation errors for values of $\beta < 0.01$, and there is 3 dB degradation in BER when $\beta > 0.1$ compared to the perfect channel estimation case. This performance of the proposed scheme under imperfect channel estimation error could be further improved by using the existing algorithms in the literature, such as the algorithm in [157].

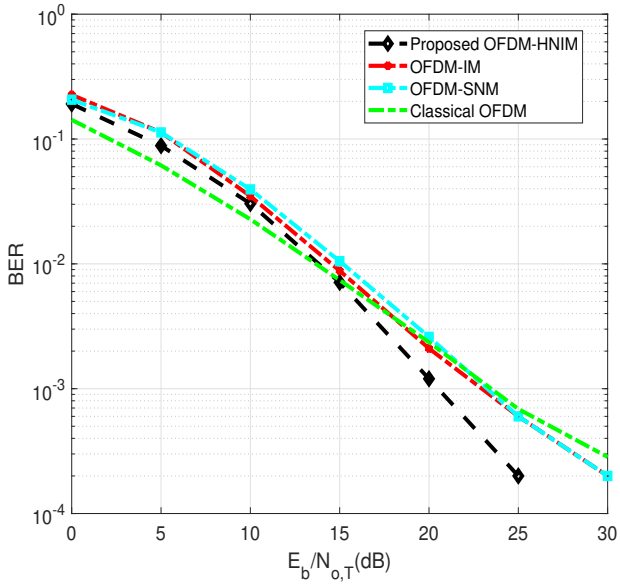

Figure 4.8: BER performance of the proposed OFDM-HNIM scheme, OFDM-IM, OFDM-SNM, and classical OFDM with imperfect CSI with $\beta = 1$, and BPSK.

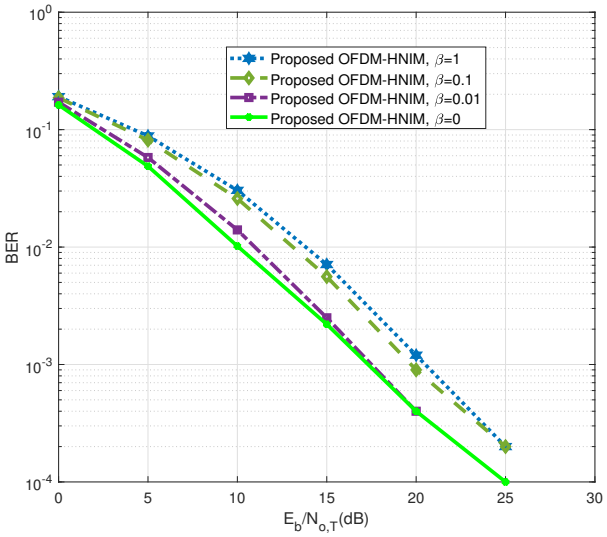

Figure 4.9: The effect of imperfect channel estimation on the proposed OFDM-HNIM scheme.

4.3. The OFDM-SGM Scheme

Here, we discuss the simulation results of the OFDM-SGM scheme. Throughput, SE and EE trade-off, and BER of the proposed OFDM-SGM scheme are compared with other existing schemes including OFDM-IM, OFDM-SNM, and plain OFDM. In our simulations, N and L are set to 64 and 4, respectively, the number of subblocks $G = N/L = 16$, and SGM bits are $p_1 = \log_2(L) = 2$ bits in each OFDM-SGM subblock. We assume the BSPK modulation of active subcarriers to utilize the full capability of the OFDM-SGM scheme. The simulated wireless channel is Rayleigh distributed and frequency-selective, as adopted in [10]. Similar signal-to-noise ratio (SNR) (or $E_b/N_{o,T}$) is considered to provide a fair comparison between the featured schemes, where E_b is the bit energy. The CP length (N_{CP}) is set to be longer than the number of channel taps to avoid intersymbol interference [158]. Furthermore, CSI is assumed not to be available at the transmitter.

The throughput performance of the OFDM-SGM compared to its counterparts under BPSK is demonstrated in **Figure 4.10**. As presented in **Figure 4.10**, the SE of OFDM-SGM under BPSK is higher than that of its competitive schemes because of having a more average number of active subcarriers in OFDM-SGM as compared to OFDM-IM. The degree of freedom offered by introducing the gap between active subcarriers as the new transmission medium enables an improved throughput performance of OFDM-SGM compared to the plain OFDM.

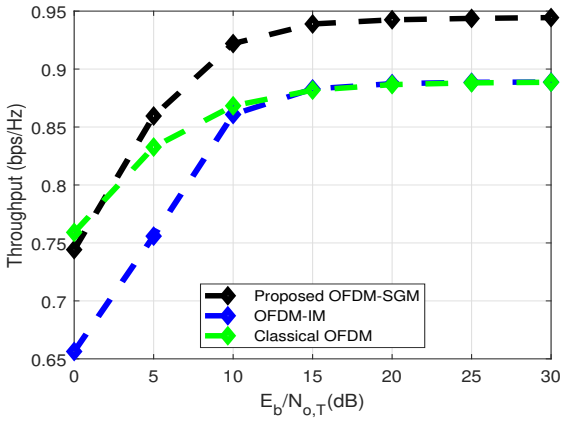

Figure 4.10: Throughput of the proposed OFDM-SGM scheme and its counterparts under BPSK.

As commonly done in the literature, we investigate the trade-off between the SE and EE for the considered modulation schemes. This trade-off is determined by the number of

active subcarriers in the OFDM block [14]. In particular, more saved energy and less SE result from having less number of active subcarriers. **Figure 4.11** exhibits the SE and EE ratios of the proposed scheme, OFDM-IM, OFDM-SNM, and the reference OFDM scheme under BPSK. It is obvious from **Figure 4.11** that the OFDM-SGM offers higher SE and EE ratios as opposed to the OFDM-IM with low activation ratio (AR), and the plain OFDM.

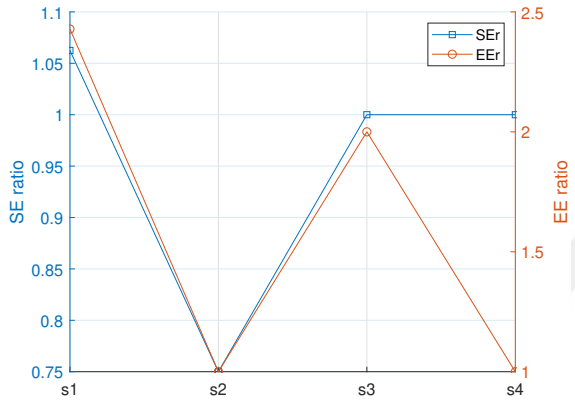

Figure 4.11: The SE ratio (SEr) and EE ratio (EEr) of the proposed scheme and its counterparts. The symbols s1, s2, s3, s4 correspond to the proposed scheme, OFDM-IM with $AR = 0.25$, OFDM-IM with $AR = 0.5$, and conventional OFDM, respectively.

Figure 4.12 shows that OFDM-SGM has improved BER performance over classical OFDM at high SNR values. Moreover, the proposed scheme with an LLR detector has comparable BER performance to OFDM-SNM and OFDM-IM. The reason for that is the gap between active subcarriers in OFDM-SGM increases the influence of active gap bits on the BER more.

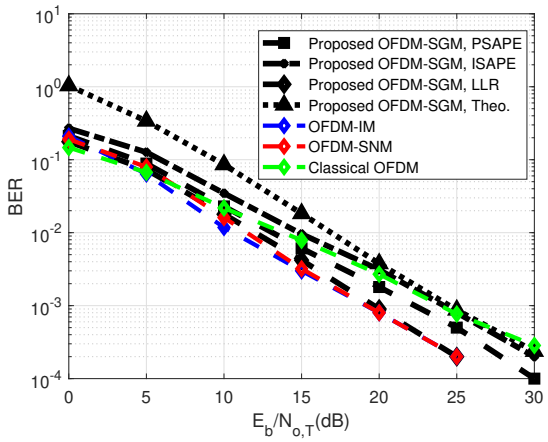

Figure 4.12: The BER performance of the OFDM-SGM, OFDM-IM, OFDM-SNM, and plain OFDM under frequency-selective Rayleigh channel with BPSK.

Table 4.2: Simulation parameters.

Modulation type	BPSK ($M = 2$)
IFFT/FFT size (N_F)	64
CP guard interval (samples)	8
Number of subblocks in each OFDM symbol (G)	16
Number of available subcarriers in each subblock (N)	4
Number of bits mapped to each subblock (p_1)	2
Multipath channel delay samples locations	[0 3 5 6 8]
Multipath channel tap power profile (dBm)	[0 -8 -17 -21 -25]

Moreover, the BER performance of the proposed OFDM-SGM when using the ISAPE detector has worse BER performance compared to that of the PSAPE detector. The reason behind this degraded BER performance of the ISAPE detector is that more error sources result from employing ISAPE as compared to the PSAPE detector. **Figure 4.12** also shows that with the growth of SNR, the obtained theoretical results become closer to the simulative ones.

4.4. The Floating OFDM-SNM For PAPR And OOBE Reduction

Here, we present the simulation results of the proposed floating OFDM-SNM scheme. PAPR and OOBE simulation results are presented in **Subsection 4.4.1** and **Subsection 4.4.2**, respectively.

The performance of the proposed scheme is investigated by computer simulations with a setup presented in **Table 4.2**. Here, an OFDM block with a specific number of available subcarriers is considered, and the active subcarriers carry the binary phase shift keying (BPSK) symbols. The HPA is ignored from the transmitter to simplify the simulated system. Furthermore, the multi-path channel is assumed to be Rayleigh distributed. The CCDF of the PAPR, PSD, and BER performances of the proposed scheme are simulated and compared with the conventional OFDM and OFDM-IM. For a fair comparison between the considered schemes, the same signal-to-noise ratio (SNR) or $E_b/N_{o,T}$ level is assumed, where E_b represents the bit energy. The simulation results related to PAPR and OOBE are presented in the following **Subsection 4.4.1** and **Subsection 4.4.2**.

4.4.1. PAPR simulation results

The PAPR performance can be enhanced, however this usually happens at the cost of increasing BER [30]. Therefore, CCDF results should be considered together with BER performance. The PAPR performance of OFDM-SNM is nearly the same as that in OFDM-IM and OFDM due to the equal distribution of the total energy over the active subcarriers. We employ the ACE and SGP [33] to reduce PAPR further, based on a proper predefined clipping threshold (A). A is set to 2.2 with a clipping ratio (CR) of 6.8485 dB, and a maximum number of iterations (J) equals 2, which makes our algorithm less complex.

The PAPR and BER performances of the OFDM-SNM with and without applying ACE/SGP are presented in **Figure 4.13** and **Figure 4.14**, respectively. We observe that it is possible to differentiate between different SAPs arrangement by finding the one which provides the lowest PAPR.

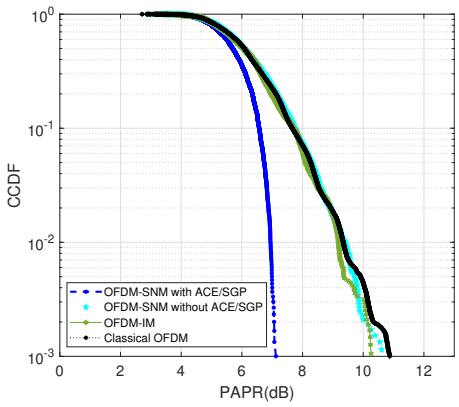

Figure 4.13: PAPR of OFDM-SNM without/with employing ACE and SGP techniques compared to OFDM-IM and conventional OFDM.

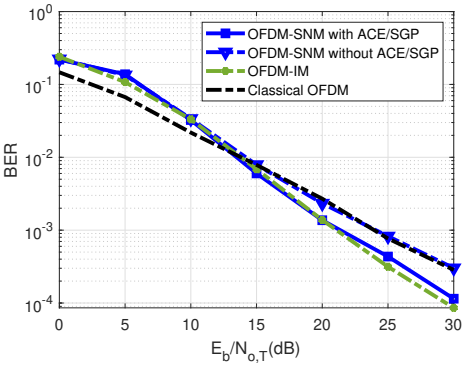

Figure 4.14: BER of OFDM-SNM without/with employing ACE and SGP techniques compared to OFDM-IM and conventional OFDM.

Figure 4.13 shows almost 3.5 dB gain in PAPR reduction performance when employing ACE/SGP as compared to the case without ACE/SGP. Also, the PAPR performance of the OFDM-IM and classical OFDM are almost the same as the ones for OFDM-SNM when ACE/SGP is not employed [31].

Figure 4.14 shows that employing ACE/SGP slightly enhances the BER performance of the OFDM-SNM compared to when ACE/SGP is not implemented. The obtained BER performances are still comparable to the ones in the OFDM-IM and plain OFDM. One main factor that contributes to the robust BER performance of our PAPR reduction technique is that the proposed scheme does not require side information. Thus, the proposed scheme does not suffer from BER degradation when receiving incorrect side information that results in the wrong recovery of the whole OFDM symbol. Hence, the proposed scheme attains a good BER performance, unlike hitherto PAPR reduction techniques where side information is needed for PAPR reduction [30]. Another critical factor that maintains the robustness of the BER performance of the proposed scheme is not introducing an increase in the average transmitted power, which is needed in some existing PAPR reduction techniques [30].

4.4.2. OOBE simulation results

It is assumed that the transmitted power to the OFDM symbol is the same among the considered transmission schemes. **Figure 4.15** shows the PSD performance of the proposed scheme in comparison with the conventional and competitive schemes. It can be clearly seen from **Figure 4.15** that there is a 2.38 dB gain in OOBE reduction by employing the proposed scheme in contrast to the conventional OFDM-SNM while a little gain when compared with the conventional OFDM and OFDM-IM.

4.5. Blind Numerology Identification For Mixed Numerologies

Simulation results are carried out in this section **Section 4.5**. The simulation results are illustrated to investigate the robustness of the proposed method. In the conducted simulations, the received mixed-numerology signals are assumed to be affected by AWGN and multipath Rayleigh fading channels. The considered multipath channel is characterized by an impulse response of length 9 and normalized power delay profile ϱ =

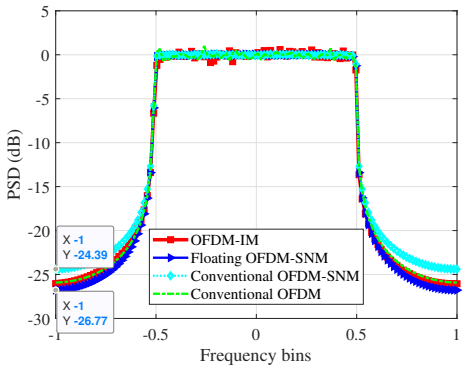

Figure 4.15: PSD of the proposed scheme and its competitive schemes.

$[0.8407, 0, 0, 0.1332, 0, 0.0168, 0.0067, 0, 0.0027]$ mW [152]. For each SNR value, we performed the simulations 10^4 times to ensure good accuracy.

For the sake of simplicity, we consider two scenarios as Scenario 1 and Scenario 2 in the conducted simulations. The base numerology with 15 kHz SCS is mixed with 30 kHz SCS and 60 kHz SCS numerologies in Scenario 1 and Scenario 2, respectively. The adopted numerology parameters are shown in **Table 4.3** [40]. The CP ratio is set as $\alpha = 1/16$. We assume an uplink transmission of two users using different numerologies with BPSK symbols carried on the activated subcarriers.

Table 4.3: The numerologies parameters in the considered scenarios.

Numerology	NUM-1	NUM-2	NUM-3
k	0	1	2
Δf_k	15 kHz	30 kHz	60 kHz
N_k	4096	2048	1024
$N_{CP,k}$	256	128	64
M_k	1024	512	256
Number of OFDM symbols	1	2	4

Figure 4.16 shows the CP correlation calculations in Algorithm 1 for Scenario 1 without considering the channel distortion and noise effects. Correct identification of the 15 kHz and 30 kHz SCSs candidate numerologies is achieved in the time domain, as shown in **Figure 4.16**. The average distances between the consecutive highest peaks are 4096 and 2048 samples, which correspond to the IFFT/FFT sizes of the 15 kHz and 30 kHz SCSs candidate numerologies, respectively.

Algorithm 2 is also simulated for the Scenario 1 without taking channel distortion and

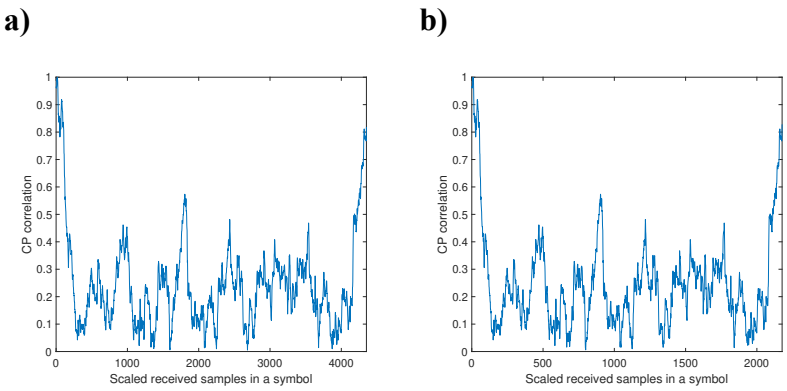

Figure 4.16: CP correlation calculations for Scenario 1 without considering noise and channel effects. **a)** 15 kHz numerology, **b)** 30 kHz numerology.

noise into consideration, as shown in **Figure 4.17**. It shows that the subband locations of the candidate numerologies can be easily identified and differentiate from each other. For example, the calculated V_u values in **Figure 4.17b** for the used band are 5.0733 and 0.0051, respectively. Therefore, it is straightforward to say that the subband location of the 30 kHz candidate numerology is the one with the lowest V_u value (i.e. the second used band with $V_u = 0.0051$).

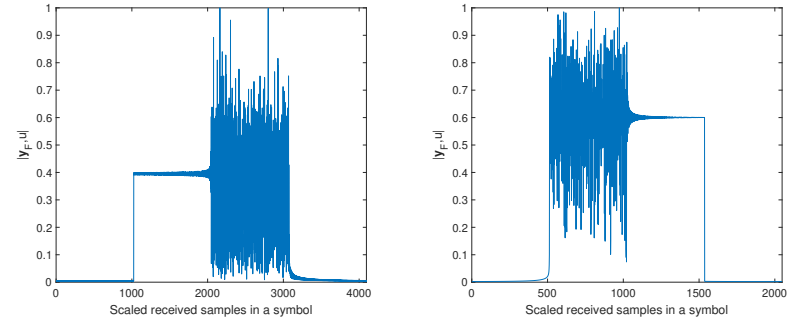

Figure 4.17: Amplitude variations plots for Scenario 1 without considering noise and channel effects. **a)** 15 kHz numerology, **b)** 30 kHz numerology.

The performance of the proposed method is compared with the non-blind approach in the traditional mixed-numerology system under AWGN and multipath Rayleigh channel. It is worth noting that prior knowledge about the candidate numerologies is known in the non-blind identification approach. **Figure 4.18** shows that the proposed algorithms provide robust accuracy results for a wide range of SNR values. More specifically, the proposed blind identification method and the non-blind approach guarantee a success rate of 100% for the considered scenarios at 0 dB of SNR under AWGN. **Figure 4.18** also shows that

the types and locations of candidate numerologies can be detected with robust accuracy in multipath conditions.

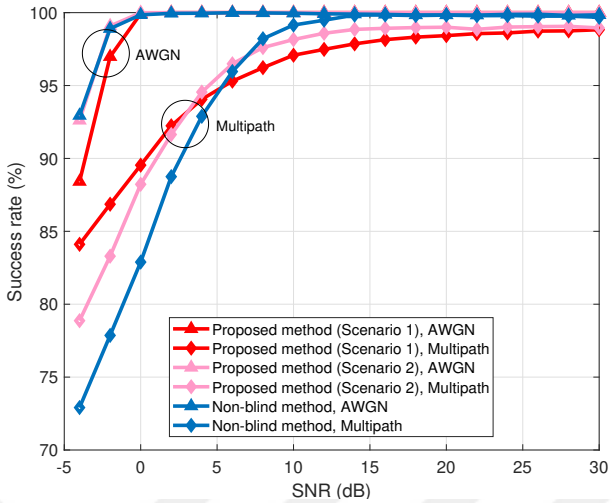

Figure 4.18: The average success rate of detecting the candidate numerologies in the considered scenarios using the proposed algorithms and the non-blind identification approach under AWGN and Rayleigh fading channel.

The BER performance of the proposed blind identification method is compared with the non-blind identification approach in the conventional mixed-numerology OFDM system. It should be noted that Scenario 1 is considered in the BER performance evaluation for the proposed method since it has worse success rate compared to the second one. As a benchmark, we also include the theoretical BER performances of the conventional OFDM [132] where single numerology is used. **Figure 4.19** shows that the proposed method is slightly worse than the theoretical BER result of the conventional OFDM under AWGN environment. Also, a slight BER difference between conventional OFDM and the non-blind identification approach in the conventional mixed-numerology system can be observed due to inserting sufficient guard bands to eliminate the effects of inter-numerology interference (INI), especially at high SNR values. This interference can be also decreased by other approaches [159], but this is out of the scope of this work. The additional blind operations performed in the proposed method introduce indispensable bits in errors. Thus, there is approximately 3 dB loss in BER performance of the proposed blind method compared to that of the non-blind one.

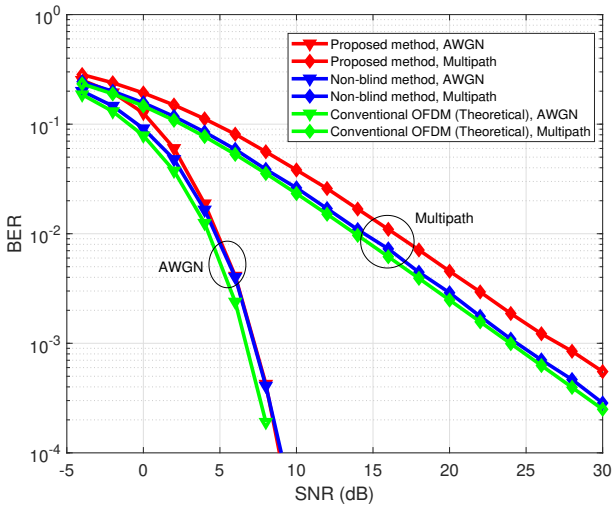

Figure 4.19: Comparison of the average BER performance of the blind/non-blind approaches in the conventional mixed-numerology system, to the theoretical BER results of the conventional OFDM under AWGN and Rayleigh fading channel.

4.6. Identification Of The Number Of Wireless Channel Taps Using Deep Neural Networks

Simulation results are carried out in section 4.6. Simulation results are presented to demonstrate and analyze the effectiveness of the proposed identification technique. The convergence performance of the proposed technique is shown in **Figure 4.20** after 1500 training epochs. The training accuracy is around 70%, about 8 points higher than the validation accuracy. When the number of epochs increases, both training and validation losses notably decrease. The achieved test accuracy is almost 62%. These preliminary results prove that our DNN converges to provide significantly higher accuracy than the existing SWISS algorithm under practical conditions where the signals are impaired by the frequency-selective fading channels. More specifically, the SWISS algorithm is a less efficient technique since pilot symbols are needed for accurate path-number identification. It has proven in [49] that the SWISS algorithm can identify exactly 9 paths with probability near 1. However, the identification obtained from NYUSIM datasets using the SWISS algorithm becomes inefficient for the number of channel taps that exceeds 9. More specifically, the SWISS algorithm achieves an average identification precision of 40.54%, which is much less than the value obtained by the proposed DNN-based approach.

However, the accuracy metric can not represent the tolerance in results. The predicted number of taps that falls within a tolerance margin from the ground truth can be seen using

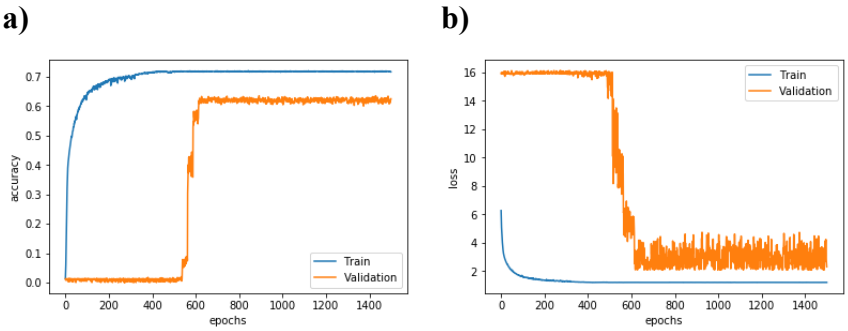

Figure 4.20: The convergence performance of the adopted DNN. **a)** Change in training/validation accuracy during training, **b)** Change in training/validation loss during training.

a confusion matrix. The obtained confusion matrix for the test set is shown in **Figure 4.21**. However, the bias effect at the bottom left in **Figure 4.21** can be explained by the nature of the channels generated from NYUSIM. These channels can have an unbalanced share of generation, causing the repetition of the number of taps in an unfair way. Thus, the bias leads to a misprediction that ultimately lowers the accuracy. Despite this unwanted effect, the overall performance of the network tends to provide a solution for the identification of the number of channel taps.

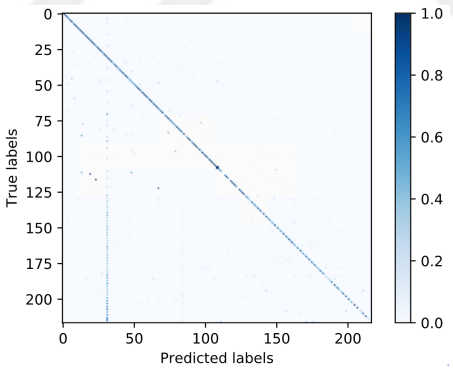

Figure 4.21: Normalized confusion matrix for test set in the proposed DNN-based method.

Furthermore, the computational complexity of the existing SWISS algorithm is very high. Particularly, the SWISS technique requires implementing one of the root-finding methods such as the Newton method to get the optimal dual variable for each class, thereby increasing the computational overhead. Also, these root-finding methods need to have initial guesses, error tolerance, and several iterations to converge to the optimal dual variable. The number of steps to convergence is in the order of $O(\log_2 S)$, where S is the predefined initial guess. Furthermore, the SWISS algorithm requires several iterations to

reach the desired accuracy for each class. On the other hand, the designed DNN saves computational complexity because it executes a constant number of matrix multiplications, independent of the channel's class.

4.7. Radar-Aided Communication Scheduling Algorithm For 5G And Beyond Networks

Simulation results are carried out in this section 4.7. The performance of the proposed approach is evaluated using system level simulation (SLS), then the key performance indicators (KPIs) are investigated.

Figure 4.22 shows the considered multi-cell scenario where the cellular topology is adopted in a single ring hexagonal structure with 7 5G BSs (gNBs), and their positions are at the center of the hexagonal cell in a square area. Users are dropped in the same area according to a uniform spatial distribution across the region of interest (ROI), which is around 7×7 km in size.

We focus on downlink transmissions without power control, as is the case in the majority of state-of-art proposals. It is assumed that BS knows the DL traffic demands that are cached in its buffer. UEs are associated to BSs based on the strongest average received power, i.e., based on distance, and do not change BS during the simulation. Fading is considered in the numerical simulations in addition to path loss, through a random variable, expressed in dB, distributed as a zero-mean Gaussian with a variance of σ^2 [160].

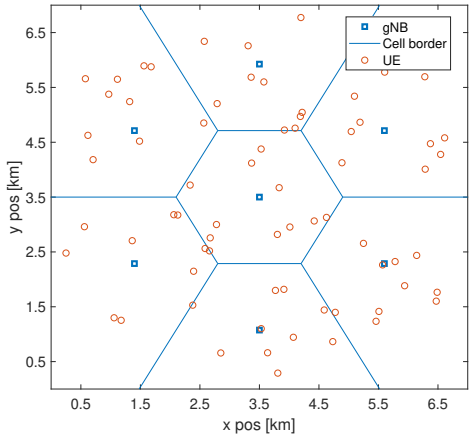

Figure 4.22: Simulation network layout.

The proposed scheduler selects the UE to transmit in each time slot. As a basic scenario,

Table 4.4: System Parameters.

Parameters/Symbols	Values/Description
Transmission bandwidth (B)	5 MHz
Carrier frequency (f_c)	5 GHz
BS transmit power (P_b^{Tx})	46 dBm
Noise PSD (N_0)	-174 dBm/Hz
Cell radius (R_c)	1400 m
Inter-site distance ($d_{k,v}$)	2425 m
Number of BSs (N_{BS})	7
Number of UEs per BSs (N_{UE-BS})	10
Total number of UEs (N_{UE})	70
Schedulers	RR, BCQI, PF
Number of available RBs (N_{rb})	15
Number of subchannels in a RB (N_c)	12
Number of available slots for scheduling (N_s)	20
Slot duration (T_s)	0.5 ms
Subchannel bandwidth (B_s)	180 kHz
Number of symbols in a RB (N_b)	7
BS configuration	Omni-directional
Transmission time interval (TTI)	2 ms
Number of Monte-Carlo Runs (N)	1000

perfect CSI is assumed to be available at the start of each time slot for schedulers and that at most one UE is allowed to transmit in each slot. The parameter specifications for the number of slots (N_s), slot duration (T_s), subchannel bandwidth (B_s), TTI, etc. can be found in **Table 4.5**. The considered scheduling inputs are imported from **Table 3.11**.

4.7.1. Simulation metrics

To understand the functioning of the proposed approach in much more detail, its performance is evaluated by considering the RR, PF, and BCQI methods in terms of average data rate (bits/s), throughput (bits/s), and SE (bits/s/Hz) over 1000 different channel realizations [101].

The average system and UE data rate, system throughput, and SE are found as follows, respectively:

$$\overline{r} = \frac{N_i}{N_{rb} N_c N_b T_s N_s} \tag{4.2}$$

$$\overline{r_k} = \frac{N_i}{N_{UE} N_s T_s} \tag{4.3}$$

$$\overline{\zeta} = \frac{N_i}{N_s T_s} \tag{4.4}$$

$$\overline{\eta} = \frac{N_i}{N_s \, TTI \, N_{rb} B_s} \tag{4.5}$$

where N_{UE}, N_i, N_{rb}, N_b, and N_c represent the total number of UEs, number of correctly received bits, number of available RBs, number of symbols in an RB, and number of subchannels in an RB, respectively.

4.7.2. State-of-art scheduling algorithms

The most commonly used scheduling methods are PF, BCQI, and RR in the literature and practice [161]. The available RBs are distributed using the PF, BCQI, and RR. The performances of PF, RR, and BCQI are analyzed under the proposed approach. For the same simulation scenario, the three scheduling techniques are used.

The PF method is one of the most widely used methods for fair scheduling [68], aiming to provide fairness while taking advantage of good channel conditions and dynamically allocating resources to UEs. It is proven in [162] that the PF is not optimal due to capacity constraints. The RR method provides RBs for UEs without considering channel conditions; this is a simple procedure that ensures fairness [163]. The BCQI method is a common channel-dependent scheduler. The channel variations between UEs are exploited in this scheduler to maximize cell throughput at the expense of fairness [164].

4.7.3. Simulation results

Here, the simulation results are presented along with their discussions. MATLAB-based SLS is used to evaluate the performance of the proposed approach. The achieved results are shown with the classical methods, i.e., PF, RR, and BCQI. During the simulations, the default parameters are listed in **Table 4.5**. The simulation results here showed the realistic case in which the signal experiences interference and noise simultaneously. Because of that, the SINR of UE has been measured when the power of the noise term is zero. Then, the SINR reduces to the signal to interference ratio (SIR). Conversely, zero interference reduces the SINR to the SNR.

Figure 4.23, **Figure 4.24**, **Figure 4.25**, and **Figure 4.26** show the performance of the proposed scheduler compared to the conventional one in terms of data rate, system throughput, and SE considering 15 available RBs. The achieved results show that the proposed scheduler, considering SINR, range, and velocity as inputs to the scheduler, is better than the conventional scheduler where SINR is only considered. It is demonstrated that the BCQI outperforms the PF and RR in terms of data rate, SE, and system throughput under the proposed scheme. The reason behind this is the channel-dependent characteristics of BCQI while assigning RBs, resulting in superior spectrum utilization. The results also show that the performance of the PF is slightly better than the RR. The RR performs the worst because it reduces throughput, data rate, and SE. On another side, it offers greater RA fairness among different UEs. It is worth noting that the throughput depends on the simulated channel state, which influences the achievable transmission rate and the UE scheduling mechanism adopted by BS.

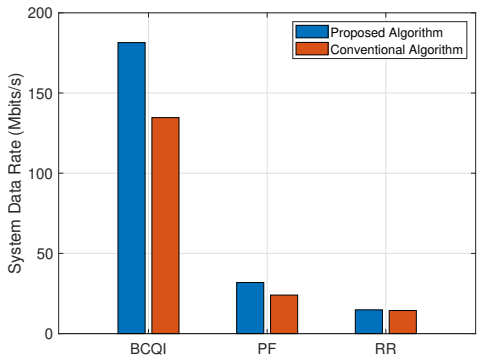

Figure 4.23: System data rate of the proposed scheduler compared to the conventional one.

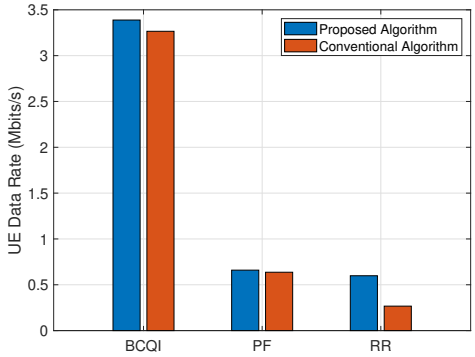

Figure 4.24: UE Data rate of the proposed scheduler compared to the conventional one.

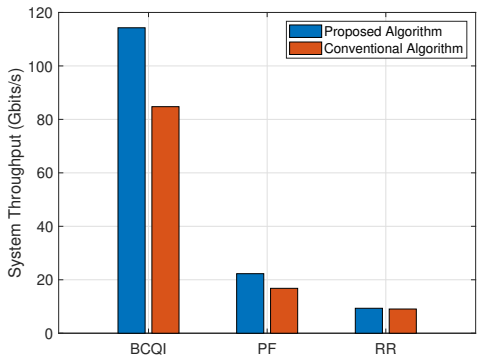

Figure 4.25: System throughput of the proposed scheduler compared to the conventional one.

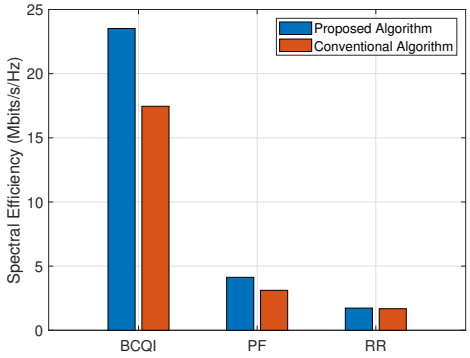

Figure 4.26: SE of the proposed scheduler compared to the conventional one.

4.8. Dynamic-Structure Resource Block Allocation Based Scheduling For 5G Systems

In **Section 4.8**, the simulation results and discussion are presented. The performance of the proposed approach is evaluated by using System-level simulations (SLS)s in MATLAB, and then the KPIs are investigated. For demonstrative simplicity, a flat fading model is assumed where the user rate is directly proportional to its allocated bandwidth fraction. The real-time traffic profiles of 5G services (eMBB, URLLC, mMTC) in our simulations are utilized for each UE. The simulation parameters are presented in **Table 4.5**.

The employed transceiver is designed as follows. The considered frame consists of random binary data bits that are encoded and modulated with the Turbo encoder and quadrature phase shift keying modulator. The Turbo encoder and decoder pair use the trellis structure with random interleaver indices. The modulated data is impaired by AWGN and extended vehicular A model channel [165]. After that, the noisy signal is demodulated

using the log-likelihood ratio detector with the Turbo decoder.

Table 4.5: The considered simulation parameters.

Transmission bandwidth	5 MHz
f_c	28000 MHz
gNB configuration	Omni-directional
Inter-site distance	2425 m
gNB transmit power	46 dBm
N_0	-174 dBm/Hz
Number of gNBs	7
Total number of UEs (N_{UE})	70
Number of eMBB UEs	20
Number of URLLC UEs	20
Number of mMTC UEs	30
$R_{bk}^{min,e}$	0.001
$R_{bk}^{min,m}$	0.005
$\epsilon_{bk}^{max,i}$	0.001

The proposed approach is evaluated by comparing its performance with the S-RBS based scheduling approach considering the conventional schedulers; RR, PF, and BCQI, in terms of data rate (Mbits/s), system throughput (Gbits/s), and SE (Mbits/s/Hz) [101]. The data rate of the proposed approach can be shown in **Figure 4.27a** and **Figure 4.28a**. Two possible cases for the number of RBs are considered: the first is when the number of RBs is 8 and 32 in the S-RBS and D-RBS, and the second is when the number of RBs is 16 and 64 in the S-RBS and D-RBS. It is clearly shown that the D-RBS is significantly improved over the S-RBS in terms of data rate for the considered scheduling approaches. The reason behind this is the flexibility and dynamicity offered by the D-RBS compared to that in the S-RBS.

a): Data rate. **b):** System throughput. **c):** SE.

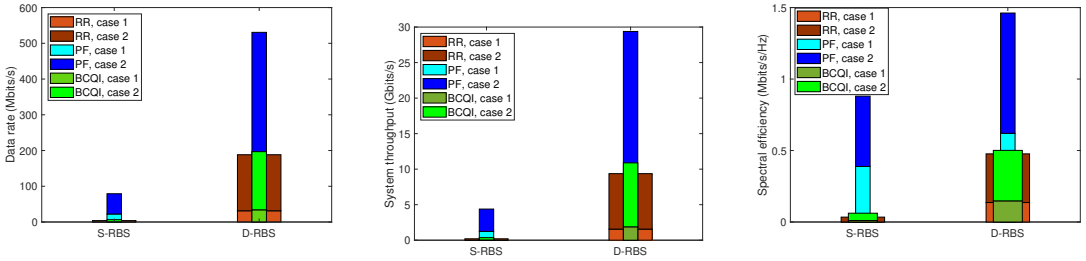

Figure 4.27: Data rate, system throughput, and SE of the proposed D-RBS based approach versus the S-RBS using the RR, PF, and BCQI schedulers.

The system throughput and SE of the proposed approach are displayed in **Figure 4.27b**,

a): Data rate. **b):** System throughput. **c):** SE.

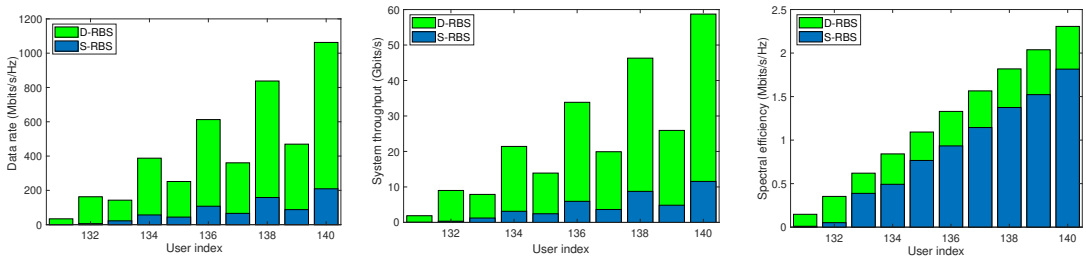

Figure 4.28: Data rate, system throughput, and SE of the proposed D-RBS based approach versus the S-RBS by considering the dynamic switching between RR and BCQI.

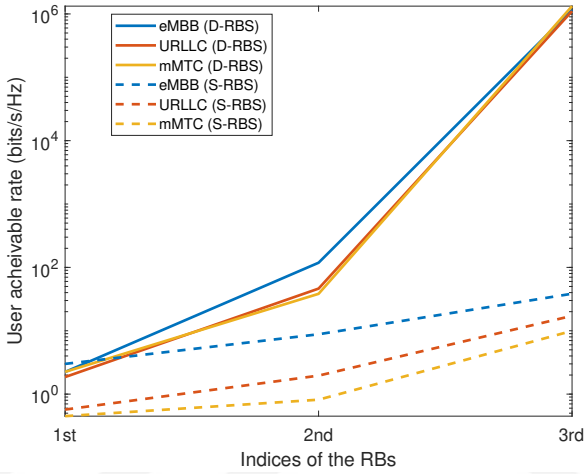

Figure 4.29: The achievable rate per user for different RBs and different services.

Figure 4.27c, **Figure 4.28b**, and **Figure 4.28c**. As observed in the obtained results, high system throughput and SE in the D-RBS are achieved through the considered scheduling algorithms due to a higher number of RBs in the same BW with D-RBS, resulting in superior spectrum utilization. Furthermore, the achievable rate per UE (bits/s/Hz) is obtained at different values of time durations and frequency sizes for different RBs. More specifically, the TTI and BW are $\{1, 0.5, 0.25\}$ ms and $\{15, 30, 60\}$ kHz, respectively, correspond to the first, second, and third indices of the RBs shown in **Figure 4.29**. It can be observed that the eMBB service has the best performance in terms of UE achievable rate as expected due to its inherent features of having a high data rate. Moreover, the D-RBS has significantly improved achievable UE rate compared to that in the S-RBS due to the degrees of freedom found in the D-RBS.

CHAPTER 5

5. CONCLUSION AND FUTURE WORK

This chapter includes some concluding remarks, insightful recommendations, and future research challenges.

5.1. Concluding Remarks

Various modulation options for the OFDM waveform are reviewed, investigated, classified, and compared in terms of their reliability, complexity, PE, OOBE, and PAPR performances. Signal plane dimensional-based classification is used to categorize the possible modulation options as: OFDM-DM and conventional and adaptive OFDM modulations exploit the 2-D signal plane. SM-OFDM, OFDM-IM, OFDM-SNM, and OFDM-PSM exploit the 3-D signal plane. As a conclusion, SM-OFDM can be preferred for its improved reliability; OFDM-IM for its high power efficiency; conventional OFDM and OFDM-DM for their simple transceiver structure; OFDM-PSM for its low OOBE; OFDM-SNM for its higher throughput when channel conditions allow BPSK modulation; and OFDM with adaptive hybrid modulation for its QoS-based adaptation. Also, the link between these different candidates for modulation and the needs of future 5G networks is shown.

We introduce a novel multi-carrier modulation scheme called OFDM-SNM that sends information not only by symbols but also by the number (instead of indices) of active subcarriers in each subblock. OFDM-SNM improves the spectral efficiency compared to that of OFDM-IM by 12.5%. Besides, different from OFDM-IM, since the active subcarriers in OFDM-SNM send information by their number instead of indices, their mapping can be configured to be floating or contiguous based on the channel quality or the ICI level between subblocks, resulting in even a better performance.

In addition to the standard signal constellation symbols, we offer a new multi-carrier transmission system called orthogonal frequency division multiplexing with hybrid number and index modulation (OFDM-HNIM) that sends additional information bits by number and index of the active subcarriers. As the modulation order increases, the proposed hybrid scheme's low-complex transceiver falls behind its counterparts in terms of throughput performance in low-order modulation formats like BPSK and QPSK. The hybrid method outperformed OFDM-IM and traditional OFDM in BER at 1.78 bits/s/Hz. Results show that our OFDM-HNIM system is channel estimation error-resistant. Due to having inactive subcarriers within the OFDM symbol of the hybrid scheme, it could be used to reduce interference among subcarriers, and enhance EE by reducing PAPR. Furthermore, it is possible to design and develop much more advanced and effective modulation techniques by integrating the recently introduced subcarrier power modulation concept in [166] and [167] with the hybrid scheme (OFDM-HNIM) to further enhance SE.

This paper introduces a novel energy-efficient multi-carrier modulation scheme termed as OFDM-subcarrier gap modulation (OFDM-SGM) that transmits extra information by the gap between the activated subcarriers beside the classical modulation symbols. The OFDM-SGM has low-complex transceivers. Also, OFDM-SGM performs better than its counterparts in terms of throughput under low modulation order. Furthermore, the upper bound on the BER of the OFDM-SGM agrees with the analyzed one. As future work, the proposed scheme will be investigated with different modulation orders and subblock sizes. Another potential research direction is combining the proposed scheme with the other existing OFDM-based modulation schemes to provide a further enhancement in different performance metrics, especially SE [27], [168], [169].

We have proposed an enhanced version of the conventional OFDM-SNM scheme to reduce PAPR and OOBE. The locations of the active subcarriers are flexibly shifted based on the PAPR performance. The best arrangement is the one that offers the minimum PAPR performance. The proposed scheme is spectrally efficient since no reserved subcarrier is used to transmit side information to the receiver for PAPR reduction purposes. Furthermore, the inherent features of the OFDM-SNM allow proposing a new OOBE optimization method in which it offers minimum OOBE within the OFDM-SNM block. The proposed energy-efficient scheme provides efficient solutions for OOBE reduction compared to conventional OFDM-SNM, OFDM-IM, and traditional OFDM. Thus, the proposed method

can limit adjacent-channel interference along with low PAPR values, thereby making it more suitable for B5G wireless networks. As future work, it is possible to further investigate the PAPR and OOBE reduction techniques for the proposed scheme in terms of different parameters, such as subblock size and the number of active subcarriers in each subblock. Furthermore, it is worth examining the effectiveness of some other OFDM-based modulation schemes [170]–[172] for PAPR and OOBE reduction.

A new identification method for mixed-numerology OFDM is proposed based on the characteristics of mixed-numerology signals in time and frequency domains. The success rates for numerology and subband location identification are very high over AWGN and frequency selective channels. By using the proposed method, the numerology and the subband location can be detected without prior information, but with a slight BER performance loss. As future work, further accuracy improvements will be investigated, especially for frequency-selective channels and asynchronous transmission.

In this paper, an end-to-end communication system is trained through a newly developed DNN to identify the number of channel taps. We achieved an improved accuracy and loss performance over the existing SWISS algorithm in identifying the number of channel taps. Our DNN system is fed by a measurement-based training dataset. The proposed method can be applied for different channel types without the need for a prior analysis. Also, the identified number of taps could help track the time variations of the wireless channel caused by the Doppler effect. The developed DNN has the potential to identify not only the number of multipath components but also their corresponding locations. As another future direction, the impacts of the noise on the proposed solution can be analyzed.

More effective scheduling algorithms are required to fulfill the needs of new applications such as radar and communication coexistence. We propose a new radar-aided scheduling algorithm in a practical vehicular communication scenario by utilizing some parameters, including range, velocity, and the conventional SINR measurements. The fundamental idea is to create the communication scheduler at the BS using the estimation of the scheduling inputs derived from the radar echo signal. The proposed scheme introduces a new degree of freedom to the scheduling design in radar-aided communication systems that leads to an efficient scheduling algorithm. The proposed scheme is evaluated in terms

of data rate, UE and system throughput, and SE. The simulation results prove that the proposed scheduler outperformed the conventional one. Moreover, the obtained results show a significant performance of the proposed scheduler using the BCQI over the PF and RR. The results show that radar can be a valuable source of side information for the communication scheduler over a millimeter-wave (mmWave) V2I link. The proposed algorithm should be viewed as a preliminary solution to demonstrate the approach's practicality, although it can be modified further. As future work, the optimal solutions could be further improved by employing more efficient optimization methods than the adopted trial and error method. Furthermore, the scheduling rules can be extended by incorporating the angular parameter from the radar echo to enhance the performance of the scheduler.

In this work, we have developed a D-RBS based scheduling approach for 5G systems. The D-RBS enables a flexible frame structure by offering small-sized RBs that can be assigned to UEs requesting various services. The PF, RR, BCQI, and the switching mechanism between RR and BCQI have been employed based on the D-RBS because it offers competitive features in RB allocation. System-level KPIs are evaluated to prove the efficiency of the proposed approach. The obtained results for the proposed approach are relatively robust against the conventional S-RBS based scheduling approach, making it a promising scheduling approach for futuristic wireless networks. In future work, different transmission modes, such as multiple input multiple output (MIMO), will be investigated under the proposed approach. Furthermore, the impact of the number of UEs and their mobility will be analyzed.

5.2. Challenges And Future Research Directions

Subsection 5.2.1 shows the applications of the considered modulation options for 5G and beyond networks based on the provided comparative evaluation. In **Subsection 5.2.2**, some other flexible modulation options for OFDM variants are discussed. **Subsection 5.2.3** exhibits envision for futuristic modulation options for beyond 5G.

5.2.1. Applications of the featured modulation options for 5G and beyond networks

New services, scenarios, and applications, as well as numerous challenging requirements, would appear in the next generation of communication networks. Single radio technology

almost cannot satisfy all of these requirements at the same time especially with diverse future services including mMTC, eMBB, and URLLC. In [173] and [174], the multi-numerology OFDM concept is introduced to provide a more flexible solution for satisfying various requirements for different services in future communication networks. The modulation option for a given waveform is expected to have a considerable impact on the waveform's capability to meet the diverse services and requirements of the next-generation wireless networks.

The featured modulation schemes have varied performances for different metrics and criteria, as presented in **Section 3.5**, where different reliability and throughput performances are achieved. **Table 5.1** and **Table 5.2** show a qualitative summary of the performance of the featured modulation schemes for an OFDM-based waveform. Thus, the possible applications of these featured modulation options for future networks can be predicted. The main criteria to assess the effectiveness of a modulation option are its reliability, SE, PE, OOBE, and complexity performances.

Table 5.1: Assessment of the featured modulation options in terms of reliability, SE and OOB leakage.

OFDM-based Modulation Scheme	**Reliability**	**Spectral Efficiency**	**OOB Leakage**
Conventional OFDM [76]	High at low SNR and low at high SNR	$\frac{N\log_2(M)}{N+N_{CP}}$	High due to the rectangular transmit pulse
OFDM-DM [77]	Low at low and high SNR	Relative loss in throughput is higher compared to plain OFDM	High
SM-OFDM [16]	High at low SE, depends on a trade-off between $N_T * N_R$ and M at high SE	$\frac{N\log_2(N_T)+\log_2(M)}{N+N_{CP}}$	Low due to significantly reduction in the interference between the transmit antennas
OFDM-IM [17]	Low at low SNR and high at high SNR	$\frac{N\left(\log_2(M^a)+\lfloor\log_2\binom{b}{a}\rfloor\right)}{(N+N_{CP})b}$	High due to the sparsity nature of the activated subcarriers
OFDM-SNM [19]	Low at low SNR and high at high SNR	$\frac{\sum_{g=1}^{G}(\log_2(b)+a(g)\log_2(M))}{N+N_{CP}}$	High due to the sparsity nature of the activated subcarriers
OFDM-PSM [20]	High at low SNR and low at high SNR	High and depends on the number of superimposed HG pulses	Low due to using localized HG pulses

The possible applications of the OFDM-SNM scheme are the ones that require relatively high transmission rate with low M, i.e. $M = 2$, to offer reduced BER values; and with a small length of the subblock, i.e. 4 subcarriers, to attain low-complex detector. Moreover, the OFDM-SNM inherent features of floating the active subcarriers could be exploited for

Table 5.2: Assessment of the featured modulation options in terms of PE and computational complexity.

OFDM-based Modulation Scheme	PE in terms of PAPR	PE in terms of transmitted power	Computational Complexity
Conventional OFDM [76]	High due to the constructive combination of subcarriers with independent phases	High due to transmitting power on all subcarriers	$O(M)$
OFDM-DM [77]	High	High due to transmitting power on all subcarriers	$O(M)$
SM-OFDM [16]	High for a large number of subcarriers	Low due to transmitting power only to single transmit antenna at a time	$O(N_T, N_R, M)$
OFDM-IM [17]	High due to sparse distribution of active subcarriers	Low due to transmitting power to fixed number of active subcarriers in each subblock	$O(M)$
OFDM-SNM [19]	High due to sparse distribution of active subcarriers	Medium and depends on the varied number of active subcarriers in each subblock	$O(b, a, M)$
OFDM-PSM [20]	High due to superimposing pulses together within the same time-frequency region	High and depends on the number of superimposed HG pulses	$O((D+1), R, U, M)$

the applications where robustness towards adjacent channel interference is preferable, especially in 5G multi-numerology design. The flexible, low-complex OFDM-IM scheme with an energy detector could be a potential candidate for the internet of things (IoT) applications where limited power of devices as well as robustness against asynchronous impairments are the main features of such applications. Furthermore, employing a low-complex compressed sensing detector in OFDM-IM alongside low activation ratio could be exploited for URLLC type of services due to low latency with high reliability performances offered by such structure.

In the next-generation wireless networks, a robust receiver towards unknown interference is needed. The number-based and index-based modulation options tailored to the OFDM waveform are promising candidates against unknown interference especially with employing a robust receiver including a low-complex, threshold-based detector. Utilizing the inactive subcarriers in the index-based and number-based modulation schemes, such as OFDM-SNM and OFDM-IM, could be helpful for 5G use cases where simpler ICI mitigation and low PAPR are crucial. The SM-OFDM scheme is suitable for mMTC use cases due to its enhanced PE and reliability along with flexibility. Due to the preferable OOB leakage performance of OFDM-PSM, it could be applied in applications where multi-user interference mitigation is favorable.

5.2.2. Other potential flexible modulation options for OFDM-based waveforms

Due to flexibility offered by the OFDM-based waveforms, there is a vital need for additional flexible modulation options for OFDM-based waveforms to be proposed. It is reasonable and advantageous to incorporate resources across various signal domains to shape a multi-dimension entity for the implementation of the presented OFDM modulation options. One example of these flexible modulation options is OFDM with subcarrier power modulation (OFDM-SPM) in which the power of subcarriers is exploited as a novel dimension to carry additional information bits beside the conventional PSK/QAM symbols. As compared to conventional OFDM, the novel OFDM-SPM scheme doubles the SE, and it uses only half the number of subcarriers required by OFDM with BPSK, and thus power is saved. The flexibility of this power-based OFDM scheme is possible by introducing more degrees of freedom for the saved power, in which it could be used for merely power saving or power reallocation, which makes the OFDM-SPM transmission scheme suitable for low complexity and power-efficient applications [169].

In the conventional transmission scheme, different QAM modulation orders are selected and applied to different subcarriers based on their corresponding subchannels' quality and/or the requirements of the service or application being used at the receiver side (i.e., Quality-of-Service (QoS) based adaptation). Particularly, given service with a certain, targeted BER requirement, the modulation orders are adaptively selected to meet the targeted BER while maximizing the transmission SE.

The presented modulation options are not only applicable to plain OFDM, but also for various OFDM variants [175]. The most common features of these OFDM variants are their application of windowing and/or filtering operation in either frequency or time domain. Example of these OFDM-like structure are filtered OFDM (f-OFDM) [176], which employs windowing or filtering operation in time domain, filter bank multicarrier (FBMC) [177] that filters the data in frequency domain at a subcarrier level, universal filtered multicarrier (UFMC) [178] that performs filtering in frequency domain at the RB level, and generalized frequency division multiplexing (GFDM) that applies a circular convolution to directly apply filtering on a time-frequency block [99]. Some examples of proposed modulation options for these OFDM variants are shown in **Table 5.3**.

Table 5.3: Modulation options for OFDM variants.

OFDM variant	Modulation option for OFDM variant	Contributions
FBMC	Circular convolution FBMC-IM [179]	Circular convolution FBMC-IM provides more OOBE suppression as compared to conventional OFDM.
GFDM	GFDM with pulse superposition modulation [100]	The acquired bandwidth efficiency of the superimposed GFDM waveform is almost 2.4 much higher than GFDM with Gaussian pulses.
UFMC	Universal Filtered OFDM with Filter Shift Keying [180]	The filter realizations carry information through the index modulation. Universal filtered OFDM with filter shift keying provides significant throughput and error performance improvements over UFMC.
f-OFDM	Spatial modulation f-OFDM [181]	In spatial modulation f-OFDM, each subcarrier within the subband is mapped to one of the transmitting antennas. Spatial modulation f-OFDM provides higher SE as a natural result of both SM and f-OFDM benefits.

5.2.3. Futuristic modulation options for beyond 5G

The presented modulation options for OFDM and its variants are not sufficient to meet diverse services in 5G and beyond networks. Further modulation schemes needed to be explored for different waveforms, not limited to OFDM and its variants, in either one-dimensional or multi-dimensional depending on the application, their requirements and capabilities. For example, the link adaptation schemes adjust over-the-air transmission parameters based on the radio channel change for both downlink and uplink. The CSI measurements for link adaptation include some parameters such as CQI, which are reported back to the transmitter. However, these conventional link adaptation hardly meets the diverse 5G and beyond networks requirements, as shown in **Figure 5.1**.

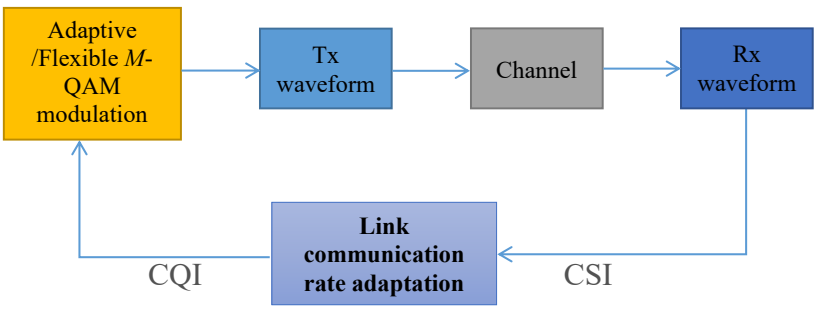

Figure 5.1: Block diagram of the conventional link adaptation.

Hence, there is a need for adaptive modulation options for a given waveform in 5G and

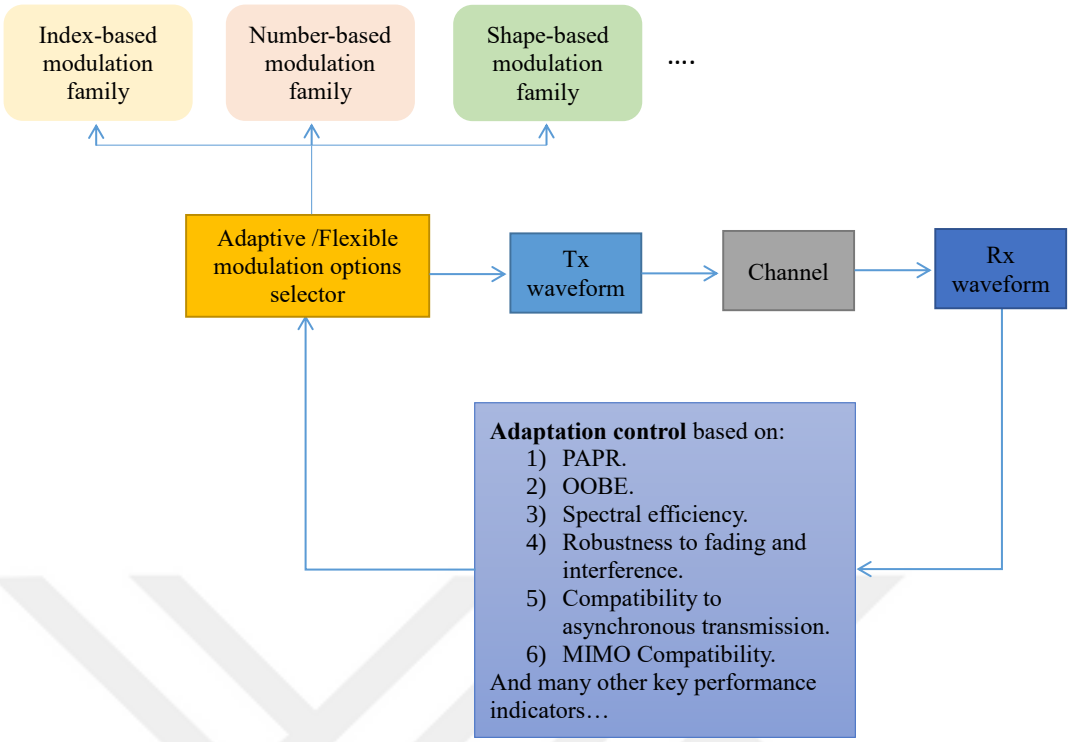

Figure 5.2: Block diagram of the adaptive modulation options selector.

beyond networks, as presented in **Figure 5.2**. It is worthy to note that there is no best modulation format, and the adopted modulation depends on the system requirements, channel model and transceiver constraints, etc. Unconventional transmission methods may have remarkable potential and impact to shape beyond 5G due to their inherently available advantages over conventional systems.

For example, index modulation schemes have been considered as alternative solutions for 5G and beyond wireless networks. One IM scheme that received a significant amount of research, due to its promising performance, is the transmitter SM as described in **Subsection 2.2.1**. One of the variants of SM systems is called receive SM (RSM) [182], where the transmitted signals from all transmit antennas are precoded, such that only a single antenna receives the modulated symbol, while the received signals at all other receive antennas include only noise. RSM is shown to require less computational complexity, measured by the number of the required real multipliers at the receiver, as compared to the transmitter SM.

Another potential IM-based candidate for beyond 5G, which attracts recent research attention, is media-based modulation (MBM) [81]. MBM offers multiple-input multiple-output

(MIMO) benefits and it introduces a completely new dimension in the channel states domain for conveying information by altering the far-field radiation pattern of reconfigurable antennas. In other words, MBM converts static Rayleigh fading to AWGN by performing the modulation of the wireless channel itself in a sense so inherent diversity is supported by MBM.

One interesting direction for designing a modulation scheme is a proper combining of multiple dimensions, such as the proposed scheme in [27] entitled "OFDM with hybrid number and index modulation" where the number and index dimensions are jointly exploited to introduce additional degree of freedoms in the modulation design.

5.2.4. Scheduling and resource allocation

In a multi-user context, efficiently and fairly allocating available time and frequency resources among users is one of the most important jobs in most centralized communication networks in order to maintain maximum throughput and reliability while minimizing interference. Channel-dependent scheduler [183] is one of the most effective scheduling algorithms utilized in the literature. The subcarriers corresponding to good subchannel gains with respect to a specific user are selected and assigned for data transmission to that specific user in this scheduler, while the remaining subcarriers are assigned to other users whose subchannels corresponding to these remaining subcarriers are in good quality.

This channel-based RA scheduler has been studied extensively for OFDM with conventional constellation modulation, for example as presented in [184]; however, to the best of authors' knowledge, there are no works reported in the literature that investigate the possibility of using such scheduler when index modulation is used with OFDM waveform. It is anticipated that OFDM-IM with its current design may deem incompatible and unsuitable to be used directly with channel-dependent scheduler. The reason for this is that, in OFDM-IM, the subcarriers selected for data transmission are dependent solely on the incoming data bits, whereas in channel-dependent scheduling, the subcarriers chosen for data transmission are dependent solely on the channel characteristics.

So, the research question that poses itself here is that "Is it practically possible to make the selected subcarriers in OFDM to be both data and channel dependent simultaneously?" if

no, then “What alternatives can be used” and if yes, then “What changes should be introduced to the transceiver structure to make the design work properly?”. These questions and others need thorough thinking and deep investigation to answer them confidently and then try to come up with novel, compatible or alternative designs to coexist and integrate subcarrier index selection modulation with subcarrier channel-based selection scheduling if possible in a seamless manner.

5.2.5. Physical layer security

In wireless communication medium, it is necessary to secure our transmission against eavesdroppers who can capture the data-carrying signals and then try to decode them [185], [186]. Naturally, using fixed modulation does not result in any secrecy gain as the transmission in this case is independent of the channel. However, channel-based adaptive constellation modulation can result in a significant secrecy performance due to the fact that the selected modulation orders in this case would be close to optimal with respect to only the legitimate receiver, resulting in a better performance; whereas the selection would be random with respect to the eavesdropper’s channel, resulting in no favourable gain to the eavesdropper.

Most of the works in the literature have focused on securing the transmission of OFDM with conventional constellation modulation, whereas very little amount of works have appeared on securing the other new types of modulation such as index modulation [187], [188]. Many of the existing physical layer security may not be directly applicable due to the differences between index and conventional data symbol modulation. Therefore, new index modulation-tailored security techniques need to be developed for securing the data sent by the indices of the transmit entities. Accordingly, more research attention should be focused on the joint security of both the information sent by indices and that sent by signal constellations.

5.2.6. Robustness to multi-access and narrow band interference

5.2.6.1. Multi-access interference (inter-user interference)

Due to the enormous increase in the amount of machine and IoT devices that are expected to be served (often simultaneously and sporadically) by communication networks; there is

an apparent, formidable need to reduce the amount of control and signaling overhead required to coordinate among users as it causes severe spectral efficiency loss and intolerant delay in the network [189]. Recently, there is a shift from coordinated, orthogonal systems such as legacy LTE networks to uncoordinated, asynchronous, and non-orthogonal systems. However, these uncoordinated, asynchronous networks would result in interference between users, degrading reliability as a consequence of reduced SINR.

To address this problem, techniques based on the usage of filtering, windowing, and guard bands are investigated in the literature [11] as natural, classical solutions to deal with this multi-user interference issue; however, these traditional solutions have drawbacks such as increasing computational complexity and reducing spectral efficiency. To address the interference between adjacent users in a more efficient manner, it has recently been shown in [190] that OFDM-IM with some modification on the subcarrier selection process has the potential to effectively alleviate adjacent user interference in asynchronous transmission systems. This has been achieved by using a data to subcarriers mapping method that gives higher activation probability to the subcarriers located in the center of each subblock. Another alternative solution to adjacent interference problem can be realized and well handled with an even better performance by OFDM-SNM scheme as the activated subcarriers in this type of modulation can be easily localized in the center of the subblocks (away from the edges of the subblocks).

5.2.6.2. Narrow-band interference

The OFDM-IM and OFDM-SNM schemes are more robust and immune to narrow-band interference than OFDM with conventional constellation modulation. The reason for that lies in the fact that in IM and SNM, OFDM symbols have a sparse nature, which results in less interference effect. One of the main reason for narrow-band interference in 5G and beyond communication systems is the emergence of new services such as URLLC ones that are basically placed and installed in a small resource portion within the data packet. Such an integration for URLLC packet causes a narrowband interference to the hosting original data packet, resulting in a severe performance degradation at the receiver. Due to the sparse characteristics of this type of interference, it is possible to mitigate it using special modulation schemes that do not utilize all subcarriers of the OFDM structure for transmission.

Consequently, the investigation and analysis of the capability of sparse modulation schemes such as OFDM-SNM and OFDM-IM in mitigating narrowband interference (especially for URLLC services) can be a subject of future research studies.

5.2.7. PAPR reduction

The OFDM-based waveforms suffer from a high PAPR, the survey in [154] includes several methods proposed to solve the PAPR problem in OFDM. To address the high PAPR problem, inherited from OFDM, in the other featured modulation options for OFDM-based waveforms, one may suggest to directly borrow the algorithms that proposed for classical OFDM. However, those techniques may not be very efficient because they do not consider the unique characteristic and features of the aforementioned modulation options for OFDM. Just recently, a few approaches for reducing the PAPR of index-based modulation schemes have appeared in the literature for OFDM-IM and SM-OFDM, respectively, as explained below.

- PAPR reduction techniques in OFDM-IM system: OFDM-IM suffers from a high PAPR problem inherited from conventional OFDM [153]. The method in [191] has been proposed to solve this PAPR issue in OFDM-IM by exploiting the inactive subcarriers in OFDM-IM. It was shown that this method outperforms the selective mapping (SLM) and active constellation extension presented in [154]. However, this method requires high computational cost for the PAPR reduction. A low computational complexity PAPR reduction method has been proposed in [127] for OFDM-IM system, and it considerably outperforms the ACE in PAPR reduction with a slight degradation in BER. Moreover, the authors in [192] proposed a scheme where the dither signals could be given more freedom (a larger radius of dithering) in average, where much better PAPR reduction performance than the scheme in [191] has been obtained at the expense of a slight BER performance degradation compared to the original OFDM-IM signal case.

- PAPR reduction techniques in SM-OFDM system: The major disadvantage of MIMO-OFDM system is having high levels of PAPR [193]. In the literature, several

algorithms proposed to reduce PAPR in SM-OFDM systems. Examples of techniques which are used for PAPR reduction of SM-OFDM systems are directed selected mapping (d-SLM) [194] and spatial shifting (SS) [195]. However, there is a need for finding much better PAPR reduction techniques for SM-OFDM transmission scheme, since such a system exhibits greater sensitivity to the signal in the HPA clipping than V-BLAST OFDM technique for the same spectral efficiency and number of antennas [128].

As seen from the literature, only a few number of studies are available on the PAPR reduction for specific OFDM modulation options. Therefore, there is a need for exploring more suitable PAPR reduction techniques for different modulation options of OFDM-based waveforms.

BIBLIOGRAPHY

[1] B. Xin, Y. Wang, W. Gao, D. Wipf, and B. Wang, "Maximal sparsity with deep networks?" in *Proc. Adv. Neural Inf. Process. Syst. (NIPS)*, Barcelona, Spain, 2016, pp. 4340–4348 (full version at arXiv:1605.01 636).

[2] M. R. Abedi, M. R. Javan, N. Mokari, E. Jorswieck *et al.*, "Dynamic frame structure for next generation wireless networks," *arXiv preprint arXiv:2002.00419*, 2020.

[3] G. D'Aria *et al.*, "Expanded 6G vision, use cases and societal values–including aspects of sustainability, security and spectrum," Technical report, Hexa-X Project, Tech. Rep., 2021.

[4] 3rd Generation Partnership Project (3GPP), "Study on Communication for Automation in Vertical Domains (CAV)," Technical Report 22.804, V16.2.0, Dec. 2018.

[5] ——, "Service Requirements for the 5G System," Technical specification 22.261, V17.1.0, Dec. 2019.

[6] G. I. Association *et al.*, "Automotive vertical sector," *White Paper 5G-PPP*, 2015.

[7] D. Vasisht, G. Zhang, O. Abari, H.-M. Lu, J. Flanz, and D. Katabi, "In-body backscatter communication and localization," in *Proceedings of the 2018 Conference of the ACM Special Interest Group on Data Communication*, 2018, pp. 132–146.

[8] T. U. of Sheffield Advanced Manufacturing Research Centre (AMRC), "Untangling the requirements of a digital twin," *White Paper*, 2021.

[9] Y. Cai, Z. Qin, F. Cui, G. Y. Li, and J. A. McCann, "Modulation and multiple access for 5G networks," *IEEE Communications Surveys Tutorials*, vol. 20, no. 1, pp. 629–646, Firstquarter 2018.

[10] A. M. Jaradat, J. M. Hamamreh, and H. Arslan, "Modulation options for OFDM-based waveforms: Classification, comparison, and future directions," *IEEE Access*, vol. 7, pp. 17 263–17 278, 2019.

[11] A. Sahin, I. Guvenc, and H. Arslan, "A survey on multicarrier communications: Prototype filters, lattice structures, and implementation aspects," *IEEE Commun. Surveys Tut.*, vol. 16, no. 3, pp. 1312–1338, 3rd Quart., 2014.

[12] T. Hwang, C. Yang, G. Wu, S. Li, and G. Y. Li, "OFDM and its wireless applications: A survey," *IEEE Trans. Veh. Technol.*, vol. 58, no. 4, pp. 1673–1694, May 2009.

[13] M. Vaezi, Z. Ding, and H. Poor, *Multiple Access Techniques for 5G Wireless Networks and Beyond*. SPRINGER INTERNATIONAL PU, 2018.

[14] M. Salah, O. A. Omer, and U. S. Mohammed, "Spectral efficiency enhancement based on sparsely indexed modulation for green radio communication," *IEEE Access*, vol. 7, pp. 31 913–31 925, 2019.

[15] D.-Z. Liu and C.-H. Wei, "DAPSK-OFDM transmissions for high date-rate digital mobile radio," in *ISCAS 2001. The 2001 IEEE International Symposium on*

Circuits and Systems (Cat. No.01CH37196), vol. 2, Sydney, NSW, Australia, May 2001, pp. 417–420.

[16] S. Ganesan, R. Mesleh, H. Ho, C. W. Ahn, and S. Yun, "On the performance of spatial modulation OFDM," in *2006 Fortieth Asilomar Conference on Signals, Systems and Computers*, Pacific Grove, CA, USA, October 2006, pp. 1825–1829.

[17] E. Basar, U. Aygolu, E. Panayirci, and H. V. Poor, "Orthogonal frequency division multiplexing with index modulation," *IEEE Transactions on Signal Processing*, vol. 61, no. 22, pp. 5536–5549, November 2013.

[18] B. Shamasundar, S. Bhat, S. Jacob, and A. Chockalingam, "Multidimensional index modulation in wireless communications," *IEEE Access*, vol. 6, pp. 589–604, 2018.

[19] A. M. Jaradat, J. M. Hamamreh, and H. Arslan, "OFDM with subcarrier number modulation," *IEEE Wireless Communications Letters*, vol. 7, no. 6, pp. 914–917, December 2018.

[20] S. Aldirmaz, A. Serbes, and L. Durak-Ata, "Spectrally efficient OFDMA lattice structure via toroidal waveforms on the time-frequency plane," *EURASIP Journal on Advances in Signal Processing*, vol. 2010, no. 1, p. 684097, July 2010. [Online]. Available: https://doi.org/10.1155/2010/684097

[21] M. Wen, X. Cheng, and L. Yang, *Index Modulation for 5G Wireless Communications*. Springer International Publishing, 2017.

[22] E. Basar, M. Wen, R. Mesleh, M. D. Renzo, Y. Xiao, and H. Haas, "Index modulation techniques for next-generation wireless networks," *IEEE Access*, vol. 5, no. 1, pp. 16 693–16 746, September 2017.

[23] Z. E. Ankaralı, B. Peköz, and H. Arslan, "Flexible radio access beyond 5G: A future projection on waveform, numerology, and frame design principles," *IEEE Access*, vol. 5, pp. 18 295–18 309, 2017.

[24] R. Y. Mesleh, H. Haas, S. Sinanovic, C. W. Ahn, and S. Yun, "Spatial modulation," *IEEE Trans. Veh. Tech.*, vol. 57, no. 4, pp. 2228–2241, July 2008.

[25] R. Abu-alhiga and H. Haas, "Subcarrier-index modulation OFDM," in *Proc. IEEE Int. Sym. Personal, Indoor and Mobile Radio Commun.* IEEE, Sep. 2009, pp. 177–181.

[26] R. Fan, Y. J. Yu, and Y. L. Guan, "Generalization of orthogonal frequency division multiplexing with index modulation," *IEEE Trans. Wirel. Commun.*, vol. 14, no. 10, pp. 5350–5359, Oct 2015.

[27] A. M. Jaradat, J. M. Hamamreh, and H. Arslan, "OFDM with hybrid number and index modulation," *IEEE Access*, pp. 1–1, 2020.

[28] A. Jaradat, J. M. Hamamreh, and H. Arslan, "Orthogonal frequency division multiplexing with subcarrier gap modulation," in *2020 IEEE 31st Annual International Symposium on Personal, Indoor and Mobile Radio Communications*, 2020, pp. 1–6.

[29] M. Elkourdi, B. Peköz, E. Güvenkaya, and H. Arslan, "Waveform design principles for 5G and beyond," in *2016 IEEE 17th Annual Wireless and Microwave Technology Conference (WAMICON)*, Florida, USA, April 2016, pp. 1–6.

[30] Y. Rahmatallah and S. Mohan, "Peak-to-average power ratio reduction in OFDM systems: A survey and taxonomy," *IEEE Communications Surveys Tutorials*, vol. 15, no. 4, pp. 1567–1592, Fourthquarter 2013.

[31] A. M. Jaradat, J. M. Hamamreh, and H. Arslan, "Modulation options for OFDM-based waveforms: Classification, comparison, and future directions," *IEEE Access*, vol. 7, pp. 17 263–17 278, 2019.

[32] Seung Hee Han and Jae Hong Lee, "An overview of peak-to-average power ratio reduction techniques for multicarrier transmission," *IEEE Wireless Communications*, vol. 12, no. 2, pp. 56–65, April 2005.

[33] E. Memisoglu, E. Basar, and H. Arslan, "Low complexity peak-to-average power ratio reduction in OFDM-IM," in *2018 IEEE International Black Sea Conference on Communications and Networking (BlackSeaCom)*, Batumi, Georgia, June 2018, pp. 1–5.

[34] J. V. De Beek, "Sculpting the multicarrier spectrum: a novel projection precoder," *IEEE Communications Letters*, vol. 13, no. 12, pp. 881–883, December 2009.

[35] S. Brandes, I. Cosovic, and M. Schnell, "Sidelobe suppression in OFDM systems by insertion of cancellation carriers," in *2005 IEEE 62nd Vehicular Technology Conference (VTC Fall).*, vol. 1, Dallas, TX, USA, September 2005, pp. 152–156.

[36] A. M. Jaradat, J. M. Hamamreh, and H. Arslan, "Floating ofdm-snm for papr and oobe reduction," in *2021 IEEE 93rd Vehicular Technology Conference (VTC2021-Spring)*. IEEE, 2021, pp. 1–5.

[37] P. Guan, D. Wu, T. Tian, J. Zhou, X. Zhang, L. Gu, A. Benjebbour, M. Iwabuchi, and Y. Kishiyama, "5G field trials: OFDM-based waveforms and mixed numerologies," *IEEE J. Sel. Areas Commun.*, vol. 35, no. 6, pp. 1234–1243, Jun. 2017.

[38] M. Iwabuchi, A. Benjebbour, Y. Kishiyama, D. Wu, T. Tian, L. Gu, Y. Cui, and T. Kashima, "5G field experimental trial on frequency domain multiplexing of mixed numerology," in *2017 IEEE 85th Veh. Tech. Conf. (VTC Spring)*, Jun. 2017, pp. 1–5.

[39] A. A. Zaidi, R. Baldemair, H. Tullberg, H. Bjorkegren, L. Sundstrom, J. Medbo, C. Kilinc, and I. Da Silva, "Waveform and numerology to support 5G services and requirements," *IEEE Commun. Mag.*, vol. 54, no. 11, pp. 90–98, Nov. 2016.

[40] *3rd Generation Partnership Project (3GPP), NR; Physical channels and modulation*, Technical Specification 38.211, ver. 15.1.0, Apr. 2018.

[41] A. Yazar and H. Arslan, "A flexibility metric and optimization methods for mixed numerologies in 5G and beyond," *IEEE Access*, vol. 6, pp. 3755–3764, 2018.

[42] A. Walter, K. Eric, and Q. Andre, "OFDM parameters estimation a time approach," in *Proc. Asilomar Conf: on Signals, Systems and Computers,*, vol. 1, Pacific Grove, California, USA, Oct./Nov. 2000, pp. 142–146.

[43] F. Liedtke and U. Albers, "Evaluation of features for the automatic recognition of OFDM signals in monitoring or cognitive receivers," *Journal of telecommunications and information technology*, vol. 84, no. 2, pp. 30–36, 2008.

[44] H. Kwon, N. N. Ratnakar, and J. Lee, "System and method for blind detection of numerology," US Patent 10,230,492, Mar. 12, 2019.

[45] A. M. Jaradat, E. Memişoğlu, and H. Arslan, "Blind numerology identification for mixed numerologies," in *2021 IEEE Wireless Communications and Networking Conference (WCNC)*, 2021, pp. 1–5.

[46] Z. Xiao, H. Wen, A. Markham, N. Trigoni, P. Blunsom, and J. Frolik, "Non-line-of-sight identification and mitigation using received signal strength," *IEEE Trans. Wireless Commun.*, vol. 14, no. 3, pp. 1689–1702, 2015.

[47] D. Li, G. Wu, J. Zhao, W.-H. Niu, and Q. Liu, "Wireless channel identification algorithm based on feature extraction and BP neural network." *JIPS*, vol. 13, no. 1, pp. 141–151, 2017.

[48] T. Blumensath and M. E. Davies, "Iterative hard thresholding for compressed sensing," *Appl. Comput. Harmon. Anal.*, vol. 27, no. 3, pp. 265–274, 2009.

[49] Z. Cheng, M. Tao, and P. Y. Kam, "Channel path identification in mmWave systems with large-scale antenna arrays," *IEEE Trans. Commun.*, vol. 68, no. 9, pp. 5549–5562, 2020.

[50] A. M. Jaradat, K. Walid Elgammal, M. K. Özdemir, and H. Arslan, "Identification of the number of wireless channel taps using deep neural networks," in *2021 19th IEEE International New Circuits and Systems Conference (NEWCAS)*, 2021, pp. 1–4.

[51] P. Popovski, K. F. Trillingsgaard, O. Simeone, and G. Durisi, "5G wireless network slicing for eMBB, URLLC, and mMTC: A communication-theoretic view," *IEEE Access*, vol. 6, pp. 55 765–55 779, 2018.

[52] M. Alsenwi, N. H. Tran, M. Bennis, A. K. Bairagi, and C. S. Hong, "eMBB-URLLC resource slicing: A risk-sensitive approach," *IEEE Communications Letters*, vol. 23, no. 4, pp. 740–743, 2019.

[53] A. K. Bairagi, M. S. Munir, M. Alsenwi, N. H. Tran, S. S. Alshamrani, M. Masud, Z. Han, and C. S. Hong, "Coexistence mechanism between eMBB and URLLC in 5G wireless networks," *IEEE Transactions on Communications*, vol. 69, no. 3, pp. 1736–1749, 2020.

[54] M. Alsenwi, N. H. Tran, M. Bennis, S. R. Pandey, A. K. Bairagi, and C. S. Hong, "Intelligent resource slicing for eMBB and URLLC coexistence in 5G and beyond: A deep reinforcement learning based approach," *IEEE Transactions on Wireless Communications*, vol. 20, no. 7, pp. 4585–4600, 2021.

[55] A. Gameiro, D. Castanheira, J. Sanson, and P. P. Monteiro, "Research challenges, trends and applications for future joint radar communications systems," *Wireless Personal Communications*, vol. 100, no. 1, pp. 81–96, 2018.

[56] B. P. Ginsburg, K. Subburaj, S. Samala, K. Ramasubramanian, J. Singh, S. Bhatara, S. Murali, D. Breen, M. Moallem, K. Dandu *et al.*, "A multimode 76-to-81GHz automotive radar transceiver with autonomous monitoring," in *2018 ieee international solid-state circuits conference-(isscc)*. IEEE, 2018, pp. 158–160.

[57] P. Kumari, J. Choi, N. González-Prelcic, and R. W. Heath, "IEEE 802.11 ad-based radar: An approach to joint vehicular communication-radar system," *IEEE Transactions on Vehicular Technology*, vol. 67, no. 4, pp. 3012–3027, 2017.

[58] A. Taha, Q. Qu, S. Alex, P. Wang, W. L. Abbott, and A. Alkhateeb, "Millimeter wave MIMO-based depth maps for wireless virtual and augmented reality," *IEEE Access*, vol. 9, pp. 48 341–48 363, 2021.

[59] N. Gonzalez-Prelcic, R. Méndez-Rial, and R. W. Heath, "Radar aided beam alignment in mmwave V2I communications supporting antenna diversity," in *2016 Information Theory and Applications Workshop (ITA)*. IEEE, 2016, pp. 1–7.

[60] Z. Chen, Z. Cao, X. He, Y. Jin, J. Li, and P. Chen, "DoA and DoD estimation and hybrid beamforming for radar-aided mmwave MIMO vehicular communication systems," *Electronics*, vol. 7, no. 3, p. 40, 2018.

[61] G. R. Muns, K. V. Mishra, C. B. Guerra, Y. C. Eldar, and K. R. Chowdhury, "Beam alignment and tracking for autonomous vehicular communication using IEEE 802.11 ad-based radar," in *IEEE INFOCOM 2019-IEEE conference on computer communications workshops (INFOCOM WKSHPS)*. IEEE, 2019, pp. 535–540.

[62] A. Ali, N. González-Prelcic, and A. Ghosh, "Passive radar at the roadside unit to configure millimeter wave vehicle-to-infrastructure links," *IEEE Transactions on Vehicular Technology*, vol. 69, no. 12, pp. 14 903–14 917, 2020.

[63] C. Jiao, Z. Zhang, C. Zhong, X. Chen, and Z. Feng, "Millimeter wave communication with active ambient perception," *IEEE Transactions on Wireless Communications*, vol. 18, no. 5, pp. 2751–2764, 2019.

[64] F. Liu, W. Yuan, C. Masouros, and J. Yuan, "Radar-assisted predictive beamforming for vehicular links: Communication served by sensing," *IEEE Transactions on Wireless Communications*, vol. 19, no. 11, pp. 7704–7719, 2020.

[65] N. C. Luong, X. Lu, D. T. Hoang, D. Niyato, and D. I. Kim, "Radio resource management in joint radar and communication: A comprehensive survey," *IEEE Communications Surveys Tutorials*, vol. 23, no. 2, pp. 780–814, 2021.

[66] M. Richart, J. Baliosian, J. Serrat, and J.-L. Gorricho, "Resource slicing in virtual wireless networks: A survey," *IEEE Transactions on Network and Service Management*, vol. 13, no. 3, pp. 462–476, 2016.

[67] M. Dianati, X. Shen, and K. Naik, "Cooperative fair scheduling for the downlink of CDMA cellular networks," *IEEE Transactions on Vehicular Technology*, vol. 56, no. 4, pp. 1749–1760, 2007.

[68] S. Mosleh, L. Liu, and J. Zhang, "Proportional-fair resource allocation for coordinated multi-point transmission in LTE-Advanced," *IEEE Transactions on Wireless Communications*, vol. 15, no. 8, pp. 5355–5367, 2016.

[69] A. Zeshan, M. Karbalayghareh, F. Miramirkhani, M. Uysal, and T. Baykas, "Comparative performance evaluation of VLC, LTE and WLAN technologies in indoor environments," in *2021 IEEE International Black Sea Conference on Communications and Networking (BlackSeaCom)*, 2021, pp. 1–6.

[70] I. Kabashkin, "Reliable V2X communications for safety-critical intelligent transport systems," in *2017 Advances in Wireless and Optical Communications (RTUWO)*, 2017, pp. 251–255.

[71] A. M. Jaradat, A. Naeem, M. I. Sağlam, M. Kartal, and H. Arslan, "Radar-aided communication scheduling algorithm for 5g and beyond networks," *IEEE Access*, vol. 10, pp. 96 403–96 413, 2022.

[72] F.-C. Kuo, K.-C. Ting, H.-C. Wang, C.-C. Tseng, and M.-W. Chen, "Differentiating and scheduling LTE uplink traffic based on exponentially weighted moving average of data rate," *Mobile Networks and Applications*, vol. 22, no. 1, pp. 113–124, 2017.

[73] T. V. Trapala, "Dynamic resource allocation for cellular networks with interference," Ph.D. dissertation, Télécom ParisTech, 2013.

[74] A. Anand, G. De Veciana, and S. Shakkottai, "Joint scheduling of URLLC and eMBB traffic in 5G wireless networks," in *IEEE INFOCOM 2018 - IEEE Conference on Computer Communications*, 2018, pp. 1970–1978.

[75] A. M. Jaradat, M. □. Sağlam, M. Kartal, and H. Arslan, "Dynamic-structure resource block allocation based scheduling for 5g systems," in *2022 IEEE 95th Vehicular Technology Conference: (VTC2022-Spring)*, 2022, pp. 1–5.

[76] T. Hwang, C. Yang, G. Wu, S. Li, and G. Y. Li, "OFDM and its wireless applications: A survey," *IEEE Transactions on Vehicular Technology*, vol. 58, no. 4, pp. 1673–1694, May 2009.

[77] H. Rohling and T. May, "OFDM systems with differential modulation schemes and turbo decoding techniques," in *2000 International Zurich Seminar on Broadband Communications. Accessing, Transmission, Networking. Proceedings (Cat. No.00TH8475)*, Zurich, Switzerland, February 2000, pp. 251–255.

[78] M. Driusso, F. Babich, M. I. Kadir, and L. Hanzo, "OFDM aided space-time shift keying for dispersive downlink channels," in *2012 IEEE Vehicular Technology Conference (VTC Fall)*, Quebec City, QC, Canada, September 2012, pp. 1–5.

[79] T. Datta, H. S. Eshwaraiah, and A. Chockalingam, "Generalized space-and-frequency index modulation," *IEEE Transactions on Vehicular Technology*, vol. 65, no. 7, pp. 4911–4924, July 2016.

[80] Q. Li, M. Wen, E. Basar, and F. Chen, "OFDM spread spectrum with index modulation," in *IEEE Globecom Workshops (GC Wkshps)*, Singapore, December 2017, pp. 1–6.

[81] A. K. Khandani, "Media-based modulation: A new approach to wireless transmission," in *2013 IEEE International Symposium on Information Theory*, Istanbul, Turkey, July 2013, pp. 3050–3054.

[82] M. Hofer, M. Simko, S. Schwarz, and M. Rupp, "Performance evaluation of differential modulation in LTE-downlink," in *2013 20th International Conference on Systems, Signals and Image Processing (IWSSIP)*, Bucharest, Romania, July 2013, pp. 179–182.

[83] R. Mesleh and A. Alhassi, *Space Modulation Techniques*. Wiley, 2018.

[84] R. Y. Mesleh, H. Haas, S. Sinanovic, C. W. Ahn, and S. Yun, "Spatial modulation," *IEEE Transactions on Vehicular Technology*, vol. 57, no. 4, pp. 2228–2241, July 2008.

[85] P. Yang, Y. Xiao, B. Zhou, and S. Li, "Initial performance evaluation of spatial modulation OFDM in LTE-based systems," in *2011 6th International ICST Conference on Communications and Networking in China (CHINACOM)*, Harbin, China, August 2011, pp. 102–107.

[86] X. Cheng, M. Zhang, M. Wen, and L. Yang, "Index modulation for 5G: Striving to do more with less," *IEEE Wireless Communications*, vol. 25, no. 2, pp. 126–132, April 2018.

[87] T. Mao, Z. Wang, Q. Wang, S. Chen, and L. Hanzo, "Dual-mode index modulation aided OFDM," *IEEE Access*, vol. 5, pp. 50–60, Sep. 2017.

[88] T. Mao, Q. Wang, and Z. Wang, "Generalized dual-mode index modulation aided OFDM," *IEEE Commun. Lett.*, vol. 21, no. 4, pp. 761–764, Apr. 2017.

[89] M. Wen, E. Basar, Q. Li, B. Zheng, and M. Zhang, "Multiple-mode orthogonal frequency division multiplexing with index modulation," *IEEE Trans. Commun.*, vol. 65, no. 9, pp. 3892–3906, Sept 2017.

[90] S. Dang, G. Ma, B. Shihada, and M. Alouini, "Enhanced orthogonal frequency-division multiplexing with subcarrier number modulation," *IEEE Internet of Things Journal*, vol. 6, no. 5, pp. 7907–7920, October 2019.

[91] *NR numerology scaling and alignment*, R1-166364, Aug. 2016.

[92] N. M. Idrees, M. R. Petit, and A. Springer, "Identification of taps in time-variant multipath channels for 3GPP LTE-downlink," in *Proc. Eur. Wireless*, Budapest, Hungary, 2015, pp. 1–6.

[93] A. Adhikary, E. Al Safadi, M. K. Samimi, R. Wang, G. Caire, T. S. Rappaport, and A. F. Molisch, "Joint spatial division and multiplexing for mm-Wave channels," *IEEE J. Sel. Areas Commun.*, vol. 32, no. 6, pp. 1239–1255, 2014.

[94] U. Demirhan and A. Alkhateeb, "Radar aided 6G beam prediction: Deep learning algorithms and real-world demonstration," in *2022 IEEE Wireless Communications and Networking Conference (WCNC)*. IEEE, 2022, pp. 2655–2660.

[95] H. Holma and A. Toskala, *LTE for UMTS: Evolution to LTE-Advanced*. John Wiley & Sons, 2011.

[96] F. Afroz, R. Subramanian, R. Heidary, K. Sandrasegaran, and S. Ahmed, "SINR, RSRP, RSSI and RSRQ measurements in long term evolution networks," *International Journal of Wireless & Mobile Networks*, 2015.

[97] W. Liu, M. Kulin, T. Kazaz, A. Shahid, I. Moerman, and E. De Poorter, "Wireless technology recognition based on RSSI distribution at sub-nyquist sampling rate for constrained devices," *Sensors*, vol. 17, no. 9, p. 2081, 2017.

[98] W. Kozek and A. F. Molisch, "Nonorthogonal pulse shapes for multicarrier communications in doubly dispersive channels," *IEEE Journal on Selected Areas in Communications*, vol. 16, no. 8, pp. 1579–1589, October 1998.

[99] G. Fettweis, M. Krondorf, and S. Bittner, "GFDM-generalized frequency division multiplexing," in *VTC Spring 2009 - IEEE 69th Vehicular Technology Conference*, Barcelona, Spain, April 2009, pp. 1–4.

[100] E. Çatak and L. Durak-Ata, "An efficient transceiver design for superimposed waveforms with orthogonal polynomials," in *2017 IEEE International Black*

Sea Conference on Communications and Networking (BlackSeaCom), Istanbul, Turkey, June 2017, pp. 1–5.

[101] J. S. E. Dahlman, S. Parkvall, *4G: LTE/LTE-Advanced for Mobile Broadband*. Academic press, 2013.

[102] A. Othman, S. Y. Ameen, and H. Al-Rizzo, "Dynamic switching of scheduling algorithm for uplink LTE system," *International Journal of Computing and Network Technology*, vol. 6, no. 3, 2018.

[103] M. E. Sahin, I. Guvenc, and H. Arslan, "Optimization of energy detector receivers for UWB systems," in *IEEE 61st Veh. Tech. Conf.*, vol. 2, May 2005, pp. 1386–1390 Vol. 2.

[104] M. Chiani and D. Dardari, "Improved exponential bounds and approximation for the Q-function with application to average error probability computation," in *Proc. IEEE GLOBECOM Conf.*, 2002, pp. 1399–1402.

[105] H. Jafarkhani, *Space-Time Coding*. Cambridge, UK: Cambridge University Press, 2005.

[106] M. Wen, Y. Zhang, J. Li, E. Basar, and F. Chen, "Equiprobable subcarrier activation method for OFDM with index modulation," *IEEE Commun. Lett.*, vol. 20, no. 12, pp. 2386–2389, Dec. 2016.

[107] E. Basar, U. Aygolu, E. Panayirci, and H. V. Poor, "Orthogonal frequency division multiplexing with index modulation," *IEEE Trans. Signal Process.*, vol. 61, no. 22, pp. 5536–5549, Nov 2013.

[108] S. Dang, J. P. Coon, and G. Chen, "Adaptive OFDM with index modulation for two-hop relay-assisted networks," *IEEE Trans. Wirel. Commun.*, vol. 17, no. 3, pp. 1923–1936, Mar. 2018.

[109] S. Dang, G. Chen, and J. P. Coon, "Lexicographic codebook design for OFDM with index modulation," *IEEE Trans. Wirel. Commun.*, vol. 17, no. 12, pp. 8373–8387, Dec. 2018.

[110] D. Tsonev, S. Sinanovic, and H. Haas, "Enhanced subcarrier index modulation (SIM) OFDM," in *2011 IEEE GLOBECOM Workshops (GC Wkshps)*, Dec. 2011, pp. 728–732.

[111] Z. Wang, S. Dang, and D. T. Kennedy, "Multi-hop index modulation-aided OFDM with decode-and-forward relaying," *IEEE Access*, vol. 6, pp. 26 457–26 468, 2018.

[112] M. Wen, X. Cheng, M. Ma, B. Jiao, and H. V. Poor, "On the achievable rate of OFDM with index modulation," *IEEE Trans. Signal Process.*, vol. 64, no. 8, pp. 1919–1932, Apr. 2016.

[113] M. Wen, B. Ye, E. Basar, Q. Li, and F. Ji, "Enhanced orthogonal frequency division multiplexing with index modulation," *IEEE Trans. Wirel. Commun.*, vol. 16, no. 7, pp. 4786–4801, Jul. 2017.

[114] S. Dang, J. Li, M. Wen, and S. Mumtaz, "Distributed processing for multi-relay assisted OFDM with index modulation," *IEEE Trans. Wirel. Commun.*, vol. 18, no. 2, pp. 1318–1331, Feb. 2019.

[115] M. Chiani, D. Dardari, and M. K. Simon, "New exponential bounds and approximations for the computation of error probability in fading channels," *IEEE Trans. Wirel. Commun.*, vol. 2, no. 4, pp. 840–845, Jul. 2003.

[116] Q. Ma, P. Yang, Y. Xiao, H. Bai, and S. Li, "Error probability analysis of OFDM-IM with carrier frequency offset," *IEEE Commun. Lett.*, vol. 20, no. 12, pp. 2434–2437, Dec. 2016.

[117] Q. Li, M. Wen, H. V. Poor, and F. Chen, "Information guided precoding for OFDM," *IEEE Access*, vol. 5, pp. 19 644–19 656, 2017.

[118] Y. Ko, "A tight upper bound on bit error rate of joint OFDM and multi-carrier index keying," *IEEE Commun. Lett.*, vol. 18, no. 10, pp. 1763–1766, Oct. 2014.

[119] R. Fan, Y. J. Yu, and Y. L. Guan, "Improved orthogonal frequency division multiplexing with generalised index modulation," *IET Communications*, vol. 10, no. 8, pp. 969–974, 2016.

[120] G. Y. Li, Z. Xu, C. Xiong, C. Yang, S. Zhang, Y. Chen, and S. Xu, "Energy-efficient wireless communications: tutorial, survey, and open issues," *IEEE Wirel. Commun.*, vol. 18, no. 6, pp. 28–35, Dec. 2011.

[121] P. Loskot and N. C. Beaulieu, "Prony and polynomial approximations for evaluation of the average probability of error over slow-fading channels," *IEEE Transactions on Vehicular Technology*, vol. 58, no. 3, pp. 1269–1280, March 2009.

[122] R. Horn and C. Johnson, *Matrix Analysis*. Cambridge University Press, 2012.

[123] A. M. Jaradat, J. M. Hamamreh, and H. Arslan, "OFDM with subcarrier number modulation," *IEEE Wireless Communications Letters*, vol. 7, no. 6, pp. 914–917, Dec 2018.

[124] R. van Nee and A. de Wild, "Reducing the peak-to-average power ratio of OFDM," in *VTC '98. 48th IEEE Vehicular Technology Conference. Pathway to Global Wireless Revolution (Cat. No.98CH36151)*, vol. 3, Ottawa, Canada, May 1998, pp. 2072–2076.

[125] P. Wolniansky, G. Foschini, G. Golden, and R. Valenzuela, "V-BLAST: An architecture for realizing very high data rates over the rich-scattering wireless channel," in *1998 URSI International Symposium on Signals, Systems, and Electronics. Conference Proceedings (Cat. No.98EX167)*, vol. 2, Pisa, Italy, March 1999, pp. 295 – 300.

[126] S. M. Alamouti, "A simple transmit diversity technique for wireless communications," *IEEE Journal on Selected Areas in Communications*, vol. 16, no. 8, pp. 1451–1458, October 1998.

[127] E. Memisoglu, E. Basar, and H. Arslan, "Low complexity peak-to- average power ratio reduction in OFDM-IM," in *2018 IEEE International Black Sea Conference on Communications and Networking (BlackSeaCom)*, Batumi, Georgia, June 2018, pp. 1–5.

[128] J. Jacob, C. M. Panazio, and T. Abrão, "PAPR and saturation effects of power amplifiers in SM OFDM and V-BLAST OFDM systems," in *2014 International Telecommunications Symposium (ITS)*, Sao Paulo, Brazil, August 2014, pp. 1–5.

[129] M. Elkhodr, Q. Hassan, and S. Shahrestani, *Networks of the Future: Architectures, Technologies, and Implementations*. Taylor & Francis Incorporated, 2017.

[130] S. Gokceli, E. Basar, M. Wen, and G. K. Kurt, "Practical implementation of index modulation-based waveforms," *IEEE Access*, vol. 5, pp. 25 463–25 473, November 2017.

[131] J. Jeganathan, A. Ghrayeb, and L. Szczecinski, "Spatial modulation: optimal detection and performance analysis," *IEEE Communications Letters*, vol. 12, no. 8, pp. 545–547, August 2008.

[132] J. Proakis and M. Salehi, *Digital Communications, 5th edition*. McGraw-Hill Higher Education, New York, 2008.

[133] J. W. Cooley and J. W. Tukey, "An algorithm for the machine calculation of complex Fourier series," *Mathematics of computation*, vol. 19, no. 90, pp. 297–301, 1965.

[134] Y. Ding and B. D. Rao, "Dictionary learning-based sparse channel representation and estimation for FDD massive MIMO systems," *IEEE Trans. Wirel. Commun.*, vol. 17, no. 8, pp. 5437–5451, 2018.

[135] "Open source downloadable 5G channel simulator software," https://wireless.engineering.nyu.edu/nyusim-5g-and-6g/, accessed: 2021-03-11.

[136] S. Jaeckel, L. Raschkowski, K. Börner, and L. Thiele, "QuaDRiGa: A 3-D multi-cell channel model with time evolution for enabling virtual field trials," *IEEE Trans. Antennas Propag.*, vol. 62, no. 6, pp. 3242–3256, 2014.

[137] D. P. Kingma and J. Ba, "Adam: A method for stochastic optimization," in *Proc. Int. Conf. Learn. Represent. (ICLR)*, San Diego, CA, USA, 2015, pp. 1–15 (full version at arXiv:1412.6980).

[138] N. Kollerstrom, "Thomas simpson and 'newton's method of approximation': an enduring myth," *The Br. J. Hist. Sci.*, vol. 25, no. 3, p. 347–354, 1992.

[139] M. Mert Şahin and H. Arslan, "Multi-functional coexistence of radar-sensing and communication waveforms," in *2020 IEEE 92nd Vehicular Technology Conference (VTC2020-Fall)*, 2020, pp. 1–5.

[140] Y. Zhang, M. Alrabeiah, and A. Alkhateeb, "Reinforcement learning of beam codebooks in millimeter wave and terahertz MIMO systems," *IEEE Transactions on Communications*, vol. 70, no. 2, pp. 904–919, 2021.

[141] J. C. E. Jiménez, M. J. F.-G. García, and D. Méndez-Romero, "Pilot-assisted channel estimation," *Wiley 5G Ref: The Essential 5G Reference Online*, pp. 1–19, 2019.

[142] A. Graff, A. Ali, and N. González-Prelcic, "Measuring radar and communication congruence at millimeter wave frequencies," in *2019 53rd Asilomar Conference on Signals, Systems, and Computers*. IEEE, 2019, pp. 925–929.

[143] A. Graff, Y. Chen, N. González-Prelcic, and T. Shimizu, "Deep learning-based link configuration for radar-aided multiuser mmwave vehicle-to-infrastructure communication," *arXiv preprint arXiv:2201.04657*, 2022.

[144] H. Wymeersch, D. Shrestha, C. M. De Lima, V. Yajnanarayana, B. Richerzhagen, M. F. Keskin, K. Schindhelm, A. Ramirez, A. Wolfgang, M. F. De Guzman *et al.*, "Integration of communication and sensing in 6G: A joint industrial and academic perspective," in *2021 IEEE 32nd Annual International Symposium on*

Personal, Indoor and Mobile Radio Communications (PIMRC). IEEE, 2021, pp. 1–7.

[145] N. A. Ali, H.-A. M. Mourad, H. M. ElSayed, M. El-Soudani, H. H. Amer, and R. M. Daoud, "General expressions for downlink signal to interference and noise ratio in homogeneous and heterogeneous LTE-Advanced networks," *Journal of advanced research*, vol. 7, no. 6, pp. 923–929, 2016.

[146] S. Sarepalli, "LTE downlink scheduling algorithms," Ph.D. dissertation, 2016, copyright - Database copyright ProQuest LLC; ProQuest does not claim copyright in the individual underlying works; Last updated - 2021-05-21. [Online]. Available: https://www.proquest.com/dissertations-theses/lte-downlink-scheduling-algorithms/docview/1844988633/se-2?accountid=191742

[147] I. Poole, "Free space path loss: Details, formula, calculator," http://radio-electronics.com.

[148] H. P. Young, "Learning by trial and error," *Games and economic behavior*, vol. 65, no. 2, pp. 626–643, 2009.

[149] 3rd Generation Partnership Project (3GPP), "Study on Scenarios and Requirements for Next Generation Access Technologies, Technical Specification Group Radio Access Network," Technical Report TR 38.913, V14.0.0, Oct. 2016.

[150] C. F. Müller, G. Galaviz, Á. G. Andrade, I. Kaiser, and W. Fengler, "Evaluation of scheduling algorithms for 5G mobile systems," in *Computer Science and Engineering—Theory and Applications*. Springer, 2018, pp. 213–233.

[151] Y. Xiao, S. Wang, L. Dan, X. Lei, P. Yang, and W. Xiang, "OFDM with interleaved subcarrier-index modulation," *IEEE Commun. Lett.*, vol. 18, no. 8, pp. 1447–1450, Aug 2014.

[152] Y. Cho, J. Kim, W. Yang, and C. Kang, *MIMO-OFDM Wireless Communications with MATLAB*, ser. Wiley - IEEE. Wiley, 2010.

[153] N. Ishikawa, S. Sugiura, and L. Hanzo, "Subcarrier-index modulation aided OFDM - will it work?" *IEEE Access*, vol. 4, pp. 2580–2593, 2016.

[154] Y. Rahmatallah and S. Mohan, "Peak-to-average power ratio reduction in OFDM systems: A survey and taxonomy," *IEEE Commun. Surveys Tut.*, vol. 15, no. 4, pp. 1567–1592, Apr. 2013.

[155] Y. Acar, S. Aldirmaz, and E. Basar, "Channel estimation for OFDM-IM systems," *Turkish Journal of Electrical Engineering and Computer Sciences*, vol. 27, pp. 1908–1921, 05 2019.

[156] Meng-Han Hsieh and Che-Ho Wei, "Channel estimation for OFDM systems based on comb-type pilot arrangement in frequency selective fading channels," *IEEE Transactions on Consumer Electronics*, vol. 44, no. 1, pp. 217–225, Feb. 1998.

[157] J. M. Hamamreh, H. M. Furqan, and H. Arslan, "Secure pre-coding and post-coding for OFDM systems along with hardware implementation," in *2017 13th International Wireless Communications and Mobile Computing Conference (IWCMC)*, Jun. 2017, pp. 1338–1343.

[158] B. Muquet, Zhengdao Wang, G. B. Giannakis, M. de Courville, and P. Duhamel, "Cyclic prefixing or zero padding for wireless multicarrier transmissions?" *IEEE Transactions on Communications*, vol. 50, no. 12, pp. 2136–2148, Dec. 2002.

[159] A. B. Kihero, M. S. J. Solaija, and H. Arslan, "Inter-numerology interference for beyond 5G," *IEEE Access*, vol. 7, pp. 146 512–146 523, 2019.

[160] Z. Ren, G. Wang, Q. Chen, and H. Li, "Modelling and simulation of rayleigh fading, path loss, and shadowing fading for wireless mobile networks," *Simulation Modelling Practice and Theory*, vol. 19, no. 2, pp. 626–637, 2011.

[161] V. C. Gungor and O. G. Uyan, "QoS-aware downlink scheduling algorithm for LTE networks: A case study on edge users," in *2017 25th Signal Processing and Communications Applications Conference (SIU)*. IEEE, 2017, pp. 1–4.

[162] A. Sinha, M. Andrews, and P. Ananth, "Scheduling algorithms for 5G networks with mid-haul capacity constraints," in *2019 International Symposium on Modeling and Optimization in Mobile, Ad Hoc, and Wireless Networks (WiOPT)*, 2019, pp. 1–8.

[163] M. T. Kawser, H. Farid, A. R. Hasin, A. M. Sadik, and I. K. Razu, "Performance comparison between round robin and proportional fair scheduling methods for LTE," *International Journal of Information and Electronics Engineering*, vol. 2, no. 5, pp. 678–681, 2012.

[164] K. Arshad, "LTE system level performance in the presence of CQI feedback uplink delay and mobility," in *2015 International Conference on Communications, Signal Processing, and their Applications (ICCSPA'15)*, 2015, pp. 1–5.

[165] 3rd Generation Partnership Project (3GPP), "Evolved Universal Terrestrial Radio Access (E-UTRA); User Equipment (UE) radio transmission and reception (Release 8)," Technical Specification TS 36.101, V8.0.0, Dec. 2007.

[166] A. Hajar, J. M. Hamamreh, M. Abewa, and Y. Belallou, "A spectrally efficient OFDM-based modulation scheme for future wireless systems," in *2019 Scientific Meeting on Electrical-Electronics Biomedical Engineering and Computer Science (EBBT)*, April 2019, pp. 1–4.

[167] Y. Belallou, J. M. Hamamreh, and A. Hajar, "OFDM-subcarrier power modulation with two dimensional signal constellations," in *2019 Innovations in Intelligent Systems and Applications Conference (ASYU)*, Oct 2019, pp. 1–6.

[168] A. Hajar and J. M. Hamamreh, "The generalization of orthogonal frequency division multiplexing with subcarrier power modulation to quadrature signal constellations," *RS Open Journal on Innovative Communication Technologies*, 5 2020. [Online]. Available: https://rs-ojict.pubpub.org/pub/ofdm-spm

[169] J. M. Hamamreh, A. Hajar, and M. Abewa, "Orthogonal frequency division multiplexing with subcarrier power modulation for doubling the spectral efficiency of 6G and beyond networks," *Transactions on Emerging Telecommunications Technologies*, p. e3921, 2020.

[170] A. M. Jaradat, J. M. Hamamreh, and H. Arslan, "OFDM with hybrid number and index modulation," *IEEE Access*, vol. 8, pp. 55 042–55 053, 2020.

[171] ——, "Orthogonal frequency division multiplexing with subcarrier gap modulation," in *2020 IEEE 31th Annual International Symposium on Personal, Indoor*

and Mobile Radio Communications (PIMRC), London, UK, August 2020, pp. 1–6.

[172] A. M. Jaradat, J. M. Hamamreh, and H. Arslan, *Flexible and Cognitive Radio Access Technologies for 5G and Beyond*, 1st ed., ser. Telecommunications. London, UK: The Institution of Engineering and Technology, 10 2020, ch. 5, pp. 143–174.

[173] A. A. Zaidi, R. Baldemair, H. Tullberg, H. Bjorkegren, L. Sundstrom, J. Medbo, C. Kilinc, and I. D. Silva, "Waveform and numerology to support 5G services and requirements," *IEEE Communications Magazine*, vol. 54, no. 11, pp. 90–98, November 2016.

[174] Z. Ankarali, B. Pekoz, and H. Arslan, "Flexible radio access beyond 5G: A future projection on waveform, numerology frame design principles," *IEEE Access*, vol. 5, no. 1, pp. 18 295–18 309, March 2017.

[175] Y. Medjahdi, S. Traverso, R. Gerzaguet, H. Shaïek, R. Zayani, D. Demmer, R. Zakaria, J. Doré, M. Ben Mabrouk, D. Le Ruyet, Y. Louët, and D. Roviras, "On the road to 5G: Comparative study of physical layer in MTC context," *IEEE Access*, vol. 5, pp. 26 556–26 581, 2017.

[176] J. Abdoli, M. Jia, and J. Ma, "Filtered OFDM: A new waveform for future wireless systems," in *2015 IEEE 16th International Workshop on Signal Processing Advances in Wireless Communications (SPAWC)*, Stockholm, Sweden, June 2015, pp. 66–70.

[177] M. Bellanger, "FBMC physical layer: A primer," ICT-PHYDYAS, Tech. Rep., 2010.

[178] V. Vakilian, T. Wild, F. Schaich, S. ten Brink, and J. Frigon, "Universal-filtered multi-carrier technique for wireless systems beyond LTE," in *2013 IEEE Globecom Workshops (GC Wkshps)*, Atlanta, GA, December 2013, pp. 223–228.

[179] J. Zhang, M. Zhao, L. Zhang, J. Zhong, and T. Yu, "Circular convolution filter bank multicarrier (FBMC) system with index modulation," in *2017 IEEE 86th Vehicular Technology Conference (VTC-Fall)*, Toronto, Canada, September 2017, pp. 1–5.

[180] S. Gokceli, E. Basar, and G. K. Kurt, "Universal filtered OFDM with filter shift keying - invited paper," in *2018 IEEE 87th Vehicular Technology Conference (VTC Spring)*, Porto, Portugal, June 2018, pp. 1–5.

[181] S. Nusenu, "Spatial modulation technique for filtered-OFDM based wireless transmission," *Advances in Science, Technology and Engineering Systems Journal*, vol. 2, pp. 981–986, 07 2017.

[182] L. Yang, "Transmitter preprocessing aided spatial modulation for multiple-input multiple-output systems," in *2011 IEEE 73rd Vehicular Technology Conference (VTC Spring)*, Budapest, Hungary, May 2011, pp. 1–5.

[183] J. Lim, H. G. Myung, K. Oh, and D. J. Goodman, "Channel-dependent scheduling of uplink single carrier FDMA systems," in *IEEE Veh. Technol. Conf.*, Sep. 2006, pp. 1–5.

[184] C. Y. Wong, R. S. Cheng, K. B. Lataief, and R. D. Murch, "Multiuser OFDM with adaptive subcarrier, bit, and power allocation," *IEEE J. Sel. Areas Commun.*, vol. 17, no. 10, pp. 1747–1758, Oct. 1999.

[185] E. Guvenkaya, J. M. Hamamreh, and H. Arslan, "On physical-layer concepts and metrics in secure signal transmission," *Phy. Commun.*, vol. 25, pp. 14 – 25, Aug. 2017.

[186] J. M. Hamamreh, H. M. Furqan, and H. Arslan, "Classifications and applications of physical layer security techniques for confidentiality: A comprehensive survey," *IEEE Commun. Surveys Tut.*, vol. 21, no. 2, pp. 1773–1828, 2019.

[187] Y. Lee, H. Jo, Y. Ko, and J. Choi, "Secure index and data symbol modulation for OFDM-IM," *IEEE Access*, vol. 5, pp. 24 959–24 974, Nov. 2017.

[188] H. M. Furqan, J. M. Hamamreh, and H. Arslan, "Adaptive OFDM-IM for enhancing physical layer security and spectral efficiency of future wireless networks," *Wireless Communications and Mobile Computing*, vol. 2018, pp. 3 178 303:1–3 178 303:16, August 2018.

[189] I. Parvez, A. Rahmati, I. Guvenc, A. I. Sarwat, and H. Dai, "A survey on low latency towards 5G: RAN, core network and caching solutions," *IEEE Commun. Surveys Tut.*, pp. 1–1, 2018.

[190] S. Doğan, A. Tusha, and H. Arslan, "OFDM with index modulation for asynchronous mMTC networks," *Sensors*, vol. 18, p. 1280, Apr. 2018.

[191] J. Zheng and H. Lv, "Peak-to-average power ratio reduction in OFDM index modulation through convex programming," *IEEE Commun. Lett.*, vol. 21, no. 7, pp. 1505–1508, Jul. 2017.

[192] K. Kim, "PAPR reduction in OFDM-IM using multilevel dither signals," *CoRR*, vol. abs/1810.02533, 2018. [Online]. Available: http://arxiv.org/abs/1810.02533

[193] S. S. Hassaneen, H. Y. Soliman, k. A. Elbarbary, and A. E. Elhennawy, "Reducing the peak to average power ratio in MIMO OFDM systems," in *2013 9th International Computer Engineering Conference (ICENCO)*, Dec. 2013, pp. 128–133.

[194] R. F. H. Fischer and M. Hoch, "Directed selected mapping for peak-to-average power ratio reduction in mimo ofdm," *Electronics Letters*, vol. 42, no. 22, pp. 1289–1290, Oct 2006.

[195] T. C. W. Schenk, P. F. M. Smulders, and E. R. Fledderus, "The application of spatial shifting for peak-to-average power ratio reduction in mimo ofdm systems," in *2006 IEEE 63rd Vehicular Technology Conference*, vol. 4, May 2006, pp. 1859–1863.

CURRICULUM VITAE

Name Surname : Ahmad Mohammad Abd-alghani Jaradat

EDUCATION:

B.Sc.	: 2013, Yarmouk University, Hijjawi Faculty for Engineering Technology, The Communication Engineering Department (CME).
M.Sc.	: 2016, Yarmouk University, Hijjawi Faculty for Engineering Technology, The Communication Engineering Department (CME).

PROFESSIONAL EXPERIENCE AND REWARDS:

- Graduate Research Scholarship at Istanbul Medipol University. The scholarship covers the full tuition for the entire duration of studies.

PUBLICATIONS, PRESENTATIONS, AND PATENTS ON THE THESIS:

- A. Jaradat, J. M. Hamamreh, H. Arslan, "OFDM with Subcarrier Number Modulation," IEEE Wireless Communications Letters, 7(6), 914-917, Dec. 2018.
- A. Jaradat, J. M. Hamamreh, H. Arslan, "Modulation Options for OFDM-Based Waveforms: Classification, Comparison, and Future Directions," IEEE Access, 7(1), 17263-17278, Feb. 2019.
- A. Jaradat, J. M. Hamamreh, H. Arslan, "OFDM With Hybrid Number and Index Modulation," IEEE Access, 8(1), 55042-55053, Mar. 2020.
- A. Jaradat, A. Naeem, M. I. Sağlam, M. Kartal and H. Arslan, "Radar-Aided Communication Scheduling Algorithm for 5G and Beyond Networks," IEEE Access, vol. 10, pp. 96403-96413, 2022, doi: 10.1109/ACCESS.2022.3205641.
- A. Jaradat, J. M. Hamamreh, H. Arslan, "Floating OFDM-SNM for PAPR and OOBE Reduction," IEEE Vehicular Technology Conference (VTC-Spring), Apr. 25-28, 2021.
- A. Jaradat, J. M. Hamamreh, H. Arslan, "Orthogonal Frequency Division Multiplexing with Subcarrier Gap Modulation," IEEE International Symposium on Personal, Indoor, and Mobile Radio Communications (PIMRC), Aug. 31 – Sep. 3, 2020.
- A. Jaradat, E. Memisoglu, H. Arslan, "Blind Numerology Identification for Mixed Numerologies," IEEE Wireless Communications and Networking Conference (WCNC), Mar. 29 – Apr. 1, 2021.
- A. Jaradat, K. Elgammal, M. K. Ozdemir, H. Arslan, "Identification of the number of Wireless Channel Taps Using Deep Neural Networks," IEEE Interregional NEWCAS Conference , June 13-16, 2021.

- A. Jaradat, M. İ. Sağlam, M. Kartal and H. Arslan, "Dynamic-Structure Resource Block Allocation Based Scheduling for 5G Systems," 2022 IEEE 95th Vehicular Technology Conference: (VTC2022-Spring), Helsinki, Finland, 2022, pp. 1-5, doi: 10.1109/VTC2022-Spring54318.2022.9860447.
- A. Jaradat, J. M. Hamamreh, H. Arslan, "Generalized and Flexible Modulation Options," in Flexible and Cognitive Radio Access Technologies for 5G and Beyond, Publisher: IET, Oct. 2020.
- A. Jaradat, J. M. Hamamreh, H. Arslan, "Data transmission method using location adjusted, sub carrier number modulation, orthogonal frequency division multiplexing", WO2021137801A1, 2020.
- A. Jaradat, K. Elgammal, M. K. Ozdemir, H. Arslan, "Blind identification of channel tap numbers in wireless communication", WO2021137801A1, 2021.
- E. Memisoglu, A. Jaradat, H. Arslan, "Method for blind detection of numerology type and band in cellular communication systems and signal receiving unit operating according to said method", WO2022146364A1, 2022.

OTHER PUBLICATIONS, PRESENTATIONS, AND PATENTS:

- A. Jaradat and H. Arslan, "Physical Modification Plane: Cross MAC/PHY Scheduling and Resource Allocation," in Physical Layer Security for Wireless Sensing and Communication, Publisher: IET, 2023.

MODULATION OPTIONS FOR OFDMBASED WAVEFORMS

ORIGINALITY REPORT

15%	10%	11%	2%
SIMILARITY INDEX	INTERNET SOURCES	PUBLICATIONS	STUDENT PAPERS

PRIMARY SOURCES

1	Mohammad Tanvir Mahmud, Heung-Gyoon Ryu. "Performance Evaluation of OFDM Hybrid Number and Index Modulation for 6G Mobile System", 2021 International Conference on Information and Communication Technology Convergence (ICTC), 2021 Publication	1%
2	cosinc.medipol.edu.tr Internet Source	<1%
3	"Front Matter", Institution of Engineering and Technology (IET), 2020 Publication	<1%
4	sens.medipol.edu.tr Internet Source	<1%
5	corelab.ku.edu.tr Internet Source	<1%
6	repository.ntu.edu.sg Internet Source	<1%

7	Muhammet Kırık, Jehad M. Hamamreh. "A novel interference signal superposition algorithm for providing secrecy to subcarrier number modulation - based orthogonal frequency division multiplexing systems", Transactions on Emerging Telecommunications Technologies, 2022 Publication	<1 %
8	Tuncay Eren, Aydin Akan. "Null Subcarrier Index Modulation in OFDM Systems for 6G and Beyond", Sensors, 2021 Publication	<1 %
9	ndl.ethernet.edu.et Internet Source	<1 %
10	archive.org Internet Source	<1 %
11	doi.org Internet Source	<1 %
12	Miaowen Wen, Qiang Li, Xiang Cheng. "Index Modulation for OFDM Communications Systems", Springer Science and Business Media LLC, 2021 Publication	<1 %
13	Submitted to Mutah University in Jordan Student Paper	<1 %

14	Jehad M. Hamamreh, Abdulwahab Hajar, Mohamedou Abewa. "Orthogonal frequency division multiplexing with subcarrier power modulation for doubling the spectral efficiency of 6G and beyond networks", Transactions on Emerging Telecommunications Technologies, 2020 Publication	<1 %
15	lib.tkk.fi Internet Source	<1 %
16	scholar.uwindsor.ca Internet Source	<1 %
17	vdoc.pub Internet Source	<1 %
18	researcherstore.com Internet Source	<1 %
19	Submitted to University of Bristol Student Paper	<1 %
20	univ-usto.dz Internet Source	<1 %
21	A. Ananth, Ha H. Nguyen, Colin Howlett. "Frequency Diversity Schemes for OFDM-IM and OFDM-SNM", 2022 IEEE Wireless Communications and Networking Conference (WCNC), 2022 Publication	<1 %

22	coek.info Internet Source	<1 %
23	downloads.hindawi.com Internet Source	<1 %
24	web.itu.edu.tr Internet Source	<1 %
25	pureadmin.qub.ac.uk Internet Source	<1 %
26	scholarcommons.usf.edu Internet Source	<1 %
27	Di Zheng, Hongming Zhang, Jian Song. "OFDM With Differential Index Modulation for Visible Light Communication", IEEE Photonics Journal, 2020 Publication	<1 %
28	web-tools.uts.edu.au Internet Source	<1 %
29	tel.archives-ouvertes.fr Internet Source	<1 %
30	Yun Liu, Fei Ji, Miaowen Wen, Dehuan Wan, Beixiong Zheng. "Vector OFDM with Index Modulation", IEEE Access, 2017 Publication	<1 %
31	Lajos Hanzo, Sheng Chen, Qi Wang, Zhaocheng Wang, Tianqi Mao. "Dual-Mode	<1 %

Index Modulation Aided OFDM", IEEE Access, 2016
Publication

32	spectrum.library.concordia.ca Internet Source	<1 %
33	epubs.surrey.ac.uk Internet Source	<1 %
34	Haji M. Furqan, Jehad M. Hamamreh, Huseyin Arslan. "Adaptive OFDM-IM for Enhancing Physical Layer Security and Spectral Efficiency of Future Wireless Networks", Wireless Communications and Mobile Computing, 2018 Publication	<1 %
35	Yu-Hsuan Liu, Kate Ching-Ju Lin. "Traffic-Aware Resource Allocation for Multi-User Beamforming", IEEE Transactions on Mobile Computing, 2022 Publication	<1 %
36	Tianqi Mao, Qi Wang, Zhaocheng Wang, Sheng Chen. "Novel Index Modulation Techniques: A Survey", IEEE Communications Surveys & Tutorials, 2019 Publication	<1 %
37	docplayer.net Internet Source	<1 %
38	Domouchtsidis, Stavros G., Georgia D. Ntouni, Vasileios M. Kapinas, and George K.	<1 %

	Karagiannidis. "OFDM-IM vs FQAM: A comparative analysis", 2016 23rd International Conference on Telecommunications (ICT), 2016. Publication	
39	onlinelibrary.wiley.com Internet Source	<1 %
40	Ali Fazeli, Ha H. Nguyen, Muhammad Hanif. "Generalized OFDM-IM With Noncoherent Detection", IEEE Transactions on Wireless Communications, 2020 Publication	<1 %
41	Shaddrack Yaw Nusenu. "Spatial Modulation Technique For Filtered-OFDM Based Wireless Transmission", Advances in Science, Technology and Engineering Systems Journal, 2017 Publication	<1 %
42	repository.kaust.edu.sa Internet Source	<1 %
43	epdf.tips Internet Source	<1 %
44	www.hindawi.com Internet Source	<1 %
45	vbn.aau.dk Internet Source	<1 %

46	Jehad M. Hamamreh, Z. Esat Ankarali, Huseyin Arslan. "CP-less OFDM With Alignment Signals for Enhancing Spectral Efficiency, Reducing Latency, and Improving PHY Security of 5G Services", IEEE Access, 2018 Publication	<1 %
47	Submitted to University of Bahrain Student Paper	<1 %
48	"Multi-Carrier Systems & Solutions 2009", Springer Science and Business Media LLC, 2009 Publication	<1 %
49	Ertugrul Basar, Miaowen Wen, Raed Mesleh, Marco Di Renzo, Yue Xiao, Harald Haas. "Index Modulation Techniques for Next-Generation Wireless Networks", IEEE Access, 2017 Publication	<1 %
50	ethesis.nitrkl.ac.in Internet Source	<1 %
51	theses.gla.ac.uk Internet Source	<1 %
52	Miaowen Wen, Xiang Cheng, Liuqing Yang. "Index Modulation for 5G Wireless Communications", Springer Science and Business Media LLC, 2017 Publication	<1 %

53	Tim Schenk. "RF Imperfections in High-rate Wireless Systems", Springer Science and Business Media LLC, 2008 Publication	<1 %
54	Hüseyin Arslan. "Wireless Communication Signals", Wiley, 2021 Publication	<1 %
55	era.ed.ac.uk Internet Source	<1 %
56	es.scribd.com Internet Source	<1 %
57	repository.tudelft.nl Internet Source	<1 %
58	Ertugrul Basar. "Index modulation techniques for 5G wireless networks", IEEE Communications Magazine, 2016 Publication	<1 %
59	s3.eu-central-1.amazonaws.com Internet Source	<1 %
60	Abdulwahab Hajar, Jehad M. Hamamreh, Mohamedou Abewa, Youcef Belallou. "A Spectrally Efficient OFDM-Based Modulation Scheme for Future Wireless Systems", 2019 Scientific Meeting on Electrical-Electronics & Biomedical Engineering and Computer Science (EBBT), 2019 Publication	<1 %

61	amsdottorato.unibo.it Internet Source	<1 %
62	mafiadoc.com Internet Source	<1 %
63	research.library.mun.ca Internet Source	<1 %
64	Yahia Medjahdi, Sylvain Traverso, Robin Gerzaguet, Hmaied Shaiek et al. "On the Road to 5G: Comparative Study of Physical Layer in MTC Context", IEEE Access, 2017 Publication	<1 %
65	eprints.kfupm.edu.sa Internet Source	<1 %
66	etheses.whiterose.ac.uk Internet Source	<1 %
67	repository.up.ac.za Internet Source	<1 %
68	"Radio Access Network Slicing and Virtualization for 5G Vertical Industries", Wiley, 2021 Publication	<1 %
69	Zhenxing Chen, Yi Lu, Seog Geun Kang. "High-Dimensional OFDM with In-Phase/Quadrature Index Modulation", IEEE Access, 2021 Publication	<1 %

70	opus.lib.uts.edu.au Internet Source	<1%
71	skynet.ee.imperial.ac.uk Internet Source	<1%
72	Andrei Gabrielov, Nicolai Vorobjov. "Complexity of cylindrical decompositions of sub-Pfaffian sets", Journal of Pure and Applied Algebra, 2001 Publication	<1%
73	Miaowen Wen, Jun Li, Shuping Dang, Qiang Lia, Shahid Mumtaz, Huseyin Arslan. "Joint-Mapping Orthogonal Frequency Division Multiplexing with Subcarrier Number Modulation", IEEE Transactions on Communications, 2021 Publication	<1%
74	Qiang Li, Miaowen Wen, H. Vincent Poor, Fangjiong Chen. "Information Guided Precoding for OFDM", IEEE Access, 2017 Publication	<1%
75	sucra.repo.nii.ac.jp Internet Source	<1%
76	web.archive.org Internet Source	<1%
77	Submitted to University of Edinburgh Student Paper	<1%

78	core.ac.uk Internet Source	<1 %
79	etd.lib.metu.edu.tr Internet Source	<1 %
80	ro.uow.edu.au Internet Source	<1 %
81	"IoT as a Service", Springer Science and Business Media LLC, 2019 Publication	<1 %
82	Jinho Choi. "Chapter 168-1 Index Modulation for OFDM", Springer Science and Business Media LLC, 2018 Publication	<1 %
83	dspace.pondiuni.edu.in Internet Source	<1 %
84	knowledgecommons.lakeheadu.ca Internet Source	<1 %
85	Ertugrul Basar, Umit Aygolu, Erdal Panayirci, H. Vincent Poor. "Orthogonal Frequency Division Multiplexing With Index Modulation", IEEE Transactions on Signal Processing, 2013 Publication	<1 %
86	www.themistoklis.org Internet Source	<1 %

87	Jehad M. Hamamreh, Ertugrul Basar, Huseyin Arslan. "OFDM-Subcarrier Index Selection for Enhancing Security and Reliability of 5G URLLC Services", IEEE Access, 2017 Publication	<1 %
88	Mohammad Irfan, Sonia Aissa. "Generalization of Index-Modulation: Breaking the Conventional Limits on Spectral and Energy Efficiencies", IEEE Transactions on Wireless Communications, 2021 Publication	<1 %
89	Shuping Dang, Guoqing Ma, Basem Shihada, Mohamed-Slim Alouini. "Enhanced Orthogonal Frequency-Division Multiplexing With Subcarrier Number Modulation", IEEE Internet of Things Journal, 2019 Publication	<1 %
90	dr.ntu.edu.sg Internet Source	<1 %
91	espace.curtin.edu.au Internet Source	<1 %
92	pure.tue.nl Internet Source	<1 %
93	Jisheng Dai, Lei Zhou, Chunqi Chang, Weichao Xu. "Robust Bayesian learning approach for massive MIMO channel estimation", Signal Processing, 2020	<1 %

	Publication	
94	Jung-Hoon Noh, Seong-Jun Oh. "Distributed SC-FDMA Resource Allocation Algorithm Based on the Hungarian Method", 2009 IEEE 70th Vehicular Technology Conference Fall, 2009 Publication	<1 %
95	Lecture Notes in Computer Science, 2013. Publication	<1 %
96	e-archivo.uc3m.es Internet Source	<1 %
97	eprints.gla.ac.uk Internet Source	<1 %
98	tuat.repo.nii.ac.jp Internet Source	<1 %
99	Submitted to City University of Hong Kong Student Paper	<1 %
100	Submitted to University of Sydney Student Paper	<1 %
101	Submitted to Indian Institute of Technology Patna Student Paper	<1 %
102	Submitted to University of Mosul Student Paper	<1 %
103	etd.auburn.edu Internet Source	

		<1 %
104	hal.archives-ouvertes.fr Internet Source	<1 %
105	"Encyclopedia of Earthquake Engineering", Springer Nature America, Inc, 2015 Publication	<1 %
106	"Quality, Reliability, Security and Robustness in Heterogeneous Networks", Springer Nature, 2013 Publication	<1 %
107	"Smart Grids and Their Communication Systems", Springer Science and Business Media LLC, 2019 Publication	<1 %
108	Hakkeon Lee, Hyunsoo Kim, Sungmook Lim, Daesik Hong. "A Novel Preamble Design for Time Synchronization in OFDM-Based Multiple Numerologies", 2018 IEEE 88th Vehicular Technology Conference (VTC-Fall), 2018 Publication	<1 %
109	Madyan Alsenwi, Nguyen H. Tran, Mehdi Bennis, Shashi Raj Pandey, Anupam Kumar Bairagi, Choong Seon Hong. "Intelligent Resource Slicing for eMBB and URLLC Coexistence in 5G and Beyond: A Deep	<1 %

	Reinforcement Learning Based Approach", IEEE Transactions on Wireless Communications, 2021 Publication	
110	Prakash Chaki, Takumi Ishihara, Shinya Sugiura. "Precoded Filterbank Multicarrier Index Modulation With Non-Orthogonal Subcarrier Spacing", IEEE Transactions on Communications, 2022 Publication	<1 %
111	Sudharsan Ganesan, Raed Mesleh, Harald Ho, Chang Wook Ahn, Sangboh Yun. "On the Performance of Spatial Modulation OFDM", 2006 Fortieth Asilomar Conference on Signals, Systems and Computers, 2006 Publication	<1 %
112	Xuekun Zhang, Hongxia Bie, Qianwen Ye, Chunyang Lei, Xianfeng Tang. "Dual-Mode Index Modulation Aided OFDM With Constellation Power Allocation and Low-Complexity Detector Design", IEEE Access, 2017 Publication	<1 %
113	discovery.ucl.ac.uk Internet Source	<1 %
114	hal-supelec.archives-ouvertes.fr Internet Source	<1 %

115	ipfs.io Internet Source	<1 %
116	oatao.univ-toulouse.fr Internet Source	<1 %
117	repository.ju.edu.et Internet Source	<1 %
118	surface.syr.edu Internet Source	<1 %
119	theses.hal.science Internet Source	<1 %
120	www.diva-portal.se Internet Source	<1 %
121	"Computer Science and Engineering—Theory and Applications", Springer Science and Business Media LLC, 2018 Publication	<1 %
122	Bo Tang, Kaiyu Qin, Haibo Mei, Changwei Chen. "Iterative Clipping-Noise Compression Scheme for PAPR Reduction in OFDM Systems", IEEE Access, 2019 Publication	<1 %
123	Ferhat Yarkin, Justin P. Coon. "Set Partition Modulation", IEEE Transactions on Wireless Communications, 2020 Publication	<1 %

124	Submitted to Politecnico di Milano Student Paper	<1 %
125	Qingbo Wang, Gaoqi Dou, Jun Gao, Ran Deng. "Linear Constellation Precoded OFDM With Interleaved Subcarrier Index Modulation", IEEE Access, 2019 Publication	<1 %
126	repositorio.iscte-iul.pt Internet Source	<1 %
127	Jun Li, Yuyang Peng, Xueqin Jiang, Yier Yan, Prabhat Ranjan. "Enhanced Index Modulated OFDM Spread Spectrum", IEEE Access, 2018 Publication	<1 %
128	Monika Jain, Anirudh Agarwal, Divyang Rawal, Ranjan Gangopadhyay. "Adaptive bit and power allocation for dual mode index modulation based OFDM system", Physical Communication, 2020 Publication	<1 %
129	Submitted to School of Business and Management ITB Student Paper	<1 %
130	Siyao Lu, Ibrahim A. Hemadeh, Mohammed El-Hajjar, Lajos Hanzo. "Compressed Sensing-Aided Space-Time Frequency Index Modulation", IEEE Transactions on Vehicular Technology, 2018	<1 %

Publication

131	Yuxin Shi, Xinjin Lu, Kai Gao, Jiang Zhu, Shilian Wang. "Subblocks Set Design Aided Orthogonal Frequency Division Multiplexing With All Index Modulation", IEEE Access, 2019 Publication	<1 %
132	Chaoyue Jin, Li Wei, Youyun Xu. "Universal Filtered OFDM Index Modulation System with Enhanced ICI compression", 2019 28th Wireless and Optical Communications Conference (WOCC), 2019 Publication	<1 %
133	openaccess.hacettepe.edu.tr:8080 Internet Source	<1 %
134	Chao Xu, Yifeng Xiong, Naoki Ishikawa, Rakshith Rajashekar et al. "Space-, Time-and Frequency-Domain Index Modulation for Next-Generation Wireless: A Unified Single-/Multi-Carrier and Single-/Multi-RF MIMO Framework", IEEE Transactions on Wireless Communications, 2021 Publication	<1 %
135	Qi Wang, Tianqi Mao, Zhaocheng Wang. "Chapter 4 Index Modulation-Aided OFDM for Visible Light Communications", IntechOpen, 2017 Publication	<1 %

136	w3.antd.nist.gov Internet Source	<1 %
137	Yonggu Lee, Hanseong Jo, Youngwook Ko, Jinho Choi. "Secure Index and Data Symbol Modulation for OFDM-IM", IEEE Access, 2017 Publication	<1 %
138	espace.inrs.ca Internet Source	<1 %
139	ir.lib.uwo.ca Internet Source	<1 %
140	repositorio.uc.cl Internet Source	<1 %
141	Khaled Ben Letaief. "Uplink Scheduling with QoS Provisioning for Cognitive Radio Systems", 2007 IEEE Wireless Communications and Networking Conference, 03/2007 Publication	<1 %
142	Submitted to Paramus High School Student Paper	<1 %
143	Thien Van Luong, Youngwook Ko. "Spread OFDM-IM With Precoding Matrix and Low-Complexity Detection Designs", IEEE Transactions on Vehicular Technology, 2018 Publication	<1 %
	aaltodoc.aalto.fi	

144	Internet Source	<1 %
145	eprints.whiterose.ac.uk Internet Source	<1 %
146	pastel.archives-ouvertes.fr Internet Source	<1 %
147	psasir.upm.edu.my Internet Source	<1 %
148	publik.tuwien.ac.at Internet Source	<1 %
149	unsworks.unsw.edu.au Internet Source	<1 %
150	web.ecs.baylor.edu Internet Source	<1 %
151	www.escholar.manchester.ac.uk Internet Source	<1 %
152	www.ijrte.org Internet Source	<1 %
153	www10.cs.fau.de Internet Source	<1 %
154	Giridhar K, Abhay Mohan M V. "Accurate Signal Recovery in UHF Band Reuse-1 Cellular OFDMA Downlinks", Institute of Electrical and Electronics Engineers (IEEE), 2021 Publication	<1 %

155	Jianping Zheng, Hongmei Lv. "A Semidefinite Relaxation Approach to OFDM-IM Detection in Rapidly Time-Varying Channels", IEEE Access, 2018 Publication	<1 %
156	Mehmet Mert Sahin, Huseyin Arslan. "Multi-functional Coexistence of Radar-Sensing and Communication Waveforms", 2020 IEEE 92nd Vehicular Technology Conference (VTC2020-Fall), 2020 Publication	<1 %
157	Ping Yang, Marco Di Renzo, Yue Xiao, Shaoqian Li, Lajos Hanzo. "Design Guidelines for Spatial Modulation", IEEE Communications Surveys & Tutorials, 2015 Publication	<1 %
158	Praveenkumar Korrai, Eva Lagunas, Shree Krishna Sharma, Symeon Chatzinotas, Ashok Bandi, Bjorn Ottersten. "A RAN Resource Slicing Mechanism for Multiplexing of eMBB and URLLC Services in OFDMA Based 5G Wireless Networks", IEEE Access, 2020 Publication	<1 %
159	S. A. Adegbite, S. G. McMeekin, B. G. Stewart. "A PAPR Reduction and Data Decoding for SLM Based OFDM Systems without SI", 2015 IEEE 81st Vehicular Technology Conference (VTC Spring), 2015	<1 %

	Publication	
160	Sarath Gopi, Sheetal Kalyani, Lajos Hanzo. "Coherent and Non-Coherent Multilayer Index Modulation", IEEE Access, 2019 Publication	<1 %
161	Saud Althunibat, Raed Mesleh, Ertugrul Basar. "Differential Subcarrier Index Modulation", IEEE Transactions on Vehicular Technology, 2018 Publication	<1 %
162	Tho Le-Ngoc, Ruikai Mai. "Hybrid Massive MIMO Precoding in Cloud-RAN", Springer Science and Business Media LLC, 2019 Publication	<1 %
163	Xiaoying Zhang, Lei Zhang, Pei Xiao, Dongtang Ma, Jibo Wei, Yu Xin. "Mixed Numerologies Interference Analysis and Inter-Numerology Interference Cancellation for Windowed OFDM Systems", IEEE Transactions on Vehicular Technology, 2018 Publication	<1 %
164	harvest.usask.ca Internet Source	<1 %
165	hexa-x.eu Internet Source	<1 %
166	ijmtst.com Internet Source	<1 %

167	keep.lib.asu.edu Internet Source	<1%
168	open.library.ubc.ca Internet Source	<1%
169	repositorio.unicamp.br Internet Source	<1%
170	www.isca-speech.org Internet Source	<1%
171	www.mdpi.com Internet Source	<1%
172	www.scribd.com Internet Source	<1%
173	"5G Mobile Communications", Springer Science and Business Media LLC, 2017 Publication	<1%
174	"Full-Duplex Communications for Future Wireless Networks", Springer Science and Business Media LLC, 2020 Publication	<1%
175	"OFDM", Springer Science and Business Media LLC, 2011 Publication	<1%
176	Ahmet Kaplan, Mehmet Can, Ibrahim Altunbas, Gunes Karabulut Kurt, Defne Kucukyavuz. "LDPC Coded OFDM-IM	<1%

Performance Evaluation Under Jamming Attack", 2020 International Conference on Information and Communication Technology Convergence (ICTC), 2020
Publication

177	Binh Vo, Ha H. Nguyen. "Performance comparison of IM-based OFDM and OFDM with multiple constellations", IEICE Communications Express, 2017 Publication	<1 %
178	Chafika Tata, Nassima Fellag, Michel Kadoch. "New Courteous Algorithm for Uplink Scheduling in LTE-Advanced and 5G Networks", Journal of Computer Networks and Communications, 2020 Publication	<1 %
179	Dongkyu Kim, Haesoon Lee, Daesik Hong. "A Survey of In-Band Full-Duplex Transmission: From the Perspective of PHY and MAC Layers", IEEE Communications Surveys & Tutorials, 2015 Publication	<1 %
180	Fernando Gregorio, Gustavo González, Christian Schmidt, Juan Cousseau. "Signal Processing Techniques for Power Efficient Wireless Communication Systems", Springer Science and Business Media LLC, 2020 Publication	<1 %

181	Gao, Qian, Jonathan H. Manton, Gang Chen, and Yingbo Hua. "Constellation Design for a Multicarrier Optical Wireless Communication Channel", IEEE Transactions on Communications, 2014. Publication	<1 %
182	Haysam Dahman. "Performance evaluation of space-time-frequency spreading for MIMO OFDM-CDMA systems", EURASIP Journal on Advances in Signal Processing, 2011 Publication	<1 %
183	Joydev Ghosh, Huseyin Haci, Neeraj Kumar, Khaled AlUtaibi, Sadiq M. Sait, Chakchai So-In. "A novel channel model and optimal power control schemes for mobile mmWave two-tier networks", Institute of Electrical and Electronics Engineers (IEEE), 2022 Publication	<1 %
184	K.G. Paterson, V. Tarokh. "On the existence and construction of good codes with low peak-to-average power ratios", IEEE Transactions on Information Theory, 2000 Publication	<1 %
185	Manav R. Bhatnagar. "Making Two-Way Satellite Relaying Feasible: A Differential Modulation Based Approach", IEEE Transactions on Communications, 2015 Publication	<1 %

186	Martoyo, Ihan. "Frequency domain equalization in CDMA detection.", Universität Karlsruhe, 2005. Publication	<1 %
187	Niu, Binglai, Vincent W.S. Wong, and Robert Schober. "Downlink Scheduling with Transmission Strategy Selection for Multi-Cell MIMO Systems", IEEE Transactions on Wireless Communications, 2012. Publication	<1 %
188	Signals and Communication Technology, 2016. Publication	<1 %
189	Teng Li. "Power Spectral Density Comparison for the Clipped OFDM-Type Signals", 2010 Second International Conference on Networks Security Wireless Communications and Trusted Computing, 04/2010 Publication	<1 %
190	Thalanany, Sebastian. "Connectivity", Mobile Evolution, 2015. Publication	<1 %
191	Victor Farias Monteiro, Diego Aguiar Sousa, Tarcisio Ferreira Maciel, Francisco Rodrigo Porto Cavalcanti et al. "Distributed RRM for 5G Multi-RAT Multiconnectivity Networks", IEEE Systems Journal, 2018 Publication	<1 %

192	Xiaoqi Wang, Chaoqin Gan, Shibao Wu, Yitong Chen, Yixin Chen. "Founding AP's IVM and related IHM for subway LiFi network", Optical Switching and Networking, 2022 Publication	<1 %
193	docs.lib.purdue.edu Internet Source	<1 %
194	dspace.cc.tut.fi Internet Source	<1 %
195	escholarship.org Internet Source	<1 %
196	ir.canterbury.ac.nz Internet Source	<1 %
197	jultika.oulu.fi Internet Source	<1 %
198	orbilu.uni.lu Internet Source	<1 %
199	pure.southwales.ac.uk Internet Source	<1 %
200	qspace.library.queensu.ca Internet Source	<1 %
201	researchonline.jcu.edu.au Internet Source	<1 %
202	researchspace.ukzn.ac.za Internet Source	<1 %

203	rs-ojict.pubpub.org Internet Source	<1 %
204	ruor.uottawa.ca Internet Source	<1 %
205	saieecontent.blob.core.windows.net Internet Source	<1 %
206	uos-app00353-si.soton.ac.uk Internet Source	<1 %
207	upcommons.upc.edu Internet Source	<1 %
208	www.arehna.di.uoa.gr Internet Source	<1 %
209	www.comonsens.org Internet Source	<1 %
210	www.cs.ucr.edu Internet Source	<1 %
211	www.eurasip.org Internet Source	<1 %
212	www.groundai.com Internet Source	<1 %
213	www.ittc.ku.edu Internet Source	<1 %
214	www.itu.int Internet Source	<1 %

215	www.research.manchester.ac.uk Internet Source	<1 %
216	www.semanticscholar.org Internet Source	<1 %
217	zombiedoc.com Internet Source	<1 %
218	Huawei Zhou, Guohai Liu, Wenxiang Zhao, Xiaodong Yu, Menghu Gao. "Dynamic Performance Improvement of Five-Phase Permanent-Magnet Motor With Short-Circuit Fault", IEEE Transactions on Industrial Electronics, 2018 Publication	<1 %
219	Lou Zhao, Derrick Wing Kwan Ng, Jinhong Yuan. "Multi-User Precoding and Channel Estimation for Hybrid Millimeter Wave Systems", IEEE Journal on Selected Areas in Communications, 2017 Publication	<1 %
220	Moustafa M. Nasralla, Ikram Ur Rehman. "QCI and QoS Aware Downlink Packet Scheduling Algorithms for Multi-Traffic Classes over 4G and beyond Wireless Networks", 2018 International Conference on Innovation and Intelligence for Informatics, Computing, and Technologies (3ICT), 2018 Publication	<1 %

221	Yuxin Shi, Kai Gao, Jiang Zhu, Xinjin Lu, Shilian Wang. "Orthogonal Frequency Division Multiplexing With Joint Subblocks Index Modulation", IEEE Access, 2019 Publication	<1 %
222	Baek, Myung-sun, and Hyoung-kyu Song. "Cooperative diversity technique for MIMO-OFDM uplink in wireless interactive broadcasting", IEEE Transactions on Consumer Electronics, 2008. Publication	<1 %
223	Ebubekir Memisoglu, Ertugrul Basar, Huseyin Arslan. "Fading-aligned OFDM with index modulation for mMTC services", Physical Communication, 2019 Publication	<1 %
224	Mahmut Yildirim. "ABC Algorithm-Based Subblocks Set Design for OFDM With All Index Modulation", IEEE Communications Letters, 2020 Publication	<1 %
225	Mitchell J. Grabner, Xinrong Li, Shengli Fu. "An Adaptive BLAST Successive Interference Cancellation Method for High Data Rate Perfect Space-Time Coded MIMO Systems", IEEE Transactions on Vehicular Technology, 2020 Publication	<1 %

226	Saulo Queiroz, Joao Vilela, Edmundo Monteiro. "What is the Cost of the Index Selector Task for OFDM with Index Modulation?", 2019 Wireless Days (WD), 2019 Publication	<1 %
227	Thi Thanh Huyen Le, Xuan Nam Tran, Vu-Duc Ngo, Minh-Tuan Le. "Repeated Index Modulation-OFDM With Coordinate Interleaving: Performance Optimization and Low-Complexity Detectors", IEEE Systems Journal, 2021 Publication	<1 %
228	Xiaoran Liu, Xiaoying Zhang, Lei Zhang, Pei Xiao, Jibo Wei, Haijun Zhang, Victor C. M. Leung. "PAPR Reduction Using Iterative Clipping/Filtering and ADMM Approaches for OFDM-Based Mixed-Numerology Systems", IEEE Transactions on Wireless Communications, 2020 Publication	<1 %
229	Zhiguo Sun, Pan Yan, Xiaoyan Ning, Changqing Deng. "Performance Analysis of Index Bit Errors Rate of SIM-OFDM on AWGN Channels", 2018 IEEE 18th International Conference on Communication Technology (ICCT), 2018 Publication	<1 %

Exclude quotes	On	Exclude matches	< 4 words
Exclude bibliography	On		